COUPLED CO_2 SEQUESTRATION AND ENHANCED CONDENSATE RECOVERY IN GAS CONDENSATE RESERVOIR USING EXPERIMENTAL DESIGN AND RESPONSE SURFACE METHODOLOGY

Mr. Pitipong Santagarn

A Thesis Submitted in Partial Fulfillment of the Requirements
for the Degree of Master of Engineering Program in Petroleum Engineering
Department of Mining and Petroleum Engineering
Faculty of Engineering
Chulalongkorn University
Academic Year 2011

การกักเก็บก๊าซคาร์บอนไดออกไซด์ควบคู่กับการเพิ่มการผลิตก๊าซธรรมชาติเหลวจากแหล่งกักเก็บก๊าซธรรมชาติเหลวโดยใช้หลักการออกแบบการทดลองและผลตอบสนองแบบโครงร่างพื้นผิว

นาย ปิติพงศ์ สันตะการ

วิทยานิพนธ์นี้เป็นส่วนหนึ่งของการศึกษาตามหลักสูตรปริญญาวิศวกรรมศาสตรมหาบัณฑิต
สาขาวิชาวิศวกรรมปิโตรเลียม ภาควิชาวิศวกรรมเหมืองแร่และปิโตรเลียม
คณะวิศวกรรมศาสตร์ จุฬาลงกรณ์มหาวิทยาลัย
ปีการศึกษา 2554

Thesis Title	COUPLED CO_2 SEQUESTRATION AND ENHANCED CONDENSATE RECOVERY IN GAS CONDENSATE RESERVOIR USING EXPERIMENTAL DESIGN AND RESPONSE SURFACE METHODOLOGY
By	Mr. Pitipong Santagarn
Field of Study	Petroleum Engineering
Thesis Advisor	Assistant Professor Suwat Athichanagorn, Ph.D.
Thesis Co-advisor	Kreangkrai Maneeintr, Ph.D.

Accepted by the Faculty of Engineering, Chulalongkorn University in Partial Fulfillment of the Requirements for the Master's Degree

...……. Dean of the Faculty of Engineering
(Associate Professor Boonsom Lerdhirunwong, Dr.Ing.)

THESIS COMMITTEE

….……Chairman
(Associate Professor Sarithdej Pathanasethpong)

…….Thesis Advisor
(Assistant Professor Suwat Athichanagorn, Ph.D.)

…….Thesis Co-advisor
(Kreangkrai Maneeintr, Ph.D.)

…….Examiner
(Falan Srisuriyachai, Ph.D.)

…….External Examiner
(Siree Nasakul, Ph.D.)

ปิติพงศ์ สันตะการ: การกักเก็บก๊าซคาร์บอนไดออกไซด์ควบคู่กับการเพิ่มการผลิตก๊าซธรรมชาติเหลวจากแหล่งกักเก็บก๊าซธรรมชาติเหลวโดยใช้หลักการออกแบบการทดลองและผลตอบสนองแบบโครงร่างพื้นผิว (COUPLED CO_2 SEQUESTRATION AND ENHANCED CONDENSATE RECOVERY IN GAS CONDENSATE RESERVOIR USING EXPERIMENTAL DESIGN AND RESPONSE SURFACE METHODOLOGY) อ. ที่ปรึกษาวิทยานิพนธ์หลัก: ผศ. ดร. สุวัฒน์ อธิชนากร, อ. ที่ปรึกษาวิทยานิพนธ์ร่วม: ดร. เกรียงไกร มณีอินทร์, 119 หน้า.

ปัญหาก๊าซธรรมชาติเหลวกลั่นตัวออกมาและตกค้างอยู่ในแหล่งกักเก็บก๊าซธรรมชาติเหลวเมื่อความดันภายในแหล่งกักเก็บลดลงต่ำกว่าความดันกลั่นตัว สามารถที่จะแก้ได้โดยการอัดก๊าซคาร์บอนไดออกไซด์ อันเป็นกระบวนการทำให้ก๊าซธรรมชาติเหลวเกิดการระเหยจากของเหลวกลายเป็นก๊าซอีกครั้งซึ่งเป็นผลจากการที่ความดันของแหล่งกักเก็บถูกอัดให้เพิ่มขึ้น ณ เวลาเดียวกันส่วนหนึ่งของปริมาณก๊าซคาร์บอนไดออกไซด์ที่ถูกอัดลงไปจะถูกกักเก็บภายในแหล่งกักเก็บ ผลบวกทั้งสองด้านนี้ทำให้วิธีการนี้น่าสนใจเป็นอย่างยิ่ง

จุดประสงค์ของการศึกษานี้คือ ศึกษาการประยุกต์ใช้การกักเก็บก๊าซคาร์บอนไดออกไซด์ควบคู่กับการเพิ่มการผลิตก๊าซธรรมชาติเหลวจากแหล่งกักเก็บก๊าซธรรมชาติเหลวที่ตัวแปรการออกแบบและกลยุทธ์ในการผลิตต่างๆ โดยใช้แบบจำลองแหล่งกักเก็บแบบองค์ประกอบเพื่อที่จะหาว่าแหล่งกักเก็บที่ศึกษานั้นมีศักยภาพที่จะใช้วิธีการนี้หรือไม่ ท่ามกลางระดับค่าของตัวแปรและกลยุทธ์ต่างๆซึ่งจะนำไปสู่สภาวะที่เหมาะสมในการดำเนินการโดยใช้หลักการออกแบบการทดลองและผลตอบสนองโครงร่างพื้นผิว ตัวแปรและกลยุทธ์ในการผลิตที่ศึกษาประกอบไปด้วย ค่าความสามารถในการซึมผ่าน วิธีการอัดก๊าซ (การอัดก๊าซสลับกับน้ำ กับ การอัดก๊าซคาร์บอนไดออกไซด์เพียงอย่างเดียว) ประเภทของหลุมอัดและหลุมผลิต (แนวตั้งกับแนวนอน) อัตราส่วนระหว่างค่าความสามารถในการซึมผ่านในแนวตั้งต่อแนวนอน อัตราการอัดก๊าซ ระยะห่างระหว่างหลุม เวลาที่เริ่มอัด โดยใช้ปริมาณคาร์บอนไดออกไซด์ที่ถูกกักเก็บและค่าเปอร์เซนต์การผลิตก๊าซธรรมชาติเหลวเป็นเกณฑ์ เพื่อหาสภาวะที่เหมาะสม

จากผลการศึกษา แหล่งกักเก็บที่มีค่าความสามารถในการซึมผ่านสูงมีศักยภาพที่จะดำเนินโครงการนี้ กลยุทธ์ที่เหมาะสมในการดำเนินการได้รับจากหลักการออกแบบการทดลอง ซึ่งสามารถประหยัดเวลาและค่าใช้จ่ายในการดำเนินการที่เกิดจากการใช้แบบจำลองเพียงอย่างเดียว

ภาควิชา วิศวกรรมเหมืองแร่และปิโตรเลียม ลายมือชื่อนิสิต.....

สาขาวิชา วิศวกรรมปิโตรเลียม ลายมือชื่อ อ.ที่ปรึกษาวิทยานิพนธ์หลัก.....

ปีการศึกษา 2554 ลายมือชื่อ อ.ที่ปรึกษาวิทยานิพนธ์ร่วม.....

5171609421: MAJOR PETROLEUM ENGINEERING
KEYWORDS: CO_2 STORGAE/EXPERIMENTAL DESIGN/GAS INJECTION

PITIPONG SANTAGARN. COUPLED CO_2 SEQUESTRATION AND ENHANCED CONDENSATE RECOVERY IN GAS CONDENSATE RESERVOIR USING EXPERIMENTAL DESIGN AND RESPONSE SURFACE METHODOLOGY. ADVISOR: ASST. PROF. SUWAT ATHICHANAGORN, Ph.D., CO-ADVISOR: KREANGKRAI MANEEINTR, Ph.D., 119 pp.

Valuable condensate in gas condensate reservoirs which will drop out and is left in the reservoir at reservoir pressure lower than dew point pressure can be recovered via CO_2 injection by the mechanism of condensate re-vaporization as a result of pressurization. At the same time, part of the injected CO_2 can be sequestered in the reservoir, allowing the methodology to be attractive.

The objective of this study is to investigate the application of CO_2 sequestration and enhanced condensate recovery in gas condensate reservoir for different flood design parameters and strategies using compositional reservoir simulation model. It is to better quantify the potential of reservoir condition over a wide variety of parameters and strategies with the need to find optimum operational strategies with the aid of Experimental Design and Response Surface Methodology. The parameters and strategies studied include permeability, injection scheme (water alternating gas vs. continuous CO_2 injection), injection and production well type (vertical vs. horizontal), vertical to horizontal permeability ratio, injection rate, well spacing, and injection time. The amount of CO_2 stored and condensate recovery factor are considered as two responses.

The results show that 1000-md permeability gas condensate reservoir with high kv/kh has potential to implement. Optimum strategies are provided by Experimental Design with less time and cost compared to full runs of simulation.

Department: Mining and Petroleum Engineering Student's Signature…….
Field of Study: Petroleum Engineering Advisor's Signature……..
Academic Year: 2011 Co-advisor's Signature…….

Acknowledgements

First of all, I would like to thank Asst. Prof. Suwat Athichanagorn, my thesis advisor, for giving me lots of knowledge in petroleum engineering, encouragement, useful guidance and invaluable support during this study.

Secondly, I am highly thankful to all faculty members in the Department of Mining and Petroleum Engineering who have offered me sincere friendship, invaluable support, petroleum knowledge, both of technical and friendly advices. Without them, this study would not have been completed.

Especially, I am indebted to Ms. Patamaporn Thitaram for providing some important data used in this work. I also wish to thank Mr. Jirasak Arunmongkol, for technical discussions, useful suggestion and invaluable guidance, leading me to completion of this study.

Finally, I would like to express my deep appreciation and thankfulness to my family who have always supported and encouraged me with patience throughout this hard time.

Contents

CHAPTER **Page**

CHAPTER **Page**

List of Tables

Page

Page

List of Figures

Page

Page

Page

List of Abbreviations

A	areal
AIM	Adaptive Implicit
atm	atmospheric pressure
B	formation volume factor
bbl	barrel (bbl/d : barrel per day)
BCF	billion cubic foot
BHP	bottomhole pressure
BICs	binary interaction coefficients
BTU	British thermal unit
CGR	condensate-gas ratio
c	critical
C	salinity of brine in weight percent of solid
C_1	methane
C_2	ethane
C_3	propane
i-C_4 or I-C_4	isobutane
i-C_5 or I-C_5	isopentane
n-C_4 or N-C_4	normal butane
n-C_5 or N-C_5	normal pentane
C_6	hexane
C_{7+}	alkane hydrocarbon account from heptanes forward
CO_2	carbon dioxide
Con CO_2	Continuous CO_2 injection
d	displacement
D	darcy
EOS	equation of state
ECR	enhanced condensate recovery
FVF	formation volume factor
g	gas

GPR	gas production rate
k	permeability
k_{rg}	gas relative permeability
k_{rw}	water relative permeability
k_{rog}	oil relative permeability for a system with oil, gas and connate water
k_{row}	oil relative permeability for a system with oil and water
k_{rowg}	oil relative permeability for a system with oil and water at $S_g = 0$
K_i	vapor liquid equilibrium ratio or the equilibrium vaporization ratio
OPR	oil production rate
M	[1] thousand (1,000 of petroleum unit), [2] million (dollar)
M_g	molecular weight
MSCF/D	thousand standard cubic feet per day
NaCl	sodium chloride
NEI	non-equilibrium initialization
o	oil
p	pressure
p_c	capillary pressure
p_d	dew point pressure
PR	Peng-Robinson
PVT	pressure-volume-temperature
PSIA or psia	pounds per square inch absolute
RK	Redlich-Kwong
SCAL	special core analysis
SCF	standard cubic foot
SGAS	gas saturation
SGFN	gas saturation function
SOFN	oil saturation function
SRK	Soave Redlich-Kwong

S	saturation
sb	salinity of brine
sc	*at* standard condition
STB or stb	stock-tank barrel
STB/D	stock-tank barrels per day
SWAT	water saturation
SWFN	water saturation function
T	temperature
THP	tubing head pressure
TVD	true vertical depth or total vertical depth
VLE	Volume-Liquid Equilibrium
VLP	vertical lift performance
w	water
WAG	water-alternating gas
x	distance
z	compressibility factor
Z	mole fraction of component

GREEK LETTER

ϕ	porosity
ρ	fluid density (mass/volume)
ρ	density
Δ	difference operator
ω	Pitzer acentric factor

CHAPTER I

INTRODUCTION

Due to industrial era, Carbon Dioxide (CO_2), as the by-product of demanding fossil fuels, has been increasingly released into the atmosphere. The concentration of CO_2 has been increasing unsteadily and estimation showed that half of this increase has occurred in the past 50 years. Concern over global warming which has resulted from lots of accumulated CO_2 emitted has led to ensuing climate change. Hence, there is balancing approach between increasing demand for fossil fuel and concern of climate change linked to CO_2 emission. Recommendations have been offered to mitigate the problem of increasing Green House Gas emission into the atmosphere. One of them is to increase energy consumption efficiency which stands for less produced CO_2 per amount of produced energy. The second approach is to develop and adopt efficient renewable energy in order to use less fossil fuel and consequently, less CO_2 produced is achieved. The third and promising scenario is long term sequestration of CO_2 in geological formations. Injection of CO_2 underground permanently in either depleted or mature oil or gas reservoir, deep saline formation is usually considered as the most applicable CO_2 sequestration processes owing to its capacity in addition to increased hydrocarbon recovery. Among various types of geological storage fields, injection of CO_2 into gas condensate reservoir is interesting for the following main reasons:

- Gas condensate and/or natural gas reservoirs have larger storage capacity than aquifers. This is because of the high compressibility of gas, representing 30 times more compressible than oil or water [1] at typical reservoir pressures which means larger pore space to store CO_2 is left after depletion.

- CO_2 injection into gas condensate reservoirs may yield significant enhanced recovery of the valuable condensate trapped in the reservoir by liquid re-vaporization and reservoir re-pressurization.

1.1 Objectives

1. To investigate the application of coupled CO_2 sequestration and enhanced condensate recovery in gas condensate reservoir
2. To find optimum values of flood design parameters and strategies to meet the objective of maximizing amount of CO_2 stored and condensate recovery factor
3. To develop the optimization method for obtaining optimum flood design parameters and strategies using Experimental Design and Response Surface Methodology.

1.2 Expected Usefulness

1. Benefit from time and cost saving in performing exhaustive simulation runs is achieved by using Experimental Design and Response Surface Methodology. Additionally, guidelines of optimizing flood design parameters and strategies used to deal with candidate reservoirs are also obtained.
2. List of ranked factors would assist in collection of useful information from available surveillance data in case of budget constraint in order to focus on higher ranked factors.

1.3 Outline of Methodology

1. Gather and prepare data such as reservoir and fluid properties for simulation model based on Thitaram's study [2].
2. Construct base case model according to data from the first step.
3. Perform Experimental Design (D-optimal) to generate sensitivity cases from defined range of each parameter using JMP software.
4. Run 'ECLIPSE 300' compositional simulator by inputting each value of parameters and strategies for every case as generated in the previous step.
5. Required results, namely, condensate recovery factor and amount of CO_2 stored for each case are obtained from the simulation.

6. Obtained results from step 5 are added into pre-generated sensitivity table in JMP software.
7. The 'Fit Model' platform on JMP software is adopted to fit the quadratic proxy model by using regression method with least square technique.
8. Regression coefficients of both objective functions which are condensate recovery factor and amount of CO_2 stored are provided and then statistical analysis is performed to determine individual effect of parameters and strategies on both results.
9. Generate 3-D Response Surface by JMP to estimate in details of responses.
10. Validate the obtained proxy model by performing different sets of cross-validation experiments which are not used in model-construction process.
11. Comparison between predicted and simulation results according to cross-validation experiments is made using statistical test called 'Matched pair t-test' to validate the proxy model.
12. The proxy model after cross-validation process can then be used to predict optimum values of parameters and effective strategies with equally weighted combination between two results as the optimization scenario.

1.4 Thesis Outline

Chapter II reviews previous works/studies related to CO_2 injection into gas condensate reservoirs and coupled CO2 sequestration and enhanced recovery in gas condensate reservoirs.

Chapter III describes the overview of gas condensate reservoirs, phase equilibrium, hydrocarbon production from gas condensate reservoirs, CO_2 injection in gas condensate reservoir, effect of CO_2 injection on gas condensate reservoirs, fundamental of experimental design and response surface methodology.

Chapter IV describes the feature of reservoir simulation model in this study.

Chapter V discusses the results of reservoir simulation, experimental analysis for designed experiments and parameters & strategies optimization.

Chapter VI provides conclusions and recommendations for further study.

CHAPTER II

LITERATURE REVIEW

This chapter discusses previous works that are related to the effect of gas injection in gas condensate reservoir, optimal injection/production strategy in gas condensate reservoir, and also experimental design and response surface methodology applied in coupled CO_2 sequestration and enhanced hydrocarbon recovery in various types of reservoirs.

There are lots of studies associated to CO_2 injection into many types of reservoirs for both enhanced hydrocarbon recovery and CO_2 sequestration as follows:

Barrufet et al. [1] investigated the storage capacity for CO_2 sequestration of a depleted gas condensate reservoir and a saline aquifer. They found that the mass of CO_2 sequestration per volume in the equivalent aquifer model is approximately 13 times lower than that of the depleted gas condensate reservoir because of its low compressibility which allows more CO_2 storage capacity. They also suggested that over and above a certain CO_2 injection rate, it becomes meaningless to invest in bigger compressor to increase the rate in order to reduce the time of injection.

The evaluation of pressure maintenance schemes by adding gas to gas condensate reservoirs was introduced by Chaback and Williams [3]. The p-x behavior was studied by the use of a rich gas condensate with CO_2 and equi-molar mixture of N_2+CO_2 at 215 and 316 ^oF. The author revealed that addition of CO_2 can reduce the retrograde liquid formation than addition of N2+CO_2 at both temperatures. They also studied the re-vaporization process of retrograde liquid. CO_2 was significantly more effective than the mixed gases in re-vaporizing retrograde liquid.

Performance of CO_2 flooding using horizontal wells had been reported by Lim et al. [4]. Compositional simulator was used to simulate CO_2 flooding with WAG injection scheme using horizontal wells in oil reservoir by taking into account the important effects of phase behavior and mixings that are often neglected by many investigators. Sensitivity such as WAG ratio, Kv/Kh, well type combinations was studied. The results showed that the application of CO_2 flooding using horizontal wells significantly shortens project life which represents cost saving. They also

showed that the use of horizontal injectors in conjunction with vertical producers in a tertiary CO_2 WAG flood generally resulted in higher oil recovery.

Jikich et al. [5] studied Enhanced Gas Recovery (EGR) with CO_2 Sequestration by injecting CO_2 into a natural gas reservoir to investigate the amount of CO_2 sequestered and the effect of carbon dioxide on gas recovery using compositional reservoir simulator. Two injection scenarios were studied:

(1) CO_2 injection starts at the beginning of production

(2) Primary production of natural gas to the economic limit followed by injection of CO_2 for secondary gas recovery

The results showed that CO_2 injection after gas field abandonment is the best scenario. They also showed that using horizontal wells for CO_2 injection aids CO_2 storage but slightly lowers methane recovery and there is considerable increase in average CO_2 injectivity as injector length increases.

Sobers, Frailey, and Lawal [6] investigated the effects of phase behavior on the sequestration of CO_2 in depleted gas reservoirs (dry gas, wet gas, retrograde gas). By using the pressure temperature diagrams and two-phase flash calculation, it was found that Carbon Dioxide lowers the compressibility of all gas types. The results are favorable for CO_2 Sequestration because decreasing compressibility factor represents increasing storage capacity.

Ramcharack et al. [7] studied impact of Carbon Dioxide Sequestration in Gas/Condensate Recovery by conducting compositional reservoir simulation to study various CO_2-mixture injection combinations with sensitivity consisting of petrophysical parameters, injection rate, and heterogeneity. They found that more concentration of CO_2 mixed with reservoir fluid results in lower dew point pressure, lower compressibility factor and shrinking two-phase envelope and consequently more storage capacity for CO_2 is available underground. They also found that the ability for CO_2 to sweep the reservoir is compromised with the presence of reservoir heterogeneity which leads to deterioration of liquid recovery.

To complete the objective of this study, papers and studies related to Experimental Design and Response Surface Methodology were reviewed as follows:

Cheong et al. [8] presented the paper that investigates the feasibility of experimental design and analysis methods by using three examples including oil in

place equation, excel spreadsheet for oil in place, and multiple deterministic modelling of a fluvial reservoir-Mungaroo formation. It includes discussions and guidelines on how to select efficient design by using expert knowledge and a decision tree, and how the experimental response can be fitted accurately with the response surface method to develop a good surrogate equation.

Ghomian et al. [9] performed a reservoir simulation study to investigate enhanced oil recovery and sequestration of Carbon Dioxide. To meet both objectives, namely, CO_2 saturation and net present value of oil production, they studied a large number of parameters and the strategy used to flood the reservoir by Experimental Design and Response Surface Methodology. D-Optimal design was adopted because there is mixing of categorical and numerical factors as well as different levels of each factor that factorial design is unable to apply. The result has shown the optimum values of flood design parameters and optimum strategy obtained from response surface methodology to acquire the objective of maximizing hydrocarbon recovery together with maximizing CO_2 sequestered simultaneously. However, the cross-validation process is not presented in their study, leaving uncertainty on the applicability of their proxy model.

Another optimization of flood design parameters and strategy using Experimental Design and Response Surface Methodology was studied by Forooghi et al. [10]. The reservoir model was constructed using properties from a chalk reservoir. The sensitivity including injection scheme, type of wells, WAG ratio, and slug size was studied to see the effects on the first objective to maximize CO_2 stored and oil recovery while minimizing CO_2 production as the second objective with regard to economic consideration. The results showed that WASG (Water-alternating solvent gas injection) scheme is the best method beyond WAG injection and continuous CO_2 injection with horizontal producer and injector completed in the lower part of the reservoir. However, this study also presented no cross-validation process and then uncertainty on the generated model occurred as well.

The study of applying experimental design and response surface methodology into petroleum industry in Thailand was performed by Arunmongkol [11]. He studied the design optimization method of a horizontal well in a thin-oil-column reservoir in the Gulf of Thailand. Series of reservoir simulation models were conducted with

regard to experimental designs to screen out significant factors and subsequently to construct the proxy model in order to predict ultimate recovery factor of the candidate reservoirs. The model is checked by cross-validation experiments to see its applicability with statistical analysis called “matched pair t-test”. The results showed that the proxy model generated is able to screen out whether the candidate reservoirs have potential for horizontal well and also to predict ultimate recovery factor efficiently within the range of parameters used to construct the model.

CHAPTER III

THEORY AND CONCEPT

This chapter provides reviews of gas condensate reservoir, phase equilibrium, hydrocarbon production from gas condensate reservoir, CO_2 injection in gas condensate reservoir, effect of CO_2 injection on gas condensate reservoir, fundamental of experimental design and response surface methodology.

3.1 Review of Gas Condensate Reservoir

The type of reservoir fluids can be divided into five types: black oil, volatile oil, retrograde gas or gas condensate, wet gas and dry gas. Each type of reservoir fluids has unique characteristics in which the behavior of a reservoir fluid during production is determined by the shape of its phase diagram and the position of its critical point and therefore can be confirmed only by observation in the laboratory. However, it is committed to petroleum engineers to identify the type of their reservoir at the early stage of development. So, available characteristics used to identify the type of reservoir fluid are *initial producing gas oil ratio*, *gravity of the stock tank liquid*, *color of the stock tank liquid*, *oil formation volume factor*, and *mole fraction of hepthane plus*.

Gas condensate reservoir is one of the reservoirs which can be considered as the most complex reservoir. Initially, its condition begins with single phase gas. As the reservoir is depleted, the reservoir pressure will keep decreasing until it reaches the dew point pressure in which subsequently liquid starts to drop out of the gas.

3.1.1 Gas Condensate Behavior

Gas condensate or retrograde gas is one of the various types of reservoir fluid which has unique characteristics of phase diagram as illustrated in Figure 3.1.

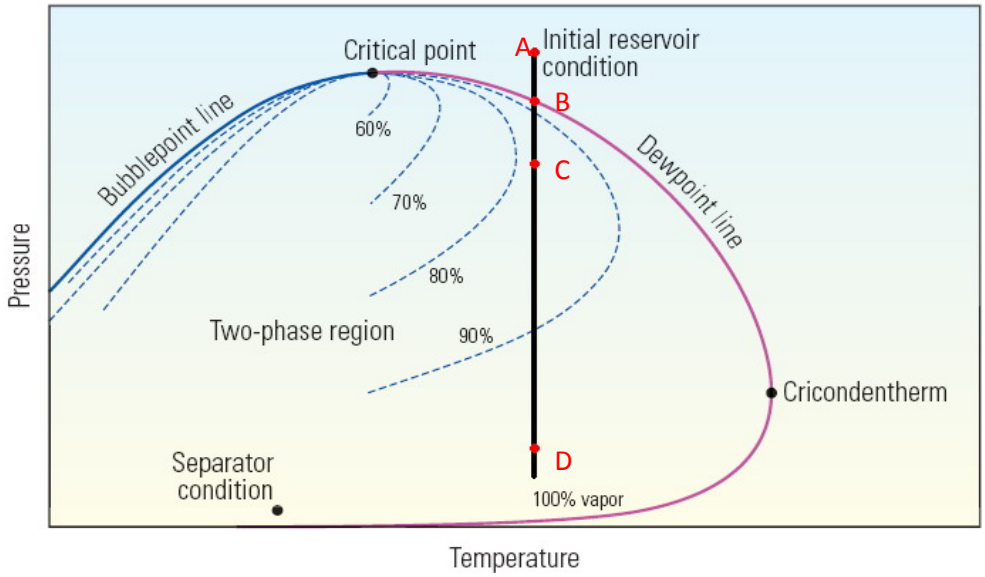

Figure 3.1: Constant composition phase diagram of a gas-condensate system (after Fan et al. [12])

The region of retrograde condensation takes place at temperatures between the critical temperature (T_C) and the cricondentherm, which is the maximum temperature above which liquid cannot be formed. Pressure-volume temperature (PVT) plot indicates single-phase behavior outside the two phase region, which is bounded by bubble point and dew point lines. In a gas-condensate reservoir, the initial reservoir condition starts with the single gas phase at point A. As the reservoir pressure is depleted, the pressure path moves down the dew point pressure at point B and therefore liquid starts to drop out of the gas. The percentage of vapor decreases with increasing liquid concentration as pressure declines from point B to C. The liquid dropout in the pore space will lead to the formation of a liquid phase and a resulting reduction in the gas production of the well together with loss of valuable heavy component hydrocarbon. This phenomenon continues until a point of maximum liquid volume is reached (point C). The liquid will re-vaporize as pressure continues declining from point C to D, yet this re-vaporization process due to pressure decline is typically below the economic life of the field, and this stage will not be reached in conventional production.

3.1.2 Regions around Gas Condensate Wellbores

The understanding of condensate formation during depletion is vital in gas condensate reservoir production. As described in previous section, when the reservoir pressure declines to the dew point pressure, liquid starts to drop out of the gas in the pore space and will jeopardize gas production. The fluid flow in gas condensate fields can be divided into three regions. The two regions near a producing well exist when the reservoir pressure is below the dew point pressure and the third region exists when the pressure is above the dew point pressure as shown in Figure 3.2.

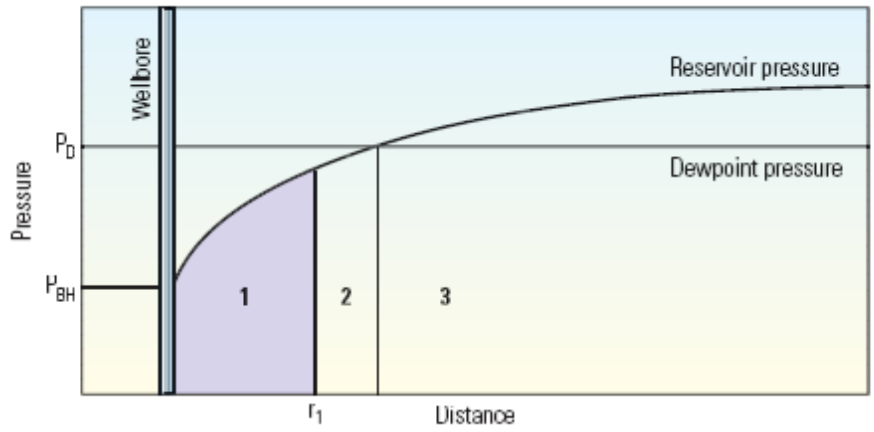

Figure 3.2: Three regions of gas condensate reservoir
(after Fan et al. [12])

Regions 1: This region is closest to a producing well in which both gas and condensate flow simultaneously at different velocities. The condensate saturation of this region is greater than the critical condensate saturation in which condensate starts to flow. The oil or condensate relative permeability increases with increasing condensate saturation while gas relative permeability decreases, which illustrates the blockage effect. Gas production suffers from restriction of condensate blockage. Less valuable heavy component is left in gas produced and it is more difficult to produce gas due to this effect.

Regions 2: In the second region, the reservoir pressure is below the dew point pressure. Liquid starts to drop out of the gas phase. The condensate saturation of this

region is less than the critical saturation. The condensate is adhered to rock surface due to interfacial tension. Hence, only gas phase is flowing.

Regions 3: This region is away from the producing well where only gas phase is present and flowing. Composition in this region is equal to the original reservoir gas.

To have insight into phase behavior and change of hydrocarbon composition within gas condensate reservoir, correlation for PVT properties of gas, dew point pressure determination, and two-phase equilibrium have to be considered.

3.1.3 Correlation for PVT Properties of Gas

Gas at low pressure which behaves as ideal gas is generally described by Charles's and Boyle's Law. The ideal gas law to relate pressure, volume, and temperature is as follows:

$$pV = nRT \tag{3.1}$$

where p = pressure (psia)
V = volume (ft^3)
n = number of pound moles
R = universal gas constant (ft^3.psia/lb-mol.°R)
T = absolute temperature (°R)

Equation 3.1 is unable to adequately describe the behavior of gas at moderate or high pressure which leads to inaccurate prediction for gas behavior because of the effect of bulk volume of gas compositions, molecules and intermolecular forces on volumetric behavior of gas. The compressibility factor or z factor is introduced to account for the deviation from ideal gas behavior. Definition of z factor is as follows:

$$z = \frac{volume\ of\ 1\ mole\ of\ real\ gas\ at\ p\ and\ T}{volume\ of\ 1\ mole\ of\ ideal\ gas\ at\ p\ and\ T} \tag{3.2}$$

Then, the correlation for real gas with the compressibility factor term is as follows:

$$pV = znRT \tag{3.3}$$

As a result, all volumetric properties of gas can be determined by using real-gas law as described in Equation 3.3

- Gas density calculation is given below

$$\rho_g = \frac{pM_g}{zRT} \tag{3.4}$$

where ρ_g = gas density (lb/ft^3)

M_g = apparent molecular weight of gas (lb/lb-mole)

- The gas isothermal compressibility is given below

$$\mathrm{c} = -\frac{1}{\mathrm{V_g}}\left(\frac{\partial \mathrm{V_g}}{\partial \mathrm{p}}\right)_{\mathrm{T}} = \frac{1}{\mathrm{p}} - \frac{1}{\mathrm{z}}\left(\frac{\partial \mathrm{z}}{\partial \mathrm{p}}\right)_{\mathrm{T}} \tag{3.5}$$

where c = isothermal compressibility (psi^{-1})

V_g = volume of gas (ft^3)

- Gas volume factor, *Bg*, is defined as the ratio of gas volume at specified *p* and *T* to the gas volume at standard conditions, which is given as follows:

$$B_g = \left(\frac{p_{sc}}{T_{sc}}\right)\frac{ZT}{p} \tag{3.6}$$

where p_{sc} = pressure at standard condition (psia)

T_{sc} = temperature at standard condition (°R)

For customary units (p_{sc} = 14.7 psia and T_{sc} = 520 °R), this is

$$B_g = 0.02827\frac{ZT}{p} \tag{3.7}$$

3.1.4 Dew Point Pressure Determination

As described previously, when the reservoir pressure drops to the dew-point pressure, the liquid starts to drop out of the single gas phase which will affect gas composition. Phase behavior is dependent on gas composition together with pressure and temperature. Therefore, dew point pressure determination is required for interpreting phase behavior.

Nemeth and Kenedy [13] proposed a correlation for calculating dew point pressure in gas condensate reservoir as follows:

$$\ln P_d = A_1\left[z_{CO_2} + z_{H_2S} + z_{C_6} + 2\left(z_{C_3} + z_{C_4}\right) + 0.4z_{C_1} + 0.2z_{N_2}\right] + A_2 z_{C_7} + \frac{A_3 z_{C_1}}{z_{C_1} + 0.002}$$

$$A_4 T + A_5\left(z_{C_{7+}} M_{C_{7+}}\right) + A_6\left(z_{C_{7+}} M_{C_{7+}}\right)^2 + A_7\left(z_{C_{7+}} M_{C_{7+}}\right)^3 + \frac{A_8 M_{C_{7+}}}{z_{C_{7+}} + 0.001}$$

$$A_9\left[\frac{M_{C_{7+}}}{z_{C_{7+}} + 0.001}\right]^2 + A_{10}\left[\frac{M_{C_{7+}}}{z_{C_{7+}} + 0.001}\right]^3 + A_{11} \qquad (3.8)$$

where

P_d	=	dew point pressure, psia	T	=	temperature, ^oR
Z	=	mole fraction of component	M	=	molecular weight
ρ	=	density, gm/ml	A_1	=	-2.0623054
A_2	=	6.6259728	A_3	=	$-4.4670559 \times 10^{-3}$
A_4	=	1.0448346×10^{-4}	A_5	=	3.2673714×10^{-2}
A_6	=	$-3.6453277 \times 10^{-3}$	A_7	=	7.4299951×10^{-5}
A_8	=	$-1.1381195 \times 10^{-1}$	A_9	=	6.2476497×10^{-4}
A_{10}	=	$-1.0716866 \times 10^{-6}$	A_{11}	=	1.0746622×10

3.2 Phase Equilibrium

Production in gas condensate reservoir is accompanied with variation of composition, temperature and pressure. This leads to change in fluid properties and also formation of new phase, namely, condensate or elimination of existing gas phase.

As changes in reservoir are often quite slow, it is reasonable to assume that all the co-existing phases, at any point in the reservoir, are in equilibrium. Equilibrium is a static condition which no changes occur in the macroscopic properties of a system with time. There are two methods commonly used to calculate the vapor-liquid equilibrium which are flash calculation and equation of state.

3.2.1 Flash calculation

Flash calculation is the simple calculation for two-phase equilibrium which involves solving simple material balance equations based on the separator condition in order to establish the phase compositions as well as amounts upon equilibrium of seperation.

Firstly, consider F moles of a hydrocarbon mixture of composition (z_i) entering a seperation unit. At the operating conditions of seperator, the mixture composition splits into L moles of liquid of component (x_i), and V moles of vapor of component (y_i). Then, by the law of conservation of mass:

$$F = L + V \tag{3.9}$$

and

$$Fz_i = Lx_i + Vy_i \tag{3.10}$$

The vapor liquid distribution coefficient, commonly known as the vapor liquid equilibrium ratio or the equilibrium vaporization ratio, K_i, is defined by

$$K_i = \frac{y_i}{x_i} \tag{3.11}$$

This quantity is known as the K-value for component i. The mole fractions of component i in liquid phase (x_i) and vapor phase (y_i) are given as

$$x_i = \frac{z_i}{\left[1 + \alpha\left(K_i - 1\right)\right]} \tag{3.12}$$

$$y_i = \frac{z_i K_i}{\left[1+\alpha\left(K_i - 1\right)\right]} \tag{3.13}$$

where $$\alpha = \frac{V(lb\ mole\ of\ the\ vapor\ leaving\ the\ separator)}{F(lb\ mole\ of\ the\ fluid\ stream\ entering\ the\ separator)} \tag{3.14}$$

3.2.2 Equations of State

Although the *K*-value approach is easily the most common representative of two-phase equilibrium, it manifests lack of generality and may result in inaccuracies of phase behavior prediction particularly near the convergence pressure. Convergence pressure is an important parameter used to determine liquid vapor equilibrium constants. Therefore, cubic equations of state (EOS's) are introduced for more efficient prediction on phase behavior and mixture composition. It is potentially able to work near the critical point and yield internally consistent densities and molar volumes. Cubic equations of state (EOS's) are simple equations relating pressure, volume, and temperature (PVT). They are able to accurately describe the volumetric and phase behavior of pure compounds and mixtures, hereby requiring only critical properties and acentric factor of each component. The equations can be employed to calculate the properties of all phases with consistency in reservoir processes that take critical conditions (miscible-gas injection and depletion of volatile-oil/gas-condensate reservoirs).

In 1873, Van Der Waals [14] introduced the first equation of state. The Van Der Waals EOS gives a simple, qualitatively accurate relation between pressure, temperature, and molar volume, as described by the equation below

$$p = \frac{RT}{v-b} - \frac{a}{v^2} \tag{3.15}$$

where a = "attraction" parameter

b = "repulsion" parameter

The Van Der Waals EOS was famously continued via so many researchers by modifying the denominator of repulsion term whereas the attraction term remains constant. The Redlich-Kwong [15] equation of state (RK EOS) has been most popular basis for developing new EOS's. Several modified Redlich-Kwong equations have found acceptance. Two popularly accepted equations of state in the petroleum industry are Redlich-Kwong (RK EOS) and Peng-Robinson (PR EOS).

Redlich-Kwong (RK EOS)

Redlich and Kwong [15] proposed an equation of state that includes temperature dependencies of the molecular attraction term as follows:

$$p = \frac{RT}{v-b} - \frac{a}{v(v+b)} \tag{3.16}$$

where

$$a = 0.42748 \frac{R^2 T_c^2}{p_c} \alpha(T_r)$$

$$b = 0.08664 \frac{RT_c}{p_c}$$

T_c = critical temperature (°R)

T_r = reduced temperature

p_c = critical pressure (psia)

p_r = reduced pressure

$\alpha\ (T_r) = T_r^{-0.5}$

Several attempts have been made to improve Volume/Liquid Equilibrium (VLE) predictions of the RK EOS by introducing a composition-dependent correction term α. Soave [16] used vapor pressures to determine the functional relation for the correction factor as follows:

$$\alpha = \left[1 + m(1 - T_r^{0.5})\right]^2 \tag{3.17}$$

$$m = 0.480 + 1.574\omega - 0.176\omega^2 \tag{3.18}$$

$$\omega = -(\log p_{vr} + 1) \quad at \ T_r = 0.7 \tag{3.19}$$

where α = 1 at critical temperature, ω is the Pitzer acentric factor for each pure substance and P_{vr} is the reduced vapor pressure

Peng-Robinson

Peng and Robinson [17] proposed a two-constant equation for improved EOS predictions and improved liquid density predictions which appears slightly different from other EOS in attraction term as shown below.

$$p = \frac{RT}{v - b} - \frac{a}{v(v + b) + b(v - b)} \tag{3.20}$$

where

$$a = 0.45724 \frac{R^2 T_c^2}{p_c} \alpha \tag{3.21}$$

$$b = 0.07780 \frac{RT_c}{p_c} \tag{3.22}$$

The values of α is obtained from

$$\alpha = \left[1 + m(1 - T_r^{0.5})\right]^2 \tag{3.23}$$

$$m = 0.37464 + 1.54226\omega - 0.26992\omega^2 \tag{3.24}$$

where α = 1 at critical temperature, ω is the Pitzer acentric factor for each pure substance

In summary, the equations of state (EOS) are used to calculate and describe the volumetric and phase behavior of gas condensate. Peng-Robinson EOS is employed in this study. Flash calculation is used to determine liquid and gas composition obtained from surface separator.

3.3 Hydrocarbon Production from Gas Condensate Reservoirs

Hydrocarbon from gas condensate reservoir can be recovered either by natural depletion or by gas injection which can be explained as follows:

(a) In natural depletion, the reservoir is produced and the liquid will later drop out of the single gas phase when the dew point pressure is reached. Condensate blockage occurs and consequently obstructs productivity of the reservoir.The condensate recovery factor of natural depletion is only 20~40% [18] as a result of this effect.

(b) Gas is injected into the reservoir for two main results. First, the reservoir pressure is to be maintained above the dew point in order to avoid condensate blockage and also prolong production life. Second, revaporization of condensate contents in the reservoir is achived by gas injection and therefore higher condensate recovery than that of natural depletion approach.

3.3.1 Miscible Fluid Displacement

The definition of miscible fluid displacement represents the displacement process in which no two-phase boundary exists between displacing fluid and displaced fluid. In this process, the displacing fluid will mix totally in all proportion with displaced fluid. The hydrocarbon recovery mechanism involved with miscible displacement comes from hydrocarbon viscosity reduction, vaporization of intermediate to heavy hydrocarbons (C_5-C_{30}), and development of multi-contact miscibility. These processes can be characterized into 4 types [19] as follows:

1.) High pressure gas injection
2.) Enriched gas injection
3.) LPG slug injection
4.) Alcohol slug injection

In this study, pure CO_2 injection which is classified as high pressure gas injection or vaporizing-gas miscible process is selected to achieve the objectives. Overview of this type of injection method is detailed by investigation on ternary diagram for hydrocarbon system.

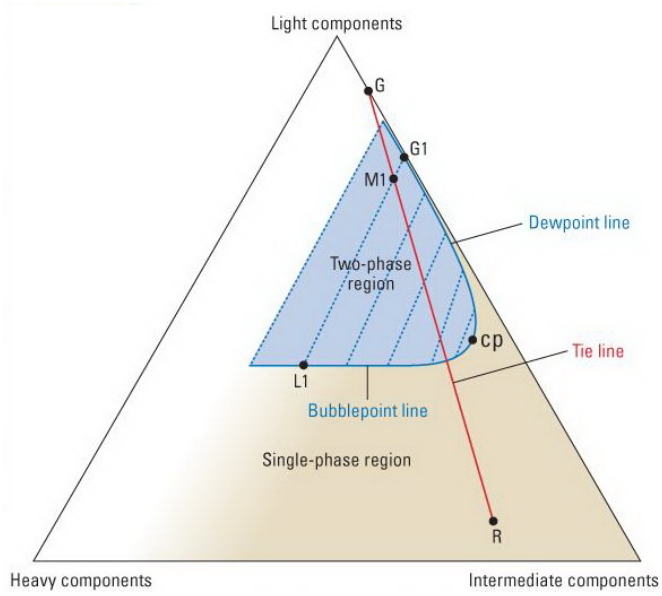

Figure 3.3: Ternary diagram for hydrocarbon system

Figure 3.3 represents the fundamental process of miscible hydrocarbon displacement by using ternary diagram for hydrocarbon process. The diagram is a visual representative of phase behavior of three components: light components (methane, inert gas), intermediate components (C_2-C_6), and heavy components (C_{7+}). The phase behavior of gases and liquids are function of pressure, temperature and composition which define the phase envelope enclosing all compositions that will split into two phases when brought to specific pressure and temperature. The region where two-phase exists is called two-phase region. The upper curve of the phase diagram defines the dew point curve, while the lower curve defines the bubble point curve. The dew point and bubble point curves join at the critical composition, cp. The tie lines represented by blue dashed lines in two-phase region show two-point connection between dew point curve or vapour curve and bubble point curve or liquid curve which account for equilibrium composition of gas and liquid. For high pressure gas injection or lean gas injection, the injected gas represented by point G comes to contact with reservoir oil which is rich in intermediate components (C_2-C_6)

represented by point R. The process is non-miscible by considering tie line between the two points which pass through two-phase region in which both gas and oil are not in equilibrium. Phase exchange takes place and then gas G takes intermediate components from oil R. Consequently, gas becomes richer with intermediate components and is represented by point G1 lying on dewpoint curve while oil becomes leaner and is represented by point L1 lying on bublepoint curve. Gas G1 will then comes to contact with original oil R and develop richer gas. Finally, the gas composition reaches critical composition (point cp) which is miscible with oil R. The miscible bank is subsequently formed and displacement by miscible process is achieved.

3.3.2 Minimum Miscibility Pressure

To achieve miscible condition between CO_2 injected and hydrocarbon gas in the reservoir, Minimum Miscibility Pressure (MMP) has to be achieved. MMP is the lowest pressure at which first-contact or multiple-contact miscibility can be achieved. At MMP, the interfacial tension is zero and no interface exists between the fluids or, in other word, single phase is achieved. Zero interfacial tension contributes to recovery of residual condensate trapped in the reservoir and consequently enhanced condensate recovery can be achieved by miscible CO_2 injection.

Therefore, determination of MMP for CO_2 injection should be done to achieve miscible injection though immiscible injection at pressure lower than MMP can also displaces hydrocarbon gas efficiently but better condensate recovery is gained if miscible condition occurs. Internal MMP-IOR report [20] suggested the correlations for MMP determination in gas condensate reservoir with CO_2 injection. It stated that the average of the three correlations; The Conquist correlation [21], the Glaso correlation [22], the Yuan *et al* correlation [23], was likely to estimate the CO_2 MMP with +/- 20% error within certain range of parameters (API Gravity 33-49 and temperature 71-250°F)

The three MMP correlations are as follows:

a.) The Cronquist Correlation

$$MMP_{pure\ CO2} = 15.988\ T^{X}\ \text{psi} \tag{3.26}$$

where T is the reservoir temperature (^oF) and

$X = 0.744206 + 0.0011038*MWC5P + 0.0015279*MPC1$

where MWC5P is the molecular weight of the pentanes plus heavier fraction

MPC1 is the mole percent of the methane plus nitrogen fraction

b.) The Glasø Correlation

$$MMP_{pure\ CO2} = 810.0 - 3.404\ M_{C7+} + (1.7E\text{-}9*U1*\exp(U_2))\ T \quad (3.27)$$

, for mol% $C_{2\text{-}6} \geq 18\%$

$$MMP_{pure\ CO2} = 2947.9 - 3.404\ M_{C7+} + (1.7E\text{-}9*U1*\exp(U_2))\ T - 121.2F_R \quad (3.28)$$

, for mol% $C_{2\text{-}6} < 18\%$,

where M_{C7+} is the molecular weight of the C_{7+} fraction,

$U_1 = (M_{C7+})^{3.730}$

$U_2 = 786.8\ M_{C7+}^{-1.058}$

T is the reservoir temperature (^oF) and F_R is the mol% of the $C_{2\text{-}6}$ fraction

c.) The Yuan *et al* Correlation

$$MMP_{pure\ CO2} = a_1 + a_2M_{C7+} + a_3P_{C2\text{-}6} + (a_4 + a_5M_{C7+} + a_6P_{C2\text{-}6} / M_{C7+}^2)\ T + (a_7 + a_8M_{C7+} + a_9M_{C7+}^2 + a_{10}P_{C2\text{-}6})\ T^2 \quad (3.29)$$

where M_{C7+} is the molecular weight of the C7+ fraction,

$P_{C2\text{-}6}$ is the mole percent of intermediate components (C_2-C_6)

a_1 - a_7 are coefficients as shown by Table 3.1

Table 3.1: Coefficients for Yuan *et al* correlation [23]

a_1	-1.4634E+03
a_2	6.6120E+00
a_3	-4.4979E+01
a_4	2.1390E+00
a_5	1.1667E-01
a_6	8.1661E+03
a_7	-1.2258E-01
a_8	1.2883E-03
a_9	-4.0152E-06
a_{10}	-9.2577E-04

As a result, the average MMP from these three correlations calculated in this study is 2,794.76 psia.

3.3.3 CO_2 Sequestration

In CO_2 sequestration aspect, the objective to store as much as amount of CO_2 is the primary goal. Physical properties of CO_2 are of importance to CO_2 storage underground. The properties prevail its density and viscosity, and thus its occupied volume and mobility which affect amount of CO_2 stored. Large volume change is associated with CO_2 phase change, so it is preferable to store CO_2 under physical condition that is not close to phase boundary to avoid unexpected volume and mobility changes [24]. Figure 3.4 shows CO_2 phase diagram.

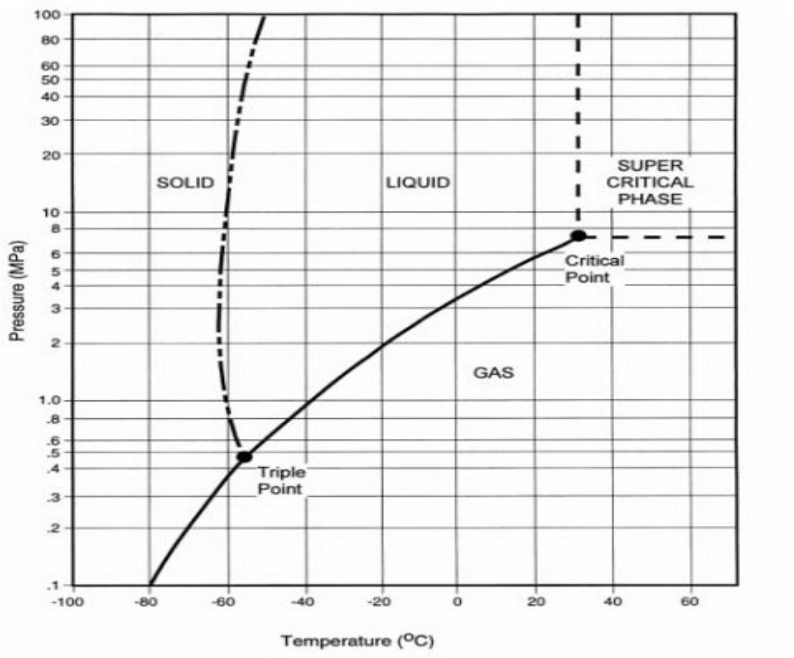

Figure 3.4: CO_2 phase diagram [25]

It can be seen from Figure 3.4 that CO_2 behaves as gas, liquid, solid or supercritical fluid depending on pressure and temperature. CO_2 will reach supercritical phase at certain temperature and pressure, temperature over 32°C or 90 °F and pressure over 7.8 MPa or 1,131 psia. Supercritical phase is the condition in which CO_2 behavior has both properties of gas and liquid at a temperature and pressure above its critical point, where distinct liquid and gas

phases do not exist. At this phase, CO_2 will travel and fill the shape of container easily like gas whereas it is dense like liquid to occupy much less volume required for available tiny pore spaces. Thus, it is desirable in CO_2 sequestration process to store CO_2 under supercritical phase or liquid CO_2. The large denser of CO_2 relative to in-situ gas means that CO_2 will migrate downward and occupies much less pore space in order to achieve as much as amount of CO_2 stored as the objective of this study. For example, one ton of liquid-CO_2 at a density of 785 kg/m^3 (i.e. 22°C and 7 MPa or 50°C and 15MPa) occupies 1.27 m^3,while at standard temperature and pressure, at the ground surface, one ton of CO_2 occupies 512 m^3[26]. Furthermore, the larger viscosity of CO_2 relative to in-situ gas stands for displacement of reservoir gas by CO_2 will be a favorable mobility ratio displacement with fewer inclination of gas fingering. CO_2 is denser and more viscous than hydrocarbon lean gas at all relevant conditions for gas reservoirs and CO_2 will generally be supercritical in deep depleted reservoirs with depth greater than 2600 feet [27].

3.3.4 CO_2 Dispersion

For CO_2 injection into gas condensate reservoir, the important issues involve the effect of miscible mixing of gases dominated by dispersion in a single phase flow as CO_2 displaces in-situ gas. The large volume and large extent of gas reservoirs may reduce efficiency of dispersion related to time scale or injection time. The efficiency of CO_2 injection in gas condensate reservoirs depends strongly on the phase behavior of mixtures of the gas with the liquid [27]. CO_2 is miscible with hydrocarbon gas. Components in the gas may dissolve in the condensate and in the water, while some components present in the condensate and some water transfer to the vapor phase.

An important parameter which reflects the amount of mixing between the displaced and displacing fluid is the width of the dispersion zone. The width of dispersion zone is the distance between the locations at which the CO_2 concentration is 0.1 and 0.9 mole fraction. The width of dispersion zone can be calculated from the correlation proposed by Shtepani [27].

$$x_{0.1} \_ x_{0.9} = 3.625\sqrt{K_l t} \tag{3.30}$$

K_l is the longitudinal dispersion coefficient, and t is time after CO_2 injection begins

This section should be included in case size of reservoir is varied to see its effect. However, this section is out of the scope of this study and is therefore not taken into account.

3.3.5 WAG (Water-Alternating Gas) injection

WAG or water- alternating gas injection is one type of injection schemes used in recovery process. It can be used as alternative method in place of pure gas injection. Its characteristic is different from continuous gas injection. Water is injected alternately with gas in order to control mobility ratio of gas injected for early breakthrough phenomena which results in poor sweep efficiency. Theoretically, water is denser than gas and has higher viscosity. Injected water will increases viscosity of gas or, in other words, reduces mobility of injected gas which prevents gas fingering detrimental to effective recovery process. WAG process is illustrated by Figure 3.5.

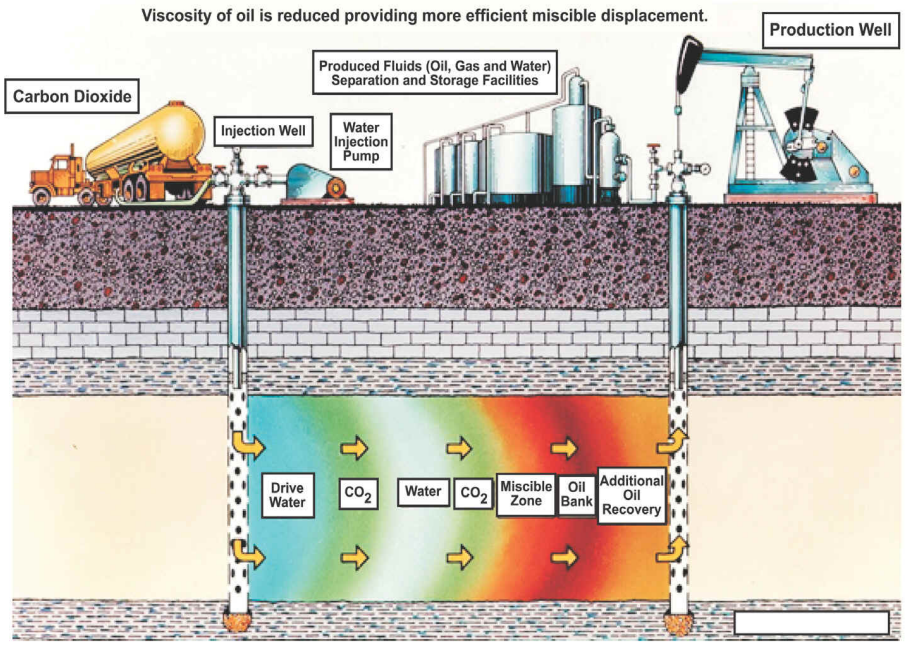

Figure 3.5: The Schematic of CO_2-WAG process [28]

Factors affecting WAG process

1. WAG ratio is a rate ratio of water to gas injected usually in the same unit. The unit can either be in reservoir condition (rb/day) or in standard condition (stb/day). The same rate of both water and gas or WAG ratio =1 is commonly taken for easy control. Since gas formation volume factor changes with reservoir pressure, it is difficult to control the process. It is thus recommended that down-hole rate (rb/day of water and gas) is used as controlling criteria.
2. Slug size is a period of one cycle for water and gas injection. Its unit is usually adopted in a month-duration. For example, 4-month slug size means that the water or gas injected first for 2 months and then the other is injected for 2 months in 1-WAG ratio basis. If 2-wag ratio is observed, it accounts for water injection for 2.67 months and then gas injection for 1.33 months as well.

3.4 Effect of CO_2 Injection on Gas Condensate Reservoir

Understanding of the effect of CO_2 injection on gas condensate reservoir is necessary. Ramcharak et al. [8] studied phase behavior and saturation pressure simulation for CO_2-gas condensate mixture as shown in Figure 3.6 and Figure 3.7.

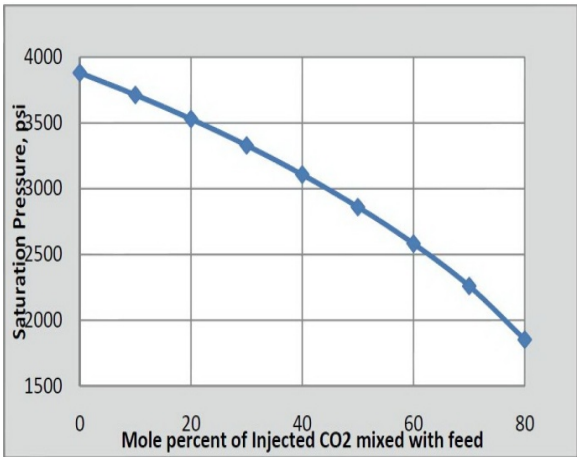

Figure 3.6: Effects of CO_2 mole percent on two-phase envelope for CO_2-gas condensate mixture (after Ramcharak et al. [8])

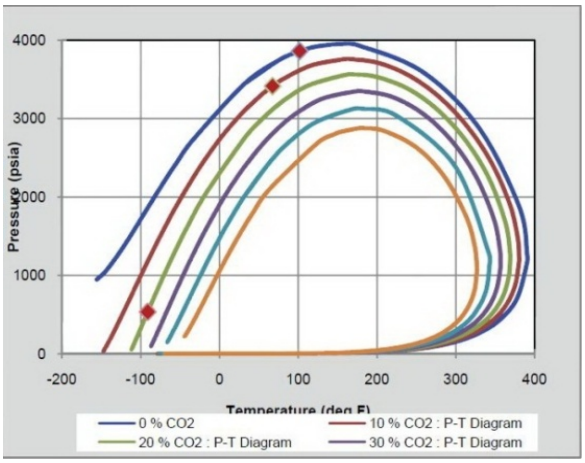

Figure 3.7: Effect of CO_2 concentration on saturation pressure of CO_2-gas mixture (after Ramcharak et al. [8])

The trends observed in Figure 3.6 show the relative "drying effect" of carbon dioxide, which is explained by the shrinking two-phase envelope as CO_2 concentration increases. The shrinking of the two-phase envelope indicates partial re-vaporization of the condensed liquid into the gaseous phase.

The effect is increasing with increasing CO_2 concentration. The trends of decreasing cricondenbar with increasing carbon dioxide indicate a tendency for liquid to move into its vapor phase easier. All these trends emphasize the "drying effect" of carbon dioxide. With regard to the objective of this study, more space becomes available with the recovery of the re-vaporized liquid and in-situ gas, thus allowing for more carbon dioxide to be sequestered and stored. Figure 3.7 illustrates the general trend of saturation pressure that decreases with increasing carbon dioxide concentration. This suggests that liquid drop-out occurs at lower pressures with increasing CO_2 concentration or conversely more reservoir fluid is in the gaseous phase. Their study also shows the predicted compressibility factor for the CO_2-gas condensate mixture. It was obviously observed that with increasing carbon dioxide concentration, the mixture compressibility factor decreases which also means that number of mole of mixture increases, thus allowing more CO_2 to be mixed with gas and stored in the pore spaces.

3.5 Fundamental of Experimental Design and Response Surface Methodology

3.5.1 Experimental Design

Experimental design is a statistical technique that consists of purposeful changes of the inputs (factors) to a process (3D geological model in this study) in order to observe the changes in the output (responses) (Montgomery [29]) as illustrated in Figure 3.8.

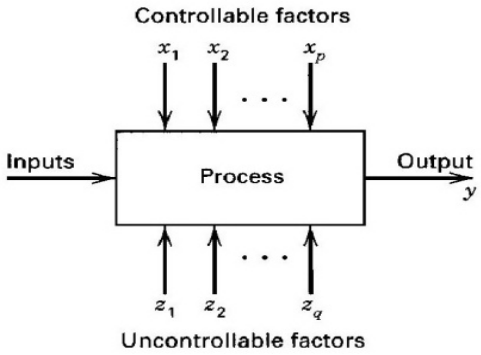

Figure 3.8: Process system (after Montgomery [29])

Experimental design is a strategy in which the input variables are varied simultaneously in a series of experimental runs according to a predefined pattern to obtain the experimental response. In other words, each experimental run will have a specific combination of input variable levels based on the design matrix. Then, the results will be analysed using statistical equation modelling methods, such as response surface equation modelling to extract the relationship between the input variables and the output response(s). The methodology ensures that precise conclusions can be achieved about the entire experiment with fewer runs. This allows obtaining the maximum information of a given process at a minimum procedure.

There are a number of experimental designs such as full factorial design, factorial design, Plackett-Burman design, Central Composite design, and D-Optimal design.

3.5.1.1 Overview of Types of Experimental Design

a) One variable at a time (OVAT)

This type of experimental design considers varying one variable while the other parameters are kept constant at a time. It can be illustrated by Figure 3.10. The effect of each factor is defined as a change in response produced by a variation in levels of that factor.

In two-level experimental design, levels of each factor which consist of low level and high level are represented by + and – referred to high level and low level respectively. If 3-factor experiment is considered, 0 will be added as a representative of mid level.

In Figure 3.9, effect of each factor is typically denoted by a capital letter of the factor concerned. For instance, "A" refers to main effect of factor A whereas "AB" refers to interaction effect of factor A and factor B. Interaction effect accounts for change in response due to variation of the factor considered at different levels of other factors, namely, all factors are varied together. For notation of factor combinations of an experimental run, two different methods are widely used. For the first method, a series of capital Latin letters stands for names of factors varied in individual experiments. Each name of factor is followed by superscript "-" and "+".

For example, A^-B^+ stands for experimental run at low level of factor A and high level of factor B. Alternatively, this combination can be expressed using the second method by the means that high level is represented by lower case letter whereas low level is represented by the absence of the corresponding letter. Therefore, A^-B^+ can be alternatively represented by "b".

It is obviously shown in Figure 3.10 that OVAT considers only main effect of each factor. For instance, main effect of A can be achieved as $A^+B^- - A^-B^-$ regardless of the values at high level of B. For the main effect of B, it can be attained in similar manners. This will cause erroneous interpretation if interaction effect of A and B is significant.

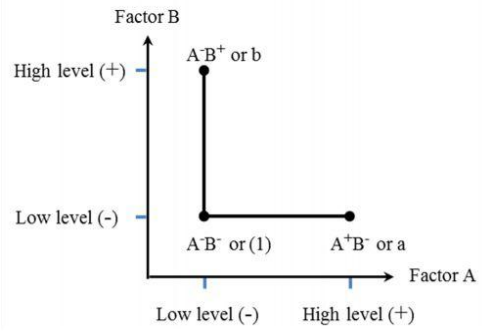

Figure 3.9: OVAT design with two factors conducted at two levels (after Montgomery [29])

b) Full factorial designs

The full factorial design is a common experimental design to study both main effects and interaction effects of various factors. This type of design consists of all possible combinations of low/high levels of all factors. All levels of several design factors are varied together as shown by Figure 3.10. If all factors have the same number of levels, the total number of combination runs can be calculated by L^k, where L is the number of levels of each factor and k is the number of factors. From the Figure 3.10, two estimates of main effect of A can be determined as $A^+B^+ - A^-B^+$ and $A^+B^- - A^-B^-$ and the average main effect of A is then calculated from two estimates standing for interaction effect by consideration on change of response between levels of factor A with varying levels of factor B simultaneously. The average main effect of factor B is to be determined in the same manners.

In conclusion, full factorial design is superior to OVAT due to its capability to take into account both main effect and interaction effect. Its results are more reasonable and reliable if interaction effects between factors exist and appear to be large.

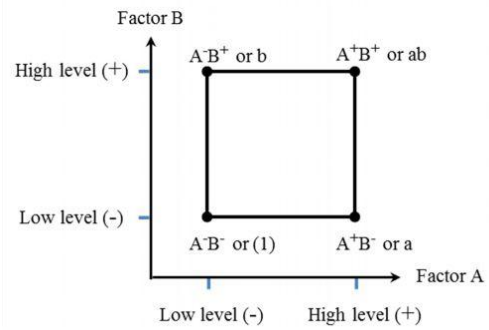

Figure 3.10: Full factorial design with two factors conducted at two levels (after Montgomery [29])

c) Fractional factorial designs

Even if full factorial design is useful on account for interaction effect involved and all possible combination runs, it requires a large number of experimental runs with increasing number of factors and increasing levels of factors which will cause time consuming and costly processes. Initially, the number of factors N with two-level design is small, represented by L^N runs, where L is level of each factor and N is number of factors, specified for a full factorial can quickly become very large with increasing L levels. For example, $2^6 = 64$ runs are required for a two-level, full factorial design with six factors. A three-level full factorial requires $3^6 = 729$ runs, which require large resources with only a modest number of factors. One solution to this problem is to use only a fraction of the runs specified by the fractional factorial design. Fractional factorial design is a portion of full factorial design in which a subset or portion of full factorial combinations is carefully chosen. For example, a 2^k full factorial design having 2^{k-p} runs is called a 1/p fraction of the 2^k design. This can be simply called 2^{k-p} fractional factorial design. Figure 3.11 shows comparison of 2^3 full factorial and 2^{3-1} fractional factorial design. Cube plot shows that fractional factorial design has only 4 experimental runs at the corner compared to 8 experimental runs of full factorial design.

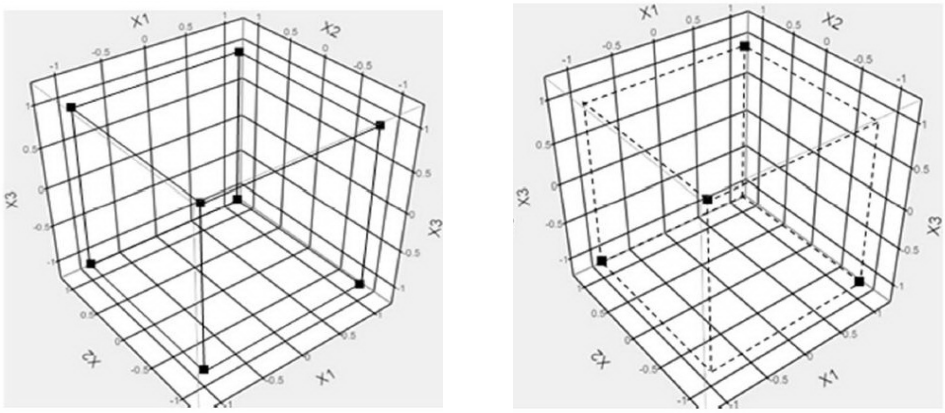

Figure 3.11: Comparison of (a) 2^3 full factorial and (b) 2^{3-1}fractional factorial design (after United States Department of Commerce, NIST/SEMATECH [30])

Even though the number of experimental runs decreases as 'p' increases, the ability to differentiate among the factors decreases because more factors are aliased. Aliases or confounding is the condition that it is impossible to differentiate two effects, which can be either main effect or interaction effect. For example, main effect of factor X_1 and X_2X_3 interaction effect are aliased which can be denoted by $[X_1] = [X_2X_3]$. In fact, when we estimate either X_1 or X_1X_2 we are really estimating $X_1+X_2X_3$ which can be denoted by $X_1 \rightarrow [X_1+X_2X_3]$.

To differentiate effects between factors, resolution of design is introduced with the basis that fractional factorial design should be performed with highest possible resolution to reduce the effects of aliases and to meet current resources of experiments. The higher the resolution, the less significant the interaction effects are, and precise interpretation of the data is consequently obtained. The definition of design resolution is so important and 2-level design resolution is herein described below:

1.) Resolution III designs: these are the designs in which no main effects are aliased with each other main effect, but main effects are aliased with two-factor interaction effects and two-factor interaction effects are aliased with each other. The 2^{3-1} design is of resolution III.

2.) Resolution IV designs: these are the designs in which no main effects are aliased with each other main effect or two-factor interaction effects

whereas two-factor interaction effects are aliased with each other. The 2^{4-1} design is of resolution IV.

3.) Resolution V designs: these are the designs in which no main effects or two-factor interaction effects are aliased with each other main effect or two-factor interaction effects, but two-factor interaction effects are aliased with three-factor interaction effects. The 2^{5-1} design is of resolution V.

d) Plackett-Burman designs

Plackett-Burman (PBD) designs are very economical two-level designs where the number of runs is a multiple of 4 rather than a power of 2 as in the case of full factorial design. They are known to be very efficient screening designs when only main effects are of interest.

e) Central composite designs

It is a 3-level experimental design which is suitable to generate the proxy model for optimization purpose of the model studied. A central composite design (CCD) contains an imbedded factorial or fractional factorial design with center points and is augmented with a group of "star points" that allow estimation of curvature, suitable to the process expected to have curvature responses. If the distance from the center of the design space to a factorial point is ±1 unit for each factor, the distance from the center of the design space to a star point is ±α with $|\alpha| >= 1$. The precise value of α depends on certain properties desired for the design and on the number of factors involved. There are 3 types of central composite designs which are circumscribed central composite designs (CCC) – $\alpha > 1$, inscribed central composite designs (CCI) – $\alpha = \pm 1$, and face-centered central composite designs (CCF) - $\alpha = \pm 1$. Figure 3.13 illustrates the face-centered central composite designs (CCF).

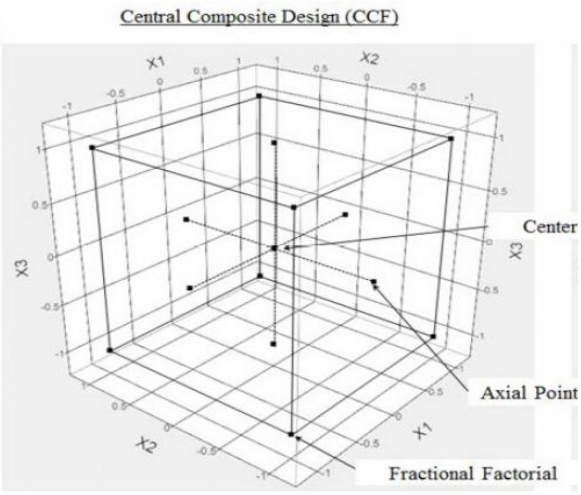

Figure 3.12: Face-centered Central Composite Design (CCF)
(after United States Department of Commerce, NIST/SEMATECH [30])

f) D-Optimal

D-optimal designs selected as a tool in this study are one form of design provided by a computer algorithm. These types of computer-aided designs are particularly useful when conventional designs do not apply. Unlike standard classical designs such as factorials fractional factorials or Central composite design, D-optimal design matrices are usually not orthogonal and effect estimates are correlated. These types of designs are always an option regardless of the type of model the experimenter wishes to fit or the objective specified for the experiment. The 'optimality' of a given D-optimal design is model dependent. That is, the experimenter must specify a model for the design before a computer can generate the specific combinations. From a set of points (e.g. a full-factorial set), an initial subset is selected according to the number of combinations desired. The methodology then iteratively exchanges design points for candidate points in an attempt to reduce the variance of the coefficients that would be estimated using this design. The reasons for using D-optimal designs instead of standard classical designs generally fall into two categories:

1. Standard factorial or fractional factorial designs require too many runs for the amount of resources or time allowed for the experiment
2. The design space is constrained (the process space contains factor setting that is not feasible or are impossible to run)

Figure 3.13 shows D-optimal design with three factors in which 3-level and 2-level factors are considered together.

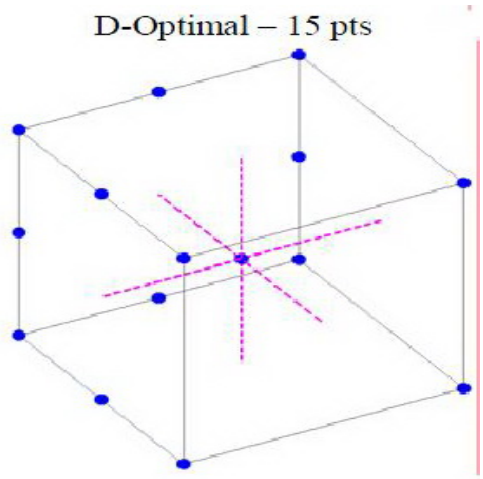

Figure 3.13: D-Optimal design with three factors
(after Yeten et al. [31])

In summary, D-Optimal design is used in this study because of its ability to deal with the process space containing factors settings that are not feasible to run by other designs (categorical factors combined with numerical factors). The design points are randomly generated from pre-defined factors and then iteratively exchanged. JMP software that is a statistical tool is used to do experimental design in this study.

3.5.2 Response Surface Methodology

Response surface methodology (RSM) explores the relationship between various variables and one or more response variables. The main idea of RSM is to use a set of designed experiments to obtain an optimal response. A response surface or a proxy model is a representation of a real system or its simulation. A response surface is constructed using regression line method with least square technique. Idea of least square technique is to minimize the vertical deviation between actual (observed) and estimated values of responses for efficient model fitting as illustrated by Figure 3.14.

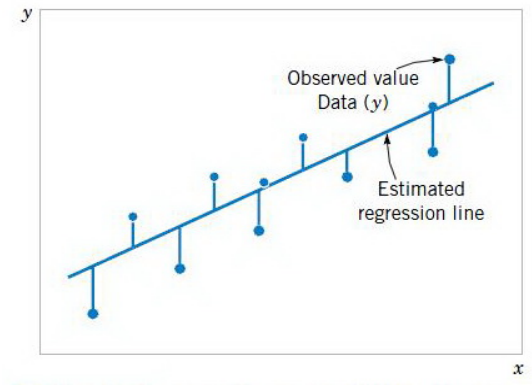

Figure 3.14: Scatter plot of observed values and estimated regression line (after Montgomery and Runger [32])

Then the regression or proxy model equation is constructed to acquire coefficients in order to fit the observed values of data with regression line as much as possible. Consider a system (Figure 3.8) in which output response variable y is a function of multiple input parameters x_i, i=1, 2,…, n

$$y = f(x_1, x_2, ..., x_n) + \varepsilon \tag{3.31}$$

Here, ε represents the random error, which has an independent normal distribution with zero expectation and uniform variance. The expected value $E(y) = f(x_1, x_2, ..., x_n)$ is called a response surface (RS). The most common models fit to the experimental data are either *linear* or *quadratic*.

A *linear model* with two factors, X_1 and X_2, can be written as

$$Y = \beta_0 + \beta_1 X_1 + \beta_2 X_2 + \beta_{12} X_1 X_2 + \varepsilon \tag{3.32}$$

Here, Y is the response for given levels of the main effects X_1 and X_2, and the X_1X_2 term is included to account for a possible interaction effect between X_1 and X_2. The constant β_0 is the response of Y when both main effects are 0.

For a more complicated example, a linear model with three factors X_1, X_2, X_3 and one response, Y, would look like

$$Y = \beta_0 + \beta_1 X_1 + \beta_2 X_2 + \beta_3 X_3 + \beta_{12} X_1 X_2 + \beta_{13} X_1 X_3 + \beta_{23} X_2 X_3 + \beta_{123} X_1 X_2 X_3 + \varepsilon \quad (3.33)$$

A second-order (quadratic) model adds three more terms to the linear model.

$$\beta_{11} X_1^2 + \beta_{22} X_2^2 + \beta_{33} X_3^2 \quad (3.34)$$

CHAPTER IV

RESEARCH METHODOLOGY

In this chapter, methodology is detailed step by step according to the outlined methodology in Chapter I in order to show the overall processes of this study. There is also description of reservoir model provided herein.

4.1 Statement of Objective and Response Factor

The main objective to perform experimental design is for modeling and optimization in accordance with research objectives of this study. Modeling objective is meant to be the representative of simulation process with good-fitting mathematical functions whereas optimization objective is to determine optimal level of each factor which leads to maximum response.

Condensate recovery factor and amount of CO_2 stored are selected as the two response factors because maximization of these two responses meets the research objective of this study. Equally weighted combination of these two response factors are set as the optimization criteria.

4.2 Selection of Parameter and Strategy Factors

There have been extensive studies on CO_2 injection into gas/gas condensate reservoirs for coupled CO_2 sequestration and enhanced condensate recovery. Each of these studies has investigated different aspects such as storage capacity for CO_2 sequestration of gas condensate reservoir [1], phase behavior study [7], engineering design [9], laboratory study to come up with CO_2 dispersion [27], and simulation on miscibility mechanism [33]. In this study, we focus on flood design parameters and strategies for coupled CO_2 sequestration and enhanced condensate recovery by using compositional numerical simulation.

Investigated parameters and strategies are as follows:

Permeability: Permeability plays a vital role in how much fluid is able to channel through the reservoir. Thus, it affects coupled CO_2 sequestration and enhanced condensate recovery. High permeability reservoir will delay condensate recovery because CO_2 will travel away from the injector all over the reservoir. So, more time is needed for CO_2 to flood hydrocarbon which will reflect the project economic in spite of high recovery at the end of production. There is in turn longer time for the reservoir pressure to reach fracture pressure, leading to more CO_2 stored in the pore space. On the other hand, low permeability reservoir provides higher condensate recovery at the early time but finally lower overall recovery is achieved due to rapid pressure decrease. Additionally, low permeability reservoir will impede the flow of CO_2 away from the injector, leading to low amount of CO_2 that can be stored. Hence, sensitivity analysis on the effect of permeability should be performed in which potential candidates are suggested for coupled CO_2-ECR project.

Injection Rate: Injection rate is one of the important flood design parameters for coupled CO_2-ECR project. Low injection rate will take longer to pressurize the reservoir and also early CO_2 breakthrough is prevented, leading to fairly high condensate whereas amount of CO_2 stored will suffer from low injection rate due to low amount of CO_2 injected into the reservoir. On the other hand, high injection rate will endanger condensate recovery due to early CO_2 breakthrough while enhancing the amount of CO_2 being injected and stored. Additionally, the effect of this parameter varies with other parameters such as permeability. For example, high injection rate in low permeability reservoir will reduce amount of CO_2 stored because fracture pressure is rapidly reached while high injection rate in high permeability reservoir will result in considerably much more amount of CO_2 stored because CO_2 is able to easily channel through the pore space and consequently fracture pressure is not reached too early.

Production/Injection Well Type: There are two common types of wells: vertical well and horizontal well. Horizontal well is physically known that it has higher contact area against the reservoir than that of a vertical well. So, a horizontal well can greater draw reservoir fluid. Therefore, a horizontal well can shorten the project life and consequently improves project economics in spite of its higher investment cost over a vertical well. In some circumstances, using combination of

horizontal and vertical wells as producers and injectors will result in better injection and production performance. However, placing a horizontal well at a proper location: top or bottom of the reservoir, is of concern to be investigated so that maximum well performance will be attained.

Well Spacing: Optimization of well spacing should be involved in coupled CO_2-ECR project. Smaller well spacing will lead to accelerated condensate recovery, contributing to the economics of project whereas low amount of CO_2 occurs due to early CO_2 breakthrough. On the other hand, larger well spacing would lead to a longer time required to sweep the reservoir, leading to poor economics but the amount of CO_2 stored is enhanced because there is more pore space available for CO_2 to be stored.

Injection Time: To fulfill the objectives of this study (maximum condensate recovery factor and maximum amount of CO_2 stored), injection at different times has to be considered: injection at initial point of production or initial injection, injection at dew point pressure, and injection after the reservoir is depleted. Condensate recovery can be obtained either from vaporized condensate by CO_2 injection or from re-pressurization. Injection at initial point of production will sustain the reservoir pressure to be above the dew-point pressure, so no condensate dropout occurs in which obtained condensate recovery is totally separated from gas produced. However, injection at the beginning will cause a lot of CO_2 to be produced with reservoir gas, and subsequently impaired condensate recovery is inflicted together with impaired amount of CO_2 stored since the fracture pressure is rapidly reached. On the other hand, injection at dew point pressure can prolong the plateau rate due to pressure maintenance above the dew-point pressure and lower CO_2 to be produced, compared to initial injection case. More amount of CO_2 can be stored due to more condensate recovery and more available pore spaces as well as longer time for fracture pressure to be reached. Finally, injection at depleted condition provides a large amount of pore space for CO_2 to be stored since a lot of hydrocarbon gas is produced prior to injection and condensate which was left in the reservoir will be re-vaporized by CO_2. Therefore, more CO_2 can be stored and more condensate recovery is obtained from re-pressurization and re-vaporization mechanisms. However, prolonged plateau rate of gas production is lost unlike injection at dew point pressure case, resulting in overall

low condensate recovery. Hence, sensitivity analysis on this factor should be performed for gaining maximum objective functions.

Injection Scheme: Injection of pure CO_2 is able to cause early CO_2 breakthrough due to its high mobility which will cause lower condensate recovery and lower storage. WAG injection of CO_2 has been proven to increase sweep efficiency but this type of injection scheme would deteriorate the total amount of CO_2 injected, causing lower stored CO_2. On the other hand, injection of pure CO_2 results in higher volume of CO_2 injected into the reservoir, leading to increasing amount of retained CO_2. Determination of efficient injection scheme for CO_2-ECR project is therefore crucial.

In addition to aforementioned parameters and strategies, one of the parameters to be considered in this study is vertical to horizontal permeability ratio. It is also investigated to account for the reservoir heterogeneity effect on coupled CO_2-ECR project.

In summary, aforementioned parameters and strategies are chosen from a large number of parameters used in CO_2-ECR project. Table 4.1 represents sensitivity table of parameters and strategies with levels of each factor for investigation on the uncertainties of all considered factors.

Table 4.1: Sensitivity table of parameters and strategies with levels of each factor

Parameters & Strategies	**Min**	**Mid**	**Max**
Permeability (md)	10	505	1000
Injection rate (Mscf/D)	4000	8000	12000
Injection well type	Vertical	Horizontal at bottom	Horizontal at top
Well spacing	Half spacing	Two-third spacing	Full spacing
Injection time	Initial	Dew point	Depleted
Production well type	Vertical	-	Horizontal at top
Injection scheme	WAG	-	Continuous CO_2
kv/kh	0.01	0.505	1.0

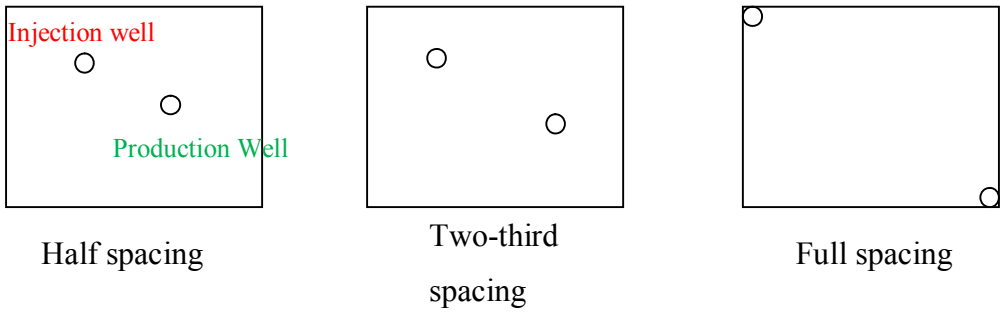

Half spacing Two-third spacing Full spacing

Figure 4.1: Top view-3 types of well spacing used in this study

Note a) Definition of ratio of well spacing is demonstrated by Figure 4.1. Spacing is a relative length to diagonal distance of the area.

b) "Horizontal at top" means the horizontal well is located at the top part of the reservoir while "Horizontal at bottom" means the horizontal well is located at the bottom part of the reservoir. Figure 4.2 illustrates location of injection well at bottom part and location of production well at top part.

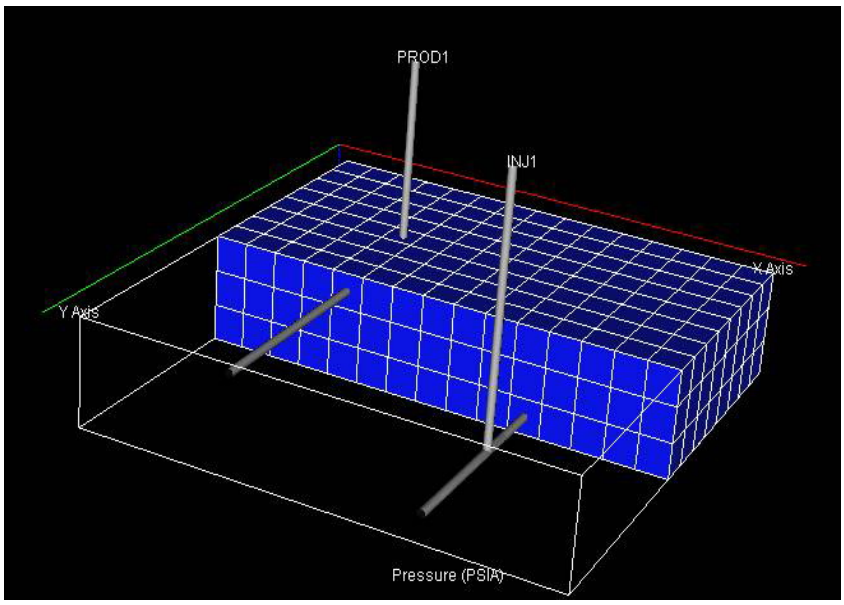

Figure 4.2: Location of horizontal injection well at the bottom part and location of horizontal production well at the top part of the reservoir

c) For injection time, "Initial" means injection starts at initial pressure, "Dew point" means injection starts when dew-point pressure is reached, and "Depleted" means injection starts when the economic limit is reached.

d) For WAG injection, WAG ratio = 1 and slug size = 2 months is used as a controlling criteria.

Experimental Design and Response Surface Methodology is proved to be a useful tool to perform a large amount of sensitivity cases with less effort and time consumption. In addition, the optimal parameters and strategies for maximizing two response factors can be obtained.

4.3 Experimental Design

Sensitivity study of all 8 parameters & strategies pre-defined in Section 4.2 will be performed by conducting experimental design. As described in Section 3.5, full factorial design includes all possible combinations of all parameters and strategies but with exhaustive resources because it will take $3^3*2^5 = 864$ cases to perform. Other

experimental designs are therefore considered to save cost and time. These designs include fractional factorial design, Plackett-Burman design, Central Composite design and D-optimal design.

Owing to mixed combinations between numerical factors (permeability, injection rate, kv/kh) and categorical factors (production well type, injection well type, well spacing, injection time and injection scheme), D-optimal design is selected. D-optimal design can deal with mixed combination between numerical factors and categorical factors whereas other designs are not able to do that. D-optimal design for all 8 factors is conducted by using statistical software 'JMP'. JMP is a versatile software for all statistical aspects. The software is able to perform Experimental Design, Response Surface Methodology, ANOVA analysis, Matched paired t-test analysis, and other statistical analyses. Interaction effects and quadratic effects are added into the design to account for response surface methodology for effective fitting of the model. Table 4.2 shows 96-case experiments provided by JMP.

Table 4.2: 96-case experiments provided by JMP

Run ID	Sensitivity Table							
	Permeability (md)	Injection rate (Mscf/D)	Injection well type	Well spacing	Injection time	Production well type	Injection scheme	kv/kh
1	10	4000	Horizontal at bottom	Full diagonal	Dew point	Vertical	WAG	0.505
2	10	4000	Horizontal at bottom	Half diagonal	Depleted	Horizontal at top	Continuous CO_2	1
3	10	4000	Horizontal at bottom	Two-third diagonal	Dew point	Horizontal at top	Continuous CO_2	0.01
4	10	4000	Horizontal at bottom	Two-third diagonal	Initial	Vertical	WAG	1
5	10	4000	Horizontal at top	Full diagonal	Dew point	Horizontal at top	Continuous CO_2	0.01
6	10	4000	Horizontal at top	Full diagonal	Initial	Vertical	WAG	0.01
7	10	4000	Horizontal at top	Half diagonal	Depleted	Horizontal at top	WAG	0.01
8	10	4000	Horizontal at top	Half diagonal	Dew point	Vertical	WAG	1
9	10	4000	Horizontal at top	Half diagonal	Initial	Vertical	Continuous CO_2	0.505
10	10	4000	Horizontal at top	Two-third diagonal	Depleted	Vertical	WAG	1
11	10	4000	Horizontal at top	Two-third diagonal	Initial	Horizontal at top	Continuous CO_2	1

Table 4.2: 96-case experiments provided by JMP (continued)

12	10	4000	Vertical	Full diagonal	Depleted	Horizontal at top	WAG	0.01
13	10	4000	Vertical	Full diagonal	Depleted	Vertical	WAG	1
14	10	4000	Vertical	Full diagonal	Initial	Horizontal at top	Continuous CO_2	1
15	10	4000	Vertical	Half diagonal	depleted	Vertical	Continuous CO_2	0.01
16	10	4000	Vertical	Half diagonal	Initial	Vertical	WAG	0.505
17	10	4000	Vertical	Two-third diagonal	Dew point	Horizontal at top	WAG	0.505
18	10	4000	Vertical	Two-third diagonal	Initial	Vertical	Continuous CO_2	0.01
19	10	8000	Horizontal at bottom	Full diagonal	Depleted	Vertical	Continuous CO_2	0.01
20	10	8000	Horizontal at bottom	Full diagonal	Initial	Horizontal at top	Continuous CO_2	0.505
21	10	8000	Horizontal at bottom	Half diagonal	Initial	Horizontal at top	WAG	1
22	10	8000	Horizontal at top	Full diagonal	Depleted	Horizontal at top	WAG	0.505
23	10	8000	Horizontal at top	Two-third diagonal	Initial	Horizontal at top	WAG	0.505
24	10	8000	Vertical	Half diagonal	Dew point	Horizontal at top	Continuous CO_2	0.505
25	10	8000	Vertical	Two-third diagonal	Dew point	Vertical	Continuous CO_2	1
26	10	12000	Horizontal at bottom	Half diagonal	Dew point	Horizontal at top	WAG	0.01
27	10	12000	Horizontal at bottom	Half diagonal	Dew point	Vertical	Continuous CO_2	1
28	10	12000	Horizontal at bottom	Two-third diagonal	Depleted	Vertical	WAG	0.01
29	10	12000	Horizontal at bottom	Two-third diagonal	Dew point	Horizontal at top	WAG	1
30	10	12000	Horizontal at bottom	Two-third diagonal	Initial	Horizontal at top	Continuous CO_2	0.505
31	10	12000	Horizontal at top	Full diagonal	Depleted	Horizontal at Top	Continuous CO_2	1
32	10	12000	Horizontal at top	Full diagonal	Initial	Vertical	Continuous CO_2	1
33	10	12000	Horizontal at top	Half diagonal	Depleted	Vertical	WAG	0.505
34	10	12000	Horizontal at top	Half diagonal	Initial	Horizontal at Top	Continuous CO_2	0.01
35	10	12000	Horizontal at top	Two-third diagonal	Dew point	Vertical	Continuous CO_2	0.01
36	10	12000	Vertical	Full diagonal	Dew point	Vertical	WAG	0.01
37	10	12000	Vertical	Two-third diagonal	Depleted	Horizontal at Top	Continuous CO_2	0.505

Table 4.2: 96-case experiments provided by JMP (continued)

38	10	12000	Vertical	Two-third diagonal	Initial	Horizontal at Top	WAG	0.01
39	505	4000	Horizontal at bottom	Half diagonal	Dew point	Vertical	Continuous CO_2	0.505
40	505	4000	Horizontal at bottom	Half diagonal	Initial	Horizontal at top	Continuous CO_2	0.01
41	505	4000	Horizontal at top	Full diagonal	Depleted	Vertical	Continuous CO_2	0.505
42	505	4000	Horizontal at top	Full diagonal	Initial	Horizontal at top	WAG	1
43	505	4000	Vertical	Two-third diagonal	Dew point	Vertical	WAG	0.505
44	505	8000	Horizontal at bottom	Full diagonal	Dew point	Horizontal at top	Continuous CO_2	1
45	505	8000	Horizontal at bottom	Half diagonal	Depleted	Vertical	WAG	0.505
46	505	8000	Horizontal at bottom	Two-third diagonal	Depleted	Horizontal at top	WAG	0.505
47	505	8000	Horizontal at bottom	Two-third diagonal	Initial	Vertical	Continuous CO_2	0.01
48	505	8000	Horizontal at top	Full diagonal	Dew point	Vertical	Continuous CO_2	0.505
49	505	8000	Horizontal at top	Half diagonal	Initial	Vertical	WAG	1
50	505	8000	Horizontal at top	Two-third diagonal	Depleted	Horizontal at top	Continuous CO_2	0.01
51	505	8000	Horizontal at top	Two-third diagonal	Dew point	Horizontal at top	WAG	0.01
52	505	8000	Vertical	Full diagonal	Depleted	Horizontal at top	Continuous CO_2	0.505
53	505	8000	Vertical	Half diagonal	Dew point	Vertical	WAG	0.01
54	505	12000	Horizontal at bottom	Full diagonal	Depleted	Vertical	WAG	1
55	505	12000	Horizontal at bottom	Full diagonal	Initial	Horizontal at top	WAG	0.01
56	505	12000	Horizontal at bottom	Two-third diagonal	Depleted	Vertical	Continuous CO_2	1
57	505	12000	Horizontal at top	Half diagonal	Dew point	Horizontal at top	Continuous CO_2	1
58	505	12000	Vertical	Full diagonal	Initial	Horizontal at top	Continuous CO_2	0.01
59	505	12000	Vertical	Half diagonal	Depleted	Horizontal at top	WAG	1
60	505	12000	Vertical	Half diagonal	Initial	Vertical	Continuous CO_2	0.01
61	505	12000	Vertical	Two-third diagonal	Initial	Vertical	WAG	1
62	1000	4000	Horizontal at bottom	Full diagonal	Depleted	Horizontal at top	Continuous CO_2	1
63	1000	4000	Horizontal at bottom	Full diagonal	Dew point	Horizontal at top	WAG	0.01

Table 4.2: 96-case experiments provided by JMP (continued)

64	1000	4000	Horizontal at bottom	Full diagonal	Initial	Vertical	Continuous CO_2	1
65	1000	4000	Horizontal at bottom	Half diagonal	Depleted	Vertical	WAG	0.01
66	1000	4000	Horizontal at bottom	Half diagonal	Dew point	Horizontal at Top	WAG	1
67	1000	4000	Horizontal at bottom	Two-third diagonal	Depleted	Vertical	Continuous CO_2	0.505
68	1000	4000	Horizontal at bottom	Two-third diagonal	Initial	Horizontal at top	WAG	0.505
69	1000	4000	Horizontal at top	Half diagonal	Depleted	Horizontal at top	WAG	0.505
70	1000	4000	Horizontal at top	Half diagonal	Dew point	Vertical	Continuous CO_2	0.01
71	1000	4000	Horizontal at top	Two-third diagonal	Dew point	Horizontal at top	Continuous CO_2	1
72	1000	4000	Horizontal at top	Two-third diagonal	Initial	Vertical	WAG	0.01
73	1000	4000	Vertical	Full diagonal	Dew point	Vertical	Continuous CO_2	0.01
74	1000	4000	Vertical	Half diagonal	Depleted	Horizontal at top	Continuous CO_2	0.505
75	1000	4000	Vertical	Half diagonal	Initial	Vertical	Continuous CO_2	1
76	1000	4000	Vertical	Two-third diagonal	Depleted	Horizontal at top	WAG	1
77	1000	8000	Horizontal at bottom	Two-third diagonal	Dew point	Vertical	WAG	0.505
78	1000	8000	Horizontal at top	Full diagonal	Dew point	Vertical	WAG	1
79	1000	8000	Horizontal at top	Full diagonal	Initial	Horizontal at top	Continuous CO_2	0.01
80	1000	8000	Horizontal at top	Half diagonal	Depleted	Vertical	Continuous CO_2	1
81	1000	8000	Vertical	Full diagonal	Initial	Vertical	WAG	0.505
82	1000	8000	Vertical	Half diagonal	Initial	Horizontal at top	WAG	0.01
83	1000	8000	Vertical	Two-third diagonal	Initial	Horizontal at top	Continuous CO_2	1
84	1000	12000	Horizontal at bottom	Full diagonal	Dew point	Vertical	Continuous CO_2	0.01
85	1000	12000	Horizontal at bottom	Half diagonal	Depleted	Horizontal at top	Continuous CO_2	0.01
86	1000	12000	Horizontal at bottom	Half diagonal	Initial	Horizontal at top	Continuous CO_2	1
87	1000	12000	Horizontal at bottom	Half diagonal	Initial	Vertical	WAG	0.01
88	1000	12000	Horizontal at top	Full diagonal	Depleted	Vertical	WAG	0.01
89	1000	12000	Horizontal at top	Half diagonal	Dew point	Horizontal at top	WAG	0.505

Table 4.2: 96-case experiments provided by JMP (continued)

90	1000	12000	Horizontal at top	Two-third diagonal	Depleted	Horizontal at top	WAG	1
91	1000	12000	Horizontal at top	Two-third diagonal	Initial	Vertical	Continuous CO_2	0.505
92	1000	12000	Vertical	Full diagonal	Depleted	Vertical	Continuous CO_2	1
93	1000	12000	Vertical	Full diagonal	Dew point	Horizontal at top	WAG	1
94	1000	12000	Vertical	Half diagonal	Dew point	Vertical	WAG	1
95	1000	12000	Vertical	Two-third diagonal	Depleted	Vertical	WAG	0.01
96	1000	12000	Vertical	Two-third diagonal	Dew point	Horizontal at top	Continuous CO_2	0.01

In this study, condensate recovery factor and amount of CO_2 stored are two response factors. So, it is necessary to perform reservoir simulation on 96-case experiments in order to obtain two response results of all cases for further analysis in the next step.

4.4 Response Surface Methodology

After obtaining the simulation response results, the results will then be added into the predefined 96-case experiment table. Model-fitting process will be performed by 'Fit Model' platform available in JMP to create a proxy model as a representative of simulation process.

At this step, the least squares technique is adopted as the method to fit the model. Subsequently, coefficients of main effects, interaction effects and quadratic effects for both objectives are obtained. The coefficients can implicitly describe which factors or interaction factors are more influential and should be investigated in details by generating a 3-D response surface plot.

Figure 4.3 shows a 3-D response surface plot provided by JMP. The 3-D response surface plot consists of the response in the y-axis accompanied with 2 factors in x-axis. The plot shows how much change the response will be when considering 2 factors varying at the same time. Interaction effects can show that change of levels of injection rate causes change of condensate recovery factor

differently depending on the level of permeability. For example, at low level of injection rate condensate recovery factor appears to increase from low level to mid level of permeability and then decrease from mid level to high level of permeability. On the other hand, at high level of injection rate condensate recovery factor appears to increase from low level to high level of permeability, representing interaction effect between injection rate and permeability.

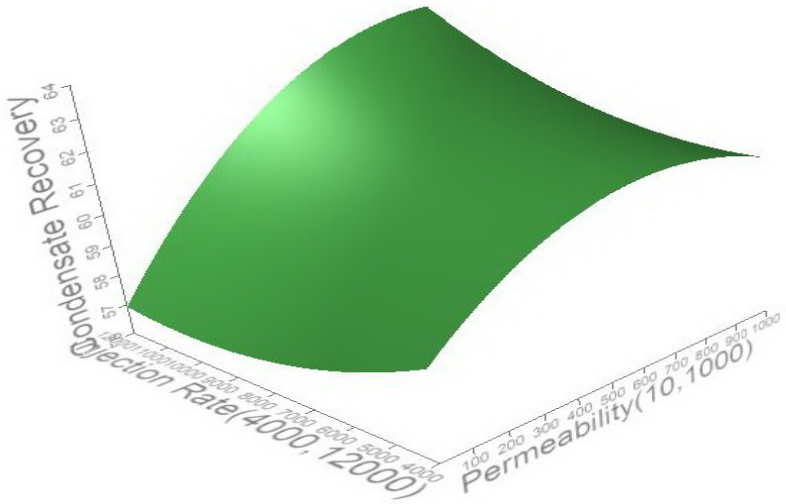

Figure 4.3: 3-D response surface plot provided by JMP

The quality of model fitting can be illustrated by Figure 4.4. Figure 4.4 represents cross-plot between actual (ECLIPSE) and predicted responses for every case. The model has a good fit if most of the points are close to 45-degree straight line. Almost all of the points fall into the interval between two dashed lines which represent 95% confidence interval of a good fit. The R^2 value of 0.92 confirms the good fit of the model. The perfect fitting is achieved when all points lie on the straight line.

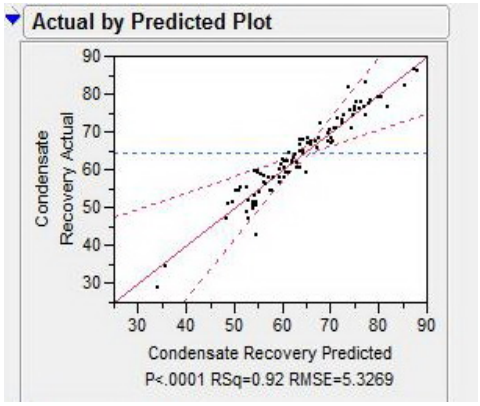

Figure 4.4: Cross-plot between actual (ECLIPSE) and predicted responses

4.5 Experiments for Proxy Cross Validation

Although the proxy model obtained from the previous step may fit well with ECLIPSE responses used to construct it, it is necessary for the experimenter to investigate applicability of the model by performing cross-validation experiments. Cross-validation experiments are experiment cases which are not used to construct the model. These experiments are randomly generated by JMP.

Since the objective of this study is to save resources and time, 30-case cross validation experiments are randomly created within levels of each factor. Table 4.3 shows 30 cases for cross validation experiments for validating the proxy model.

Subsequently, reservoir simulation will be performed for the 30 cases. Two response results are obtained and then compared to the predicted results from the proxy model. A statistical test called 'matched pairs t-test' available in JMP as shown in Figure 4.5 is used to investigate the difference between ECLIPSE results and predicted results. If the differences between them which are represented by t-test results ("Prob>|t|", "Prob>t", and "Prob<t") are all greater than 0.05, the conclusion can be drawn that the proxy model can adequately fit and consequently is applicable to determine optimum parameters and strategies for maximizing condensate recovery factor and amount of CO_2 stored in place of exhaustive simulation with less effort and time consumption.

Table 4.3: Cases for cross validation experiments

Run ID	Validation table							
	Permeability (md)	Injection rate (Mscf/D)	kv/kh	Injection well type	Well spacing	Injection time	Production well type	Injection scheme
1	604	8800	1	Horizontal at bottom	Full diagonal	Depleted	Vertical	WAG
2	406	7200	0.01	Horizontal at bottom	Two-third diagonal	Dew point	Vertical	Con CO_2
3	208	4000	0.802	Horizontal at top	Full diagonal	Initial	Vertical	Con CO_2
4	10	10400	0.604	Horizontal at top	Half diagonal	Dew point	Vertical	WAG
5	802	12000	0.208	Vertical	Full diagonal	Dew point	Horizontal at top	Con CO_2
6	1000	5600	0.406	Vertical	Two-third diagonal	Depleted	Vertical	WAG
7	802	10400	0.01	Horizontal at bottom	Half diagonal	Dew point	Horizontal at top	WAG
8	604	4000	0.406	Horizontal at bottom	Two-third diagonal	Depleted	Vertical	WAG
9	208	5600	1	Horizontal at top	Half diagonal	Initial	Horizontal at top	Con CO_2
10	1000	8800	0.802	Vertical	Full diagonal	Depleted	Horizontal at top	WAG
11	10	7200	0.208	Vertical	Half diagonal	Depleted	Vertical	Con CO_2
12	406	12000	0.604	Horizontal at bottom	Full diagonal	Depleted	Vertical	Con CO_2
13	802	4000	0.208	Horizontal at bottom	Half diagonal	Depleted	Horizontal at top	WAG
14	10	7200	0.406	Horizontal at top	Full diagonal	Dew point	Horizontal at top	Con CO_2
15	604	10400	0.01	Horizontal at top	Two-third diagonal	Depleted	Horizontal at top	WAG
16	1000	8800	0.604	Vertical	Half diagonal	Initial	Horizontal at top	Con CO_2
17	406	5600	1	Horizontal at bottom	Full diagonal	Initial	Horizontal at top	Con CO_2
18	208	12000	0.802	Horizontal at bottom	Half diagonal	Dew point	Vertical	WAG
19	208	4000	0.802	Horizontal at top	Full diagonal	Dew point	Vertical	Con CO_2
20	1000	5600	0.406	Horizontal at top	Two-third diagonal	Initial	Vertical	WAG
21	604	8800	1	Vertical	Half diagonal	Initial	Horizontal at top	Con CO_2
22	10	10400	0.604	Horizontal at bottom	Full diagonal	Initial	Horizontal at top	WAG
23	802	12000	0.208	Horizontal at bottom	Two-third diagonal	Dew point	Horizontal at top	WAG

Table 4.3: Cases for cross validation experiments (continued)

24	406	7200	0.01	Horizontal at top	Full diagonal	Initial	Vertical	WAG
25	604	7200	0.01	Horizontal at top	Two-third diagonal	Initial	Horizontal at top	Con CO_2
26	208	12000	0.208	Horizontal at bottom	Full diagonal	Dew point	Vertical	WAG
27	406	8800	1	Horizontal at bottom	Half diagonal	Dew point	Horizontal at top	Con CO_2
28	1000	10400	0.604	Horizontal at bottom	Two-third diagonal	Depleted	Horizontal at top	Con CO_2
29	10	5600	0.406	Horizontal at top	Half diagonal	Initial	Horizontal at top	WAG
30	802	4000	0.802	Vertical	Full diagonal	Dew point	Horizontal at top	WAG

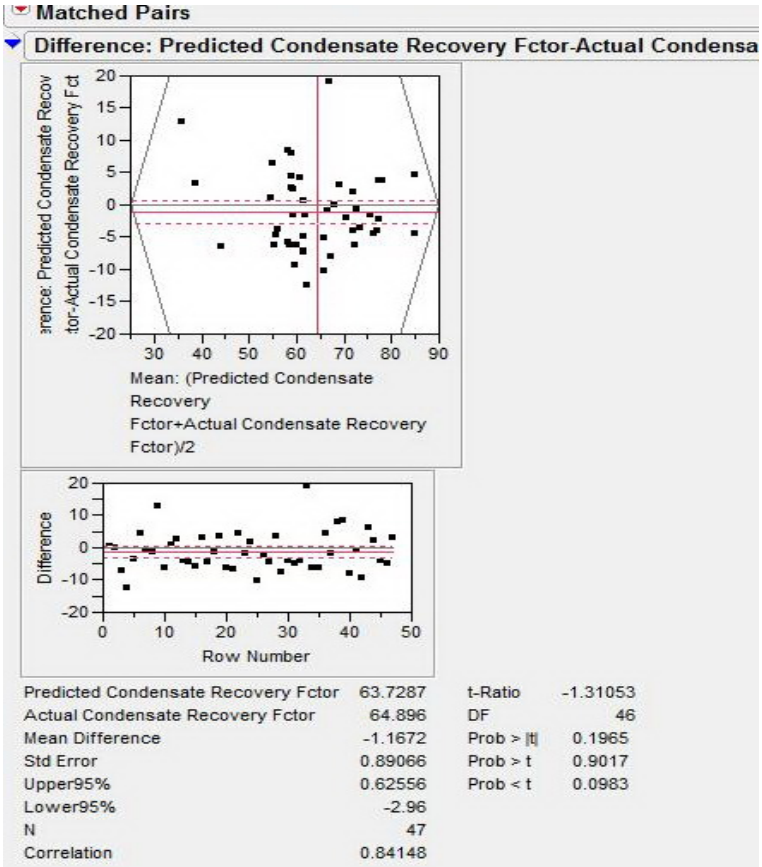

Figure 4.5: Matched pairs t-test for analysis of difference between actual (ECLIPSE) and predicted responses

4.6 Reservoir Simulation Model

Three main sections of reservoir simulation program are:

1. **PVT*i* section** PVT*i* generates the phase behavior of the reservoir fluid, dew point pressure and calculates binary interaction coefficients between components.
2. **ECLIPSE section** The compositional simulator **'**ECLIPSE 300' is used to simulate the performance of the gas condensate reservoir.
3. **VFP section** VFP constructs the wellbore model and calculates the vertical performance.

This section describes each section of the simulation program in details and how properties in each section were gathered.

4.6.1 PVTi Section

PVTi is a compositional PVT equation of state based program used for characterizing a set of fluid samples. The component type is *user defined*. In this type, the physical properties of each component such as critical pressure, critical temperature, and acentric factors can be defined by the user.

The initial fluid compositions used in this study are actual field data from Society of Petroleum Engineering papers, as shown in Table 4.4 [34].

Table 4.4: Initial composition of reservoir fluid

Component	Fraction
Methane (CH_4)	0.59991
Ethane (C_2H_6)	0.084326
Propane (C_3H_8)	0.063988
Iso-Butane (C_4H_{10})	0.034127
Normal-Butane (C_4H_{10})	0.038989
Iso-Pentane (C_5H_{12})	0.014286
Normal-Pentane (C_5H_{12})	0.013988
Hexane (C_6H_{14})	0.072718
Heptane (C_7H_{16})	0.065366
Octane (C_8H_{18})	-
Nonane (C_9H_{20})	-
Decane ($C_{10}H_{22}$)	-
Undecane ($C_{11}H_{24}$)	-
Dodecane ($C_{12}H_{26}$)	-
Carbon dioxide (CO_2)	0.012302
Nitrogen (N_2)	-

The physical properties of each component were acquired from Engineering Data Book, GPSA 1987, as shown in Table 4.5 [35].

Table 4.5: Physical properties of each component

Comp.	Boiling point (^oR)	Critical pressure (psia)	Critical temp. (^oR)	Critical volume (ft^3/lb-mole)	Molecular weight	Acentric factor
C_1	201.280	667.0	343.34	0.0988	16.043	0.0108
C_2	332.540	707.8	550.07	0.0783	30.070	0.0972
C_3	416.270	615.0	665.92	0.0727	44.097	0.1515
i-C_4	470.780	527.9	734.41	0.0714	58.123	0.1852
n-C_4	491.080	548.8	765.51	0.0703	58.123	0.1981
i-C_5	542.090	490.4	828.96	0.0684	72.150	0.2286
n-C_5	556.890	488.1	845.70	0.0695	72.150	0.2510
C_6	615.700	439.5	911.80	0.0688	86.177	0.2990
C_7	669.070	397.4	970.90	0.0682	100.204	0.3483
C_8	718.170	361.1	1023.50	0.0673	114.231	0.3978
C_9	763.400	330.7	1070.80	0.0693	128.258	0.4425
C_{10}	805.400	304.6	1112.20	0.0702	142.285	0.4881
C_{11}	844.800	287.2	1150.20	0.0366	156.310	0.5370
C_{12+}	881.160	263.9	1184.40	0.0398	170.340	0.5760
CO_2	350.765	1069.5	547.73	0.0342	44.010	0.2667
N_2	139.564	492.8	227.51	0.0510	28.013	0.0370

After inputting initial composition of reservoir fluid and physical properties of each componenet, the phase diagram and the binary interaction coefficients (BICs) will be generated as shown in Figure 4.6 and Table 4.6, respectively.

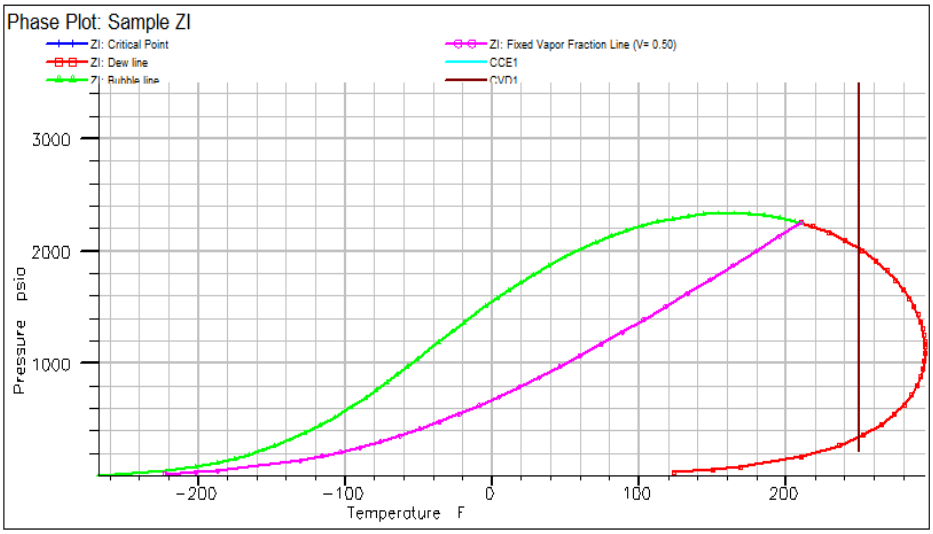

Figure 4.6: Phase diagram extracted from PVTi program

Table 4.6: Binary interaction coefficient between components calculated from PVTi program

	N_2	CO_2	C1	C2	C3	i-C4	n-C4	i-C5	n-C5	C6	C7	C8	C9	C10	C11	C12+
N_2	0	0	0.0106	0.0100	0.0100	0	0	0	0	0	0	0	0	0	0	0
CO_2	0	0	0.0153	0.0100	0.0100	0	0	0	0	0	0	0	0	0	0	0
C1	0.0106	0.0153	0	0	0	0.0196	0.0196	0.0238	0.0238	0.0288	0.0343	0.0377	0.0401	0.0419	0.0435	0.0450
C2	0.0100	0.0100	0	0	0	0.0100	0.0100	0.0100	0.0100	0.0100	0.0100	0.0100	0.0100	0.0100	0.0100	0.0100
C3	0.0100	0.0100	0	0	0	0.0100	0.0100	0.0100	0.0100	0.0100	0.0100	0.0100	0.0100	0.0100	0.0100	0.0100
i-C4	0	0	0.0196	0.0100	0.0100	0	0	0	0	0	0	0	0	0	0	0
n-C4	0	0	0.0196	0.0100	0.0100	0	0	0	0	0	0	0	0	0	0	0
i-C5	0	0	0.0238	0.0100	0.0100	0	0	0	0	0	0	0	0	0	0	0
n-C5	0	0	0.0238	0.0100	0.0100	0	0	0	0	0	0	0	0	0	0	0
C6	0	0	0.0288	0.0100	0.0100	0	0	0	0	0	0	0	0	0	0	0
C7	0	0	0.0343	0.0100	0.0100	0	0	0	0	0	0	0	0	0	0	0
C8	0	0	0.0377	0.0100	0.0100	0	0	0	0	0	0	0	0	0	0	0
C9	0	0	0.0401	0.0100	0.0100	0	0	0	0	0	0	0	0	0	0	0
C10	0	0	0.0419	0.0100	0.0100	0	0	0	0	0	0	0	0	0	0	0
C11	0	0	0.0435	0.0100	0.0100	0	0	0	0	0	0	0	0	0	0	0
C12+	0	0	0.0450	0.0100	0.0100	0	0	0	0	0	0	0	0	0	0	0

The maximum liquid dropout and dew point pressure are obtained from the PVTi section as shown in Table 4.7

Table 4.7: Maximum liquid dropout and dew point pressure of gas condensate

Case	Maximum liquid dropout (%)	Dew point pressure (psi)
Base	19	2020

4.6.2 ECLIPSE Section

Reservoir simulation is an efficient tool to describe the flow of multiphase reservoir fluid either in simple or complex geological model. Consequently, it is widely used in order to determine reservoir performance and also reservoir management.

The reservoir is constructed by amount of established volume elements, namely grid blocks, which represent geological reservoir construction. The appropriate equation is used in place of partial differential equation that describes fluid flow in the reservoir. There are 3 types of simulation which suit individual fluid considered: black oil, compositional, chemical. In this study, compositional reservoir simulation (ECLIPSE 300) is selected to describe fluid flow because the compositions of reservoir fluid change with time. One of the processes which causes compositional change is gas injection.

Input data such as reservoir properties, water/gas saturation, compositions of both reservoir and injected gas, cubic equation of state, and well condition/location as well as injection/production conditions are all specified by the user. The simulator will then incorporate all specified data to efficiently construct the model for user-required study. All the following input data are extracted from one of the 96 cases for experimental design in order to show what input data ECLIPSE requires.

4.6.2.1 Grid Section

The reservoir model is plane geometry and homogenous. The selected grid system is Cartesian coordinate. The dimensions of the reservoir are 2,250 ft x 2,250 ft x 120 ft and 8,000 ft TVD (depth of top face). The number of block is 15 x 15 x 3. Details of grid and reservoir properties specified for this study are as follows:

a) Case Definition

Simulator:	Compositional	
Model Dimensions:	Number of cells in the x-direction	15
	Number of cells in the y-direction	15
	Number of cells in the z-direction	3
Grid type:	Cartesian	
Geometry type:	Block centered	
Oil-gas-water options:	Water, gas condensate (ISGAS), CO_2 in aqueous phase	
Number of Components:	16	
Pressure saturation options (solution type):	AIM	

b) Reservoir properties

Properties:	Porosity		=	0.17	
	Permeability	kx	=	10	md
		ky	=	10	md
		kz	=	1	md
	X Grid block size		=	150	ft
	Y Grid block size		=	150	ft
	Z Grid block size		=	40	ft
	Depth of Top face (Top layer)		=	8,000	ft

Note: The correlation for permeability-porosity is obtained from previous study [34] as follows:

$$k = 0.0048e^{44.843\phi}$$

where k is permeability (mD) and $\emptyset$ is porosity (fraction)

The top view, side view, and 3D view of Base case are shown in Figures 4.7, 4.8, and 4.9, respectively.

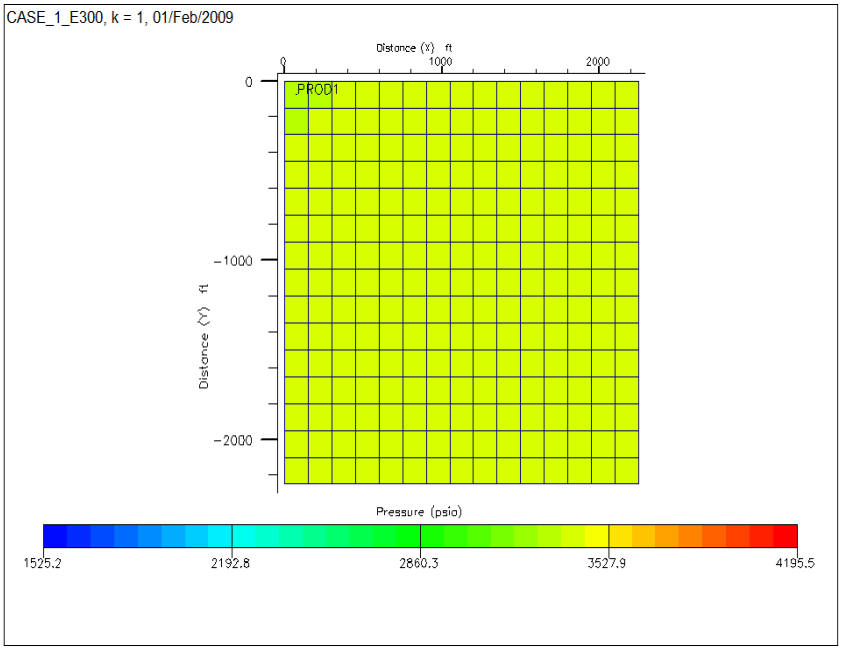

Figure 4.7: Top view of the reservoir model

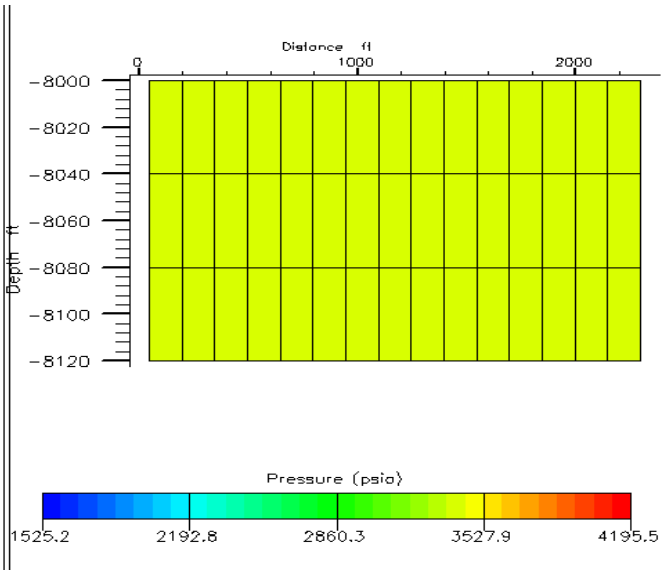

Figure 4.8: Side view of the reservoir model

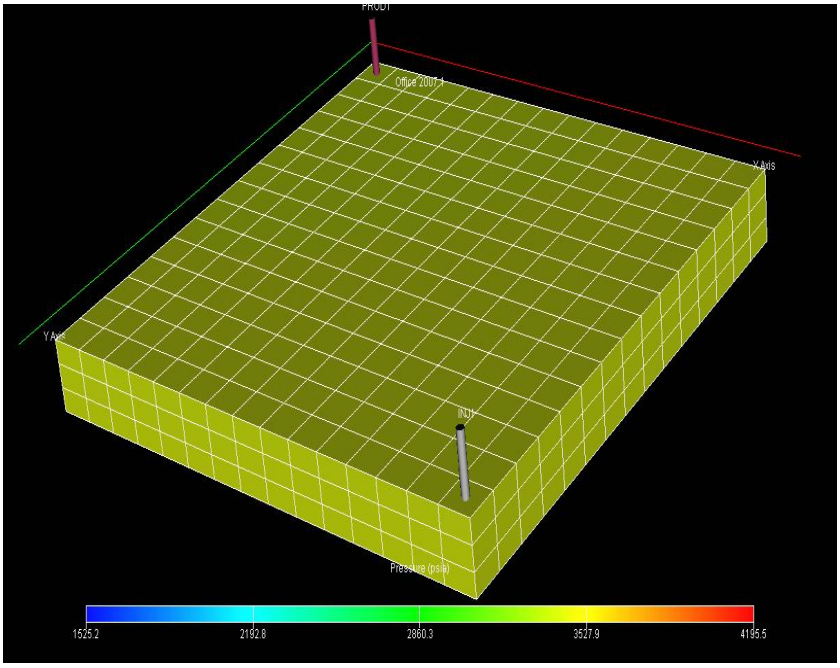

Figure 4.9: 3D view of the reservoir model

As shown in Figure 4.9, the injection and production wells are located at the corner of the reservoir or, in other word, they lie in diagonal direction. As previously stated in Section 4.2, this study includes both vertical well and horizontal well, so assumptions on their completion are to be defined. The vertical well and horizontal well are both completed for the whole interval of the reservoir. The horizontal well is located either at the top part or bottom part of the reservoir depending on the defined case and is oriented in the y-direction.

4.6.2.2 PVT section

In this section, all critical properties, initial compositions of reservoir fluid are added into the program. Peng-Robinson equation of state is selected to predict phase behavior and mixture composition changing with time. Fluid densities at surface conditions are then calculated as shown in Table 4.8.

Table 4.8: Fluid densities at surface condition

Property	Value	Units
Oil density	49.99914	lb/ft3
Water density	62.42797	lb/ft3
Gas density	0.04947417	lb/ft3

4.6.2.3 SCAL (Special Core Analysis) Section

A set of special core analysis data are collected from one of the gas fields in the Gulf of Thailand. The relation between oil relative permeabilities and oil saturation are tabulated in Table 4.9 and shown in Figure 4.10. k_{row} is the oil relative permeability for a system with oil and water only, and k_{rowg} is the oil relative permeability for a system with oil, water, and gas.

Table 4.9: Oil saturation and oil relative permeability

S_o	k_{row}	k_{rowg}
0	0	0
0.2	0	0
0.32	0.00463	0.015625
0.44	0.037037	0.125
0.56	0.125	0.421875
0.68	0.296296	1
0.95	1	1

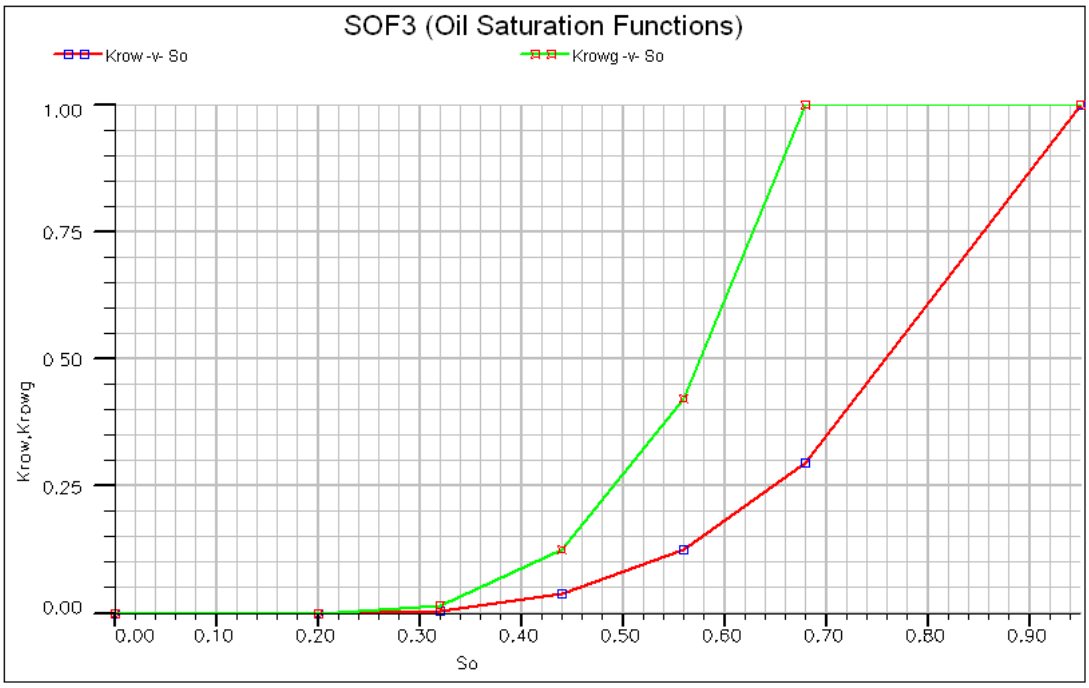

Figure 4.10: Oil relative permeability function

The relation between water relative permeability and water saturation is tabulated in Table 4.10 and shown in Figure 4.11.

Table 4.10: Water saturation and water relative permeability

S_w	k_{rw}
0.11	0
0.157	0
0.216	0
0.313	0.02
0.44	0.06
0.56	0.10
0.68	0.15
0.80	0.30
0.90	0.65

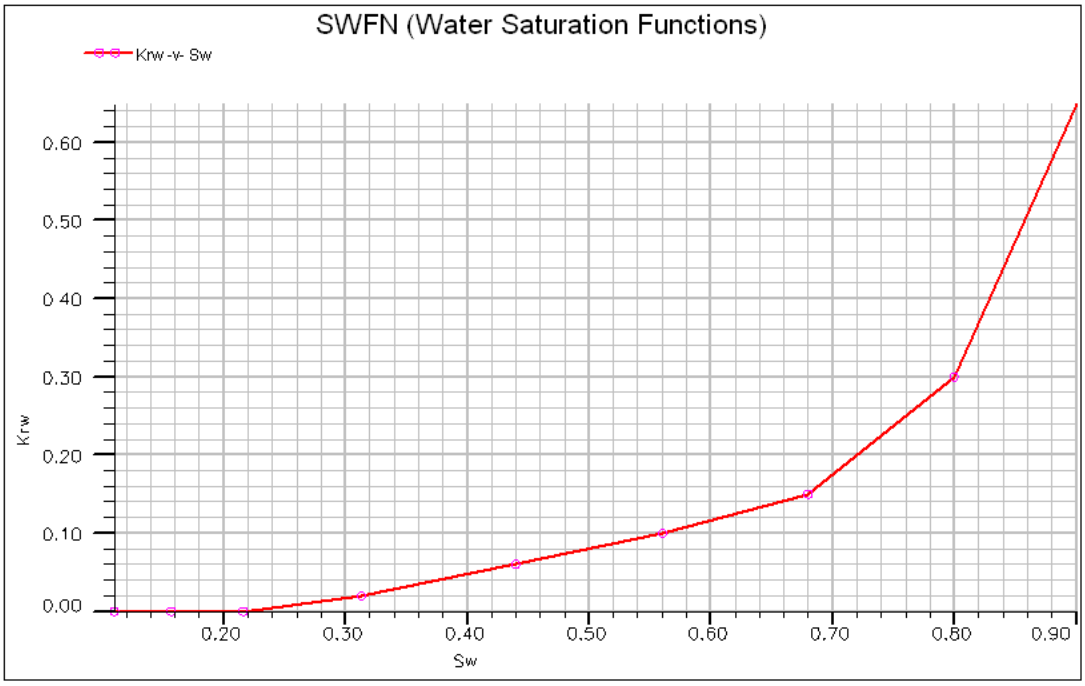

Figure 4.11: Water relative permeability as a function of water saturation

The relation between gas relative permeability and gas saturation is tabulated in Table 4.11 and shown in Figure 4.12.

Table 4.11: Gas saturation function and gas relative permeability

S_g	k_{rg}
0	0
0.10	0
0.20	0
0.30	0.20
0.40	0.40
0.60	0.85
0.70	0.90
0.80	0.92
0.90	0.95
0.95	0.95

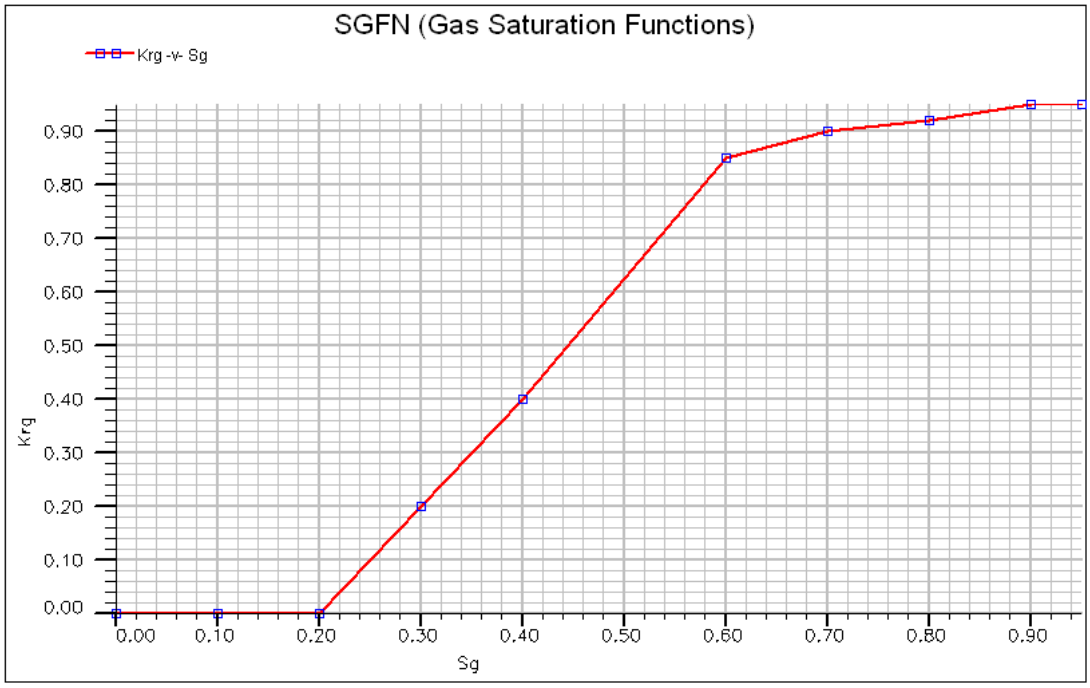

Figure 4.12: Gas relative permeability as a function of gas saturation

The relation between capillary pressure and water saturation is tabulated in Table 4.12 and shown in Figure 4.13.

Table 4.12: Water saturation function and capillary pressure

S_w	P_c (psia)
0.11	250
0.157	53
0.216	13
0.313	1
0.44	0
0.56	0
0.68	0
0.80	0
0.90	0

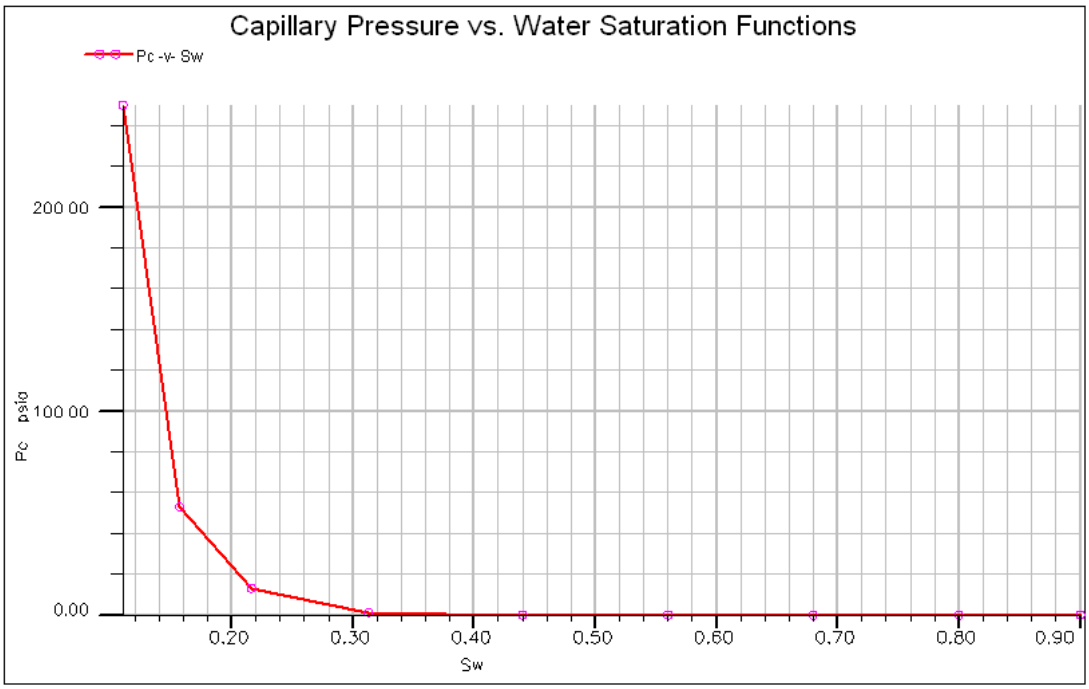

Figure 4.13: Capillary pressure as a function of water saturation

4.6.2.4 Initialization Section

Initial properties of reservoir and fluid are specified in this section for determination of Vapor/Liquid Equilibrium (VLE) using Peng-Robinson EOS. Initial fluid composition as shown in table 4.13 is specified in Non-Equilibrium Initialization (NEI) section which is used to generate consistent oil and gas compositions for each cell.

Table 4.13: Initial compositions of reservoir fluid

Component	Fraction
C1	0.59991
C2	0.084326
C3	0.063998
i-C4	0.034127
n-C4	0.038989
i-C5	0.014286
n-C5	0.013988
C6	0.072718
C7	0.0654
C8	0
C9	0
C10	0
C11	0
C12	0
CO_2	0.0123
N_2	0

The initial water saturation and initial gas saturation is 0.11 and 0.89, respectively. These values are obtained from one gas field in the Gulf of Thailand. The initial temperature is 250°F and initial pressure is 3500 psia.

4.6.2.5 Schedule Section

Well condition/location, production strategies, injection/production condition, and economical limit all are specfied at this section to come up with the development plan, production management as user-defined purpose.

Tables 4.14 - 4.22 show details of production and injection wells.

Production well

Table 4.14: Well specification (Prod1) [WELSPECS]

Well	PROD 1
I location	1
J location	1
Datum depth	8,120 ft
Preferred phase	GAS
Inflow equation	STD
Automatic shut-in instruction	SHUT
Cross flow	YES
Density calculation	SEG
Type of well model	STD

Table 4.15: Well connection data (Prod1) [COMPDAT]

Well	PROD 1
K upper	1
K lower	3
Open/shut flag	OPEN
Wellbore ID	0.5104167 ft
Direction	Z

Table 4.16: Production well control (Prod1) [WCONPROD]

Well	PROD 1
Open/shut flag	OPEN
Control	GRAT
Gas rate	8,000 MSCF/D
BHP target	700 psia
THP target	200 psia
VFP pressure table	1

Table 4.17: Production well economics limit [WECON]

Well	PROD 1
Minimum oil rate	12.57 STB/D
Minimum gas rate	100 MSCF/D
Workover procedure	NONE
End run	YES
Quantity for economic limit	RATE
Secondary workover procedure	NONE

Table 4.18: Production vertical flow performance [VFPPROD]

VFP Table Number	1
Datum depth	8,120 ft
Flow rate definition	GAS
Water fraction definition	WGR
Gas fraction definition	GOR
Fixed pressure definition	THP
Table units	FIELD
Tabulated quantity definition	BHP

Injection well

Table 4.19: Well specification (Inj1) [WELSPECS]

Well	INJ 1
I location	15
J location	15
Datum depth	8,120 ft
Preferred phase	GAS
Inflow equation	STD
Automatic shut-in instruction	SHUT
Cross flow	YES
Density calculation	SEG
Type of well model	STD

Table 4.20: Well connection data (Inj1) [COMPDAT]

Well	INJ 1
K upper	1
K lower	3
Open/shut flag	SHUT
Wellbore ID	0.5104167 ft
Direction	Z

Table 4.21: Injection well control (Inj1) [WCONINJE]

Well	INJ 1
Injector type	GAS
Open/shut flag	SHUT
Control mode	RATE
Injection pressure	4000 psia
Gas surface rate	8,000 MSCF/D

Table 4.22: Nature of injection gas (Inj1) [WINJGAS]

Well	INJ 1
Injector fluid	STREAM
Well stream	1

Table 4.23: Injection gas composition [WELLSTRE]

Well stream	1
Comp 15	1

Assumptions used in this section are as follows:

1. The minimum tubing head pressure of producer is 200 psia. This limit is a common tubing head presssure limit used in Gulf of Thailand when a booster compressor is used.
2. Economic limit for oil or condensate rate is determined by accounting for electricity consumption cost of compressor, depending on injection rate. The economic limit for natuaral depletion is defined at 5 STB/D. Therefore, all other economic limits for injection cases are obtained by compressor cost plus 5 STB/D as shown in Table 4.24. Detailed calculation of compressor cost and electricity consumption cost of compressor is provided in Appendix.
3. Injecion pressure is limited to 4,000 psia to prevent fracture of reservoir.
4. Production rate is equal to injection rate.

Table 4.24: Economic limit for this study

Injection Rate (Mscf/D)	Economic limit (STB/D)
4000	8.57
5600	10
7200	11.43
8000	12.15
8800	13.87
10400	14.3
12000	15.73

4.6.3 VFP Section

VFP or vertical flow performance represents the flow of fluid from bottomhole up to the wellhead. It is crucial to include this section in ECLIPSE simulation because ECLIPSE typically accounts for only flow behavior from the reservoir to bottom-hole. The production and injection wells of the model have the tubing diameter of 3-1/2 inches with an inner diameter of 2.992 inches. The well is perforated from 8,000 ft to 8,120 ft and the perforation interval is from the top to the bottom of the reservoir. The schematic of wellbore configuration is shown in Figure 4.14.

The vertical flow performance was generated by Production and Systems Performance analysis software (PROSPER) to describe the flow of fluid from bottomhole up to wellhead. The chosen vertical lift correlation is Fancher Brown. Fancher Brown is a no-slip hold-up correlation suitable to gas condensate well because the flow regime is normally mist flow; so the slip between liquid and gas is infinitesimal.

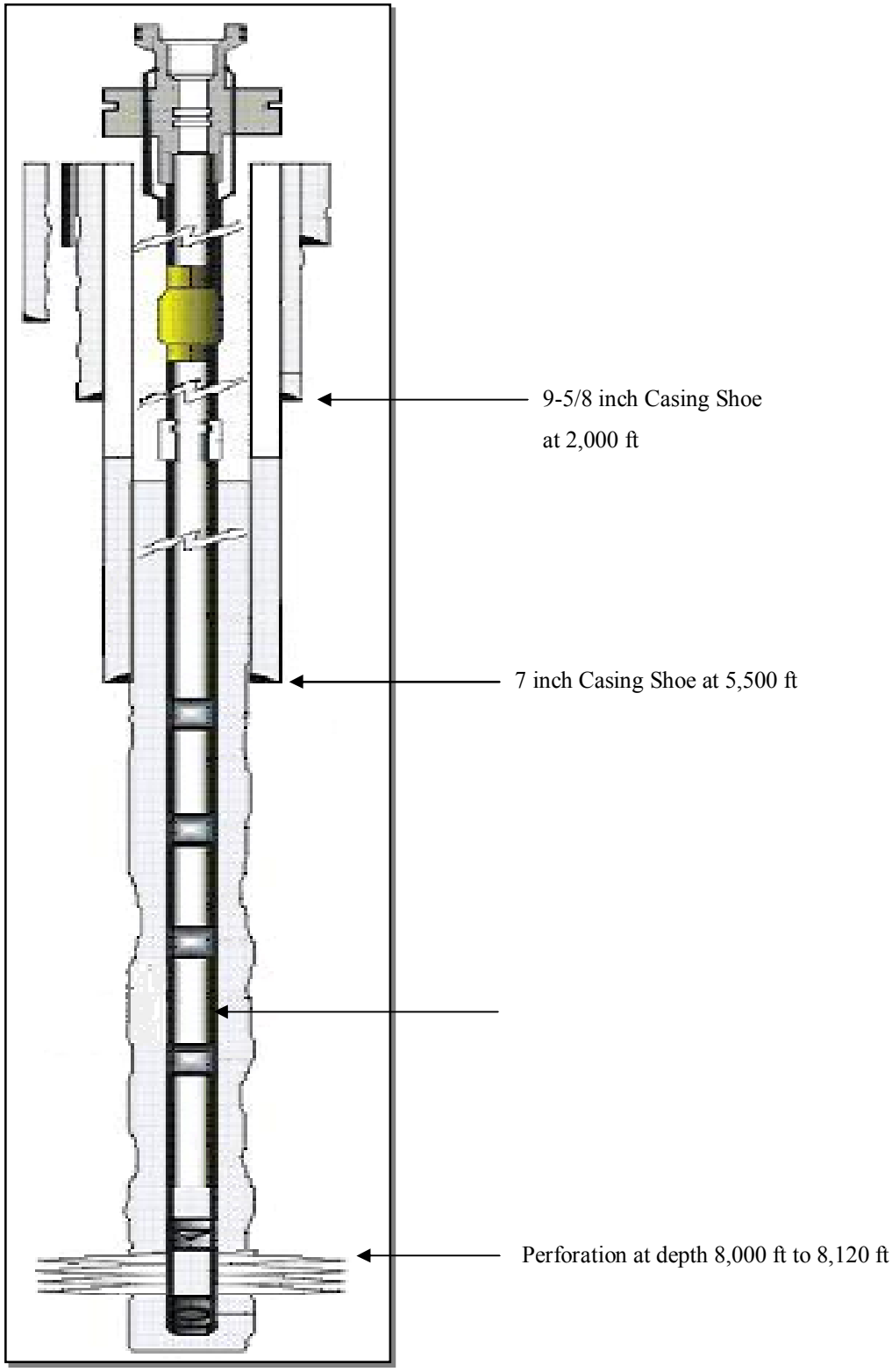

Figure 4.14: Casing and tubing flow model used in this study

CHAPTER V

RESULTS AND DISCUSSION

This chapter discusses the results obtained from Experimental Design and Response Surface Methodology processes. The quadratic proxy model is constructed by the JMP software. Cross-validation experiment is performed to see the applicability of quadratic proxy model. Lastly, optimum parameters and strategies for maximizing objective functions are obtained from the proxy model in compliance with the objective of this study.

5.1 Experimental Design and Response Surface Methodology

5.1.1 Quadratic Proxy Model

As previously described in Section 4.3, corresponding simulations are performed for 96-case experiments generated by JMP. The simulation results (condensate recovery factor and amount of CO_2 stored) are obtained from ECLIPSE and then added into pre-defined 96-case experiment table in JMP as shown in Figure 5.1. Additionally, simulation results of condensate recovery factor and amount of CO_2 stored for all 96-case experiments are shown in Table 5.1.

Simulation results obtained from ECLIPSE

	Permeability	Injection Rate	Injection Well Type	Well Spacing	Injection Time	Production Well Type	Injection Scheme	Kv/Kh	Condensate Recovery	Amount of CO2 stored
1	10	4000	Horizontal at bottom	Full Diagonal	Dew Point	Vertical	WAG	0.505	78.01	8.11
2	10	4000	Horizontal at bottom	Half Diagonal	Depleted	Horizontal at Top	Continuous CO2	1	58.32	23.33
3	10	4000	Horizontal at bottom	Two-Third Diagonal	Dew Point	Horizontal at Top	Continuous CO2	0.01	76.43	21.98
4	10	4000	Horizontal at bottom	Two-Third Diagonal	Initial	Vertical	WAG	1	67.74	6.51
5	10	4000	Horizontal at Top	Full Diagonal	Dew Point	Horizontal at Top	Continuous CO2	0.01	78.98	22.91
6	10	4000	Horizontal at Top	Full Diagonal	Initial	Vertical	WAG	0.01	74.24	8.87
7	10	4000	Horizontal at Top	Half Diagonal	Depleted	Horizontal at Top	WAG	0.01	59.47	7.84
8	10	4000	Horizontal at Top	Half Diagonal	Dew Point	Vertical	WAG	1	57.95	5.95
9	10	4000	Horizontal at Top	Half Diagonal	Initial	Vertical	Continuous CO2	0.505	34.5	12.67
10	10	4000	Horizontal at Top	Two-Third Diagonal	Depleted	Vertical	WAG	1	59.3	7.33
11	10	4000	Horizontal at Top	Two-Third Diagonal	Initial	Horizontal at Top	Continuous CO2	1	62.45	19.11
12	10	4000	Vertical	Full Diagonal	Depleted	Horizontal at Top	WAG	0.01	62.26	8.36
13	10	4000	Vertical	Full Diagonal	Depleted	Vertical	WAG	1	63.86	7.04
14	10	4000	Vertical	Full Diagonal	Initial	Horizontal at Top	Continuous CO2	1	68.16	21.04
15	10	4000	Vertical	Half Diagonal	Depleted	Vertical	Continuous CO2	0.01	54.23	23.4
16	10	4000	Vertical	Half Diagonal	Initial	Vertical	WAG	0.505	62.62	8.19
17	10	4000	Vertical	Two-Third Diagonal	Dew Point	Horizontal at Top	WAG	0.505	67.68	8.74
18	10	4000	Vertical	Two-Third Diagonal	Initial	Vertical	Continuous CO2	0.01	69.66	21.09
19	10	8000	Horizontal at bottom	Full Diagonal	Depleted	Vertical	Continuous CO2	0.01	56.31	25.15
20	10	8000	Horizontal at bottom	Full Diagonal	Initial	Horizontal at Top	Continuous CO2	0.505	81.82	23.66
21	10	8000	Horizontal at bottom	Half Diagonal	Initial	Horizontal at Top	WAG	1	42.97	4.66
22	10	8000	Horizontal at Top	Full Diagonal	Depleted	Horizontal at Top	WAG	0.505	67.07	6.66
23	10	8000	Horizontal at Top	Two-Third Diagonal	Initial	Horizontal at Top	WAG	0.505	64.38	7.16
24	10	8000	Vertical	Half Diagonal	Dew Point	Horizontal at Top	Continuous CO2	0.505	55.17	17
25	10	8000	Vertical	Two-Third Diagonal	Dew Point	Vertical	Continuous CO2	1	77.78	22.47
26	10	12000	Horizontal at bottom	Half Diagonal	Dew Point	Horizontal at Top	WAG	0.01	72.23	8.83
27	10	12000	Horizontal at bottom	Half Diagonal	Dew Point	Vertical	Continuous CO2	1	51.1	18.04
28	10	12000	Horizontal at bottom	Two-Third Diagonal	Depleted	Vertical	WAG	0.01	60.21	8.73
29	10	12000	Horizontal at bottom	Two-Third Diagonal	Dew Point	Horizontal at Top	WAG	1	74.47	7.94
30	10	12000	Horizontal at bottom	Two-Third Diagonal	Initial	Horizontal at Top	Continuous CO2	0.505	63.16	19.29
31	10	12000	Horizontal at Top	Full Diagonal	Depleted	Horizontal at Top	Continuous CO2	1	67.16	25.97
32	10	12000	Horizontal at Top	Full Diagonal	Initial	Vertical	Continuous CO2	1	66.77	20.8
33	10	12000	Horizontal at Top	Half Diagonal	Depleted	Vertical	WAG	0.505	53.3	7.89

Figure 5.1: Simulation results added into pre-defined experiment table in JMP

Table 5.1: Simulation results of condensate recovery factor and amount of CO_2 stored for all 96-case experiments

Case	Condensate recovery (%)	Amount of CO_2 stored (Bscf)	Case	Condensate recovery (%)	Amount of CO_2 stored (Bscf)	Case	Condensate recovery (%)	Amount of CO_2 stored (Bscf)
1	78.01	8.11	**33**	53.30	7.89	**65**	57.88	13.26
2	58.32	23.33	**34**	28.77	11.68	**66**	73.68	11.47
3	76.43	21.98	**35**	67.85	20.82	**67**	59.74	21.33
4	67.74	6.51	**36**	70.91	15.86	**68**	70.70	10.60
5	78.98	22.91	**37**	56.66	24.57	**69**	49.82	12.91
6	74.24	8.87	**38**	67.45	13.68	**70**	57.82	29.39
7	59.47	7.84	**39**	63.28	30.73	**71**	78.23	37.07
8	57.95	5.95	**40**	64.23	31.44	**72**	66.81	9.90
9	34.50	12.67	**41**	61.96	39.01	**73**	83.21	12.87
10	59.30	7.33	**42**	75.55	10.68	**74**	54.38	38.99
11	62.45	19.11	**43**	79.06	11.84	**75**	47.17	28.10
12	62.26	8.36	**44**	85.93	36.78	**76**	51.14	13.79
13	63.86	7.04	**45**	57.72	12.01	**77**	75.55	11.81
14	68.16	21.04	**46**	56.83	13.31	**78**	77.44	12.15
15	54.23	23.40	**47**	54.29	28.90	**79**	67.53	34.90
16	62.62	8.19	**48**	76.47	33.96	**80**	55.43	38.42
17	67.68	8.74	**49**	54.56	7.41	**81**	72.11	10.77
18	69.66	21.09	**50**	58.93	38.03	**82**	68.19	10.31
19	56.31	25.15	**51**	73.26	11.62	**83**	59.43	32.11
20	81.82	23.66	**52**	60.55	38.91	**84**	74.34	35.51
21	42.97	4.66	**53**	67.35	10.30	**85**	60.65	40.57
22	67.07	6.66	**54**	62.42	11.06	**86**	59.45	32.00
23	64.38	7.16	**55**	82.23	12.02	**87**	68.43	10.05
24	55.17	17.00	**56**	59.18	37.99	**88**	61.51	11.75
25	77.78	22.47	**57**	60.61	27.86	**89**	65.74	10.85
26	72.23	8.83	**58**	71.11	32.98	**90**	51.70	14.28
27	51.10	16.04	**59**	54.50	12.69	**91**	48.84	28.92
28	60.21	8.73	**60**	51.28	28.19	**92**	64.74	41.57
29	74.47	7.94	**61**	67.17	9.95	**93**	76.41	12.64
30	63.16	19.29	**62**	64.89	41.62	**94**	67.39	11.00
31	67.16	25.97	**63**	86.36	13.13	**95**	61.76	12.27
32	66.77	20.80	**64**	46.99	28.04	**96**	76.11	36.21

From Table 5.1, it should be noted that the amount of retained CO_2 and condensate recovery does not change in the same fashion. Higher amount of stored CO_2 does not always means higher condensate recovery and so on. Therefore,

optimum values for both condensate recovery factor and amount of CO_2 stored in which all of the uncertainties in the design space are considered.

After that, model fitting process is performed by 'Fit Model' platform available in JMP to create quadratic proxy model. Least square technique is adopted as the method to fit the model as shown by Figure 5.2

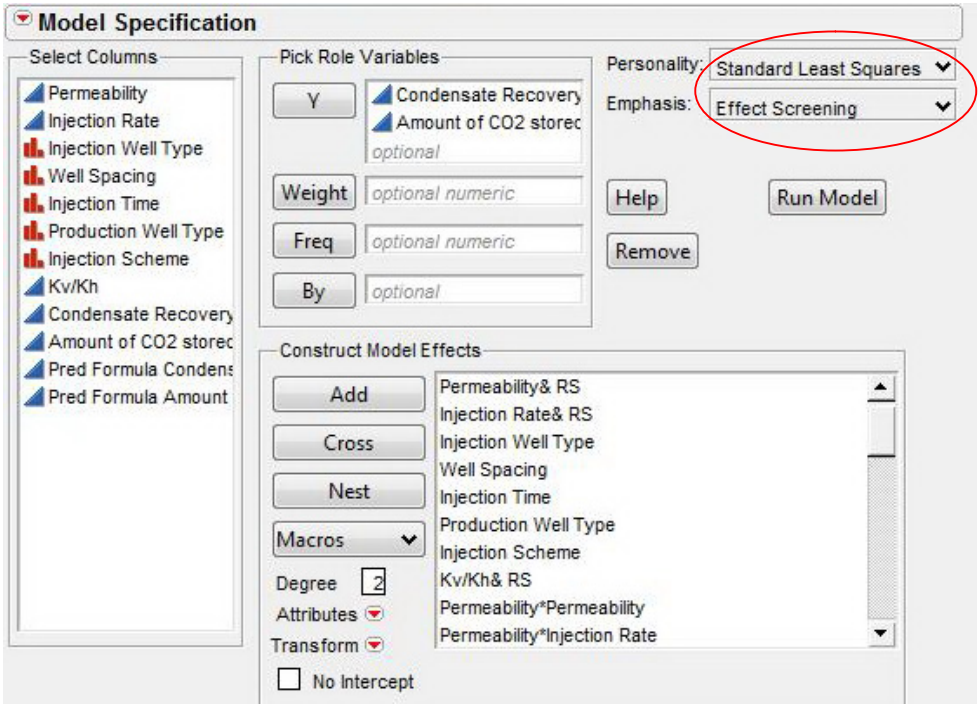

Figure 5.2: 'Fit Model' screen for fitting the model

The emphasis of this study is to see the most influential factors on coupled CO_2 sequestration and enhanced condensate recovery, which leads to optimum condition, so the 'Effect screening' emphasis is selected in this screen.

The quadratic equation with two-way interaction for fitting the proxy model is shown below for both objective functions

$$RF = \beta_0 + \sum_{i=1}^{3} \beta_i x_i + \sum_{i<j}^{3} \beta_{ij} x_i x_j + \sum_{i=1}^{3} \beta_{ii} x_i x_i + \sum_{i=1}^{3} \sum_{j=4}^{8} \beta_{ij} x_i + \sum_{i=4}^{8} \beta_i + \sum_{i<j}^{8} \beta_{ij} \quad (5.1)$$

$$CO_2 = \beta_0 + \sum_{i=1}^{3} \beta_i x_i + \sum_{i<j}^{3} \beta_{ij} x_i x_j + \sum_{i=1}^{3} \beta_{ii} x_i x_i + \sum_{i=1}^{3} \sum_{j=4}^{8} \beta_{ij} x_i + \sum_{i=4}^{8} \beta_i + \sum_{i<j}^{8} \beta_{ij} \quad (5.2)$$

where

RF = condensate recovery factor (%)

CO_2 = amount of CO_2 stored (Bscf)

β_0 = regression coefficient intercept

β_i = regression coefficient of main effect

β_{ij} = regression coefficient of interaction effect

β_{ii} = regression coefficient of quadratic (power) effect

Note that i = 1 to 3 represents numerical factors; permeability, injection rate and k_v/k_h, respectively and i = 4 to 8 represents categorical factors which are injection rate, injection well type, well spacing, injection time, production well type, and injection scheme, respectively.

The equations show that categorical factors have only regression coefficients without parameters. Only parameters of numerical factors exist when combined with categorical factors for example, $\sum_{i=1}^{3}\sum_{j=4}^{8}\beta_{ij}x_i$ has only x_i of numerical factors.

There is an important statistical principle in the analysis and interpretation. The principle called "sparsity of effects principle" states that most systems are dominated by some main effects and low-order interaction effects while most high-order interaction effects are negligible. Therefore, only two-order interaction effects are included in quadratic equations above.

As a result, quadratic proxy model is used for the fitting and the quality of fitting can be illustrated by Figure 5.3 and Figure 5.4 for condensate recovery factor and amount of CO_2 stored, respectively. Both figures present the actual by predicted plot, summary of fit and analysis of variance.

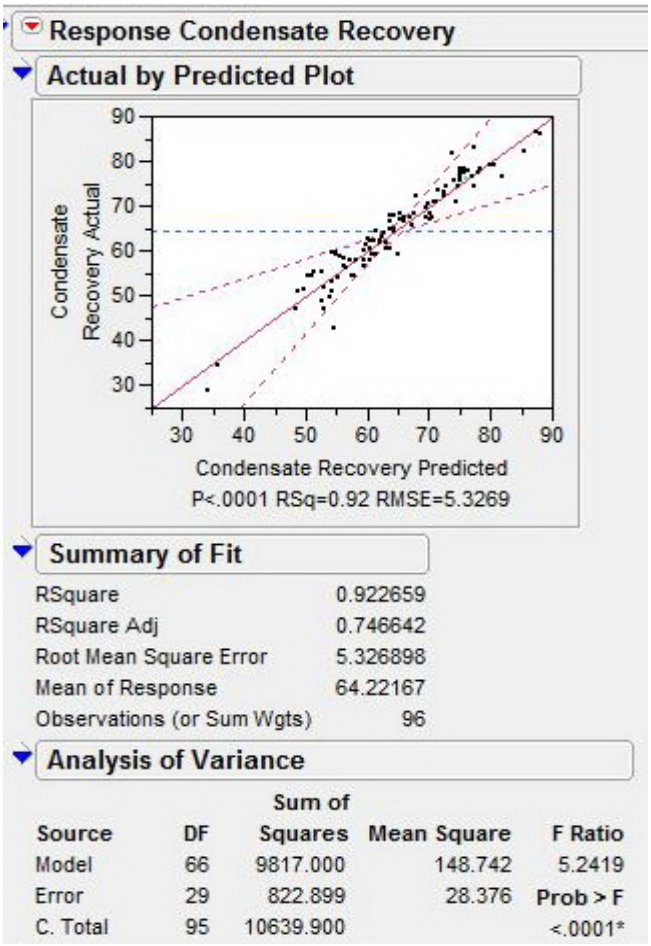

Figure 5.3: Actual by predicted plot, summary of fit and analysis of variance for condensate recovery factor

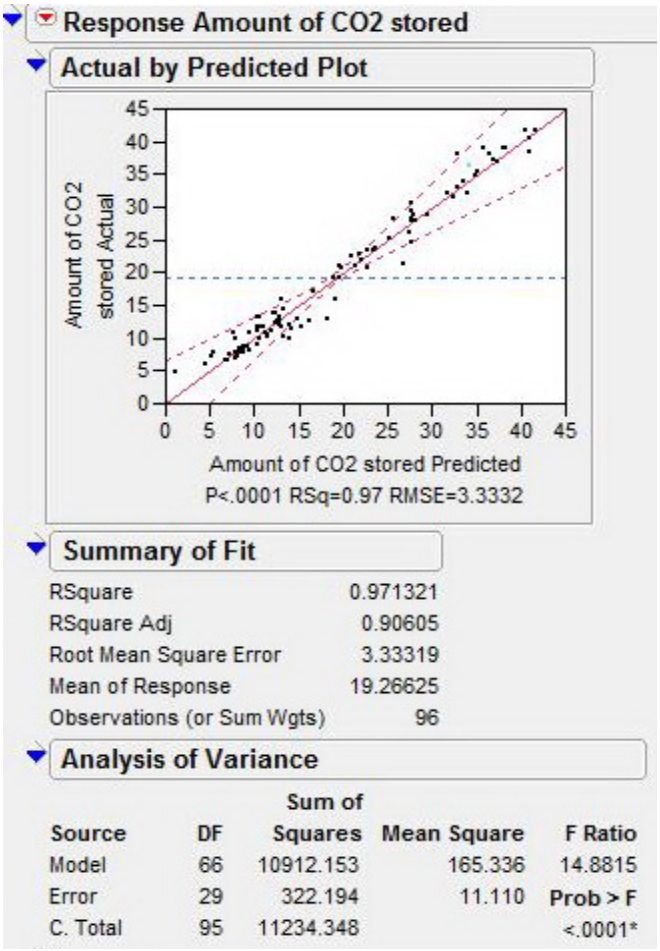

Figure 5.4: Actual by predicted plot, summary of fit and analysis of variance for amount of CO_2 stored

Both Figure 5.3 and Figure 5.4 show actual by predicted plot which is cross-plot between ECLIPSE and predicted responses for every case-experiment. In both figures, almost all ECLIPSE values represented by the points lie near the 45-degree solid straight line representing predicted values of responses and also lie within the confidence region represented by two dashed lines, all account for good model fitting. The points above the solid straight line represent under-prediction whereas the points below the solid straight line represent over-prediction. Moreover, the figures also show that fitting efficiency of amount of CO_2 stored is better than that of condensate recovery factor. All points in Figure 5.4 are closer to the solid line than those in Figure 5.3, representing better fitting.

Another representation of model fitting is summary of fit. Investigation on both figures shows that condensate recovery factor and amount of CO_2 stored have R^2= 0.92 and 0.97, respectively, representing good model fitting. The fitting efficiency of amount of CO_2 stored is greater than that of condensate recovery factor which is confirmed by its higher R^2 and lower Root Mean Square Error (RMSE). RMSE represents how much the ECLIPSE values are far away from the regression linear line or mean predicted values. In other words, lower RMSE accounts for better model-fitting.

Besides, interpretation of good model fitting can also be confirmed by Analysis of variance (ANOVA). Analysis of variance comprises of model and error, degree of freedom (DF), sum of square, mean square, F-ratio and Prob > F. Model herein means the effects of change of each parameter on the response whereas error means the difference between ECLIPSE and mean predicted responses. In this study, the experiment is set for modeling objective, and computer simulation is regarded as a deterministic method with assumption that the error is zero, so sum of squares and mean square of model are much greater than those of error as shown in Figures 5.3 and 5.4, which represents high effects of parameters on the responses. Additionally, the model effects appear significant because Prob > F is less than 0.0001 which means that each parameter effect is significantly different from other parameters in accordance with null assumption that each factor effect is not different from each other. Prob > F less than 0.0001 also means that the model has better statistical fit for the data used to construct the model. Analysis of variance also implies that the proxy model for amount of CO_2 stored has better fit than that of condensate recovery factor which is represented by higher F-ratio of amount of CO_2 stored. Higher F-ratio means that the parameter effects are massively influential to the response and therefore the model is better statistically fit.

Another representation of good model fitting is residual by predicted plot. This plot accounts for the difference between ECLIPSE and predicted responses of each case which is also called residual as shown in Figures 5.5 and 5.6 for both objective functions. From the figures, the residuals of responses randomly distribute at all predicted values, which represent random error in accordance with a statistical assumption. The residuals of condensate recovery factor appear higher than those of

amount of CO_2 stored, which account for better model fitting of amount of CO_2 stored.

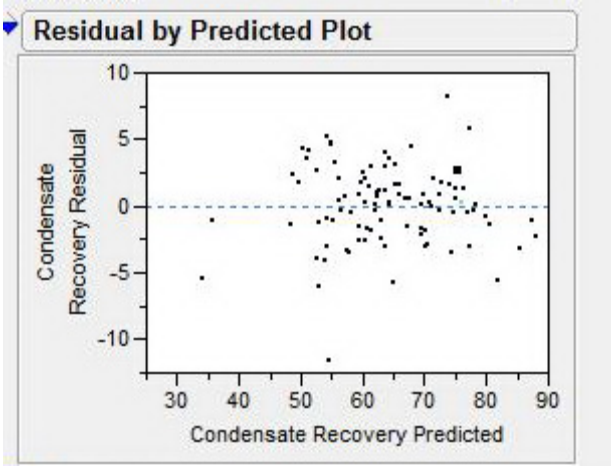

Figure 5.5: Residual by predicted plot for condensate recovery factor

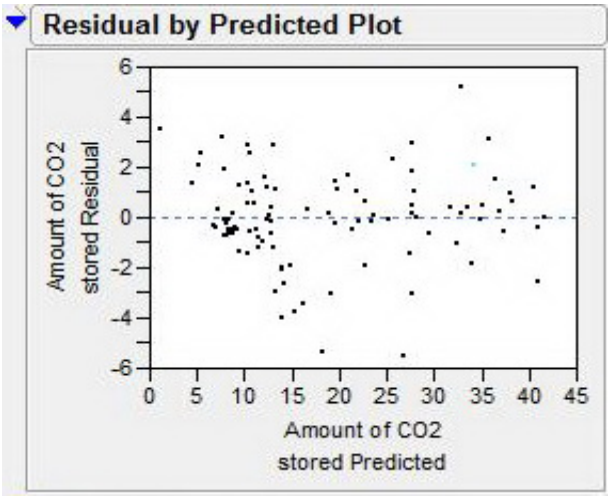

Figure 5.6: Residual by predicted plot for amount of CO_2 stored

The parameter coefficients for both objective functions are obtained from JMP as shown in Figure 5.7 and Figure 5.8. All parameters coefficients or herein "Estimates" are sorted based on the values of Prob >|t| in descending order. JMP also marks the significant parameters by '*' beside those whose Prob >|t| are less than 0.05. Prob >|t| is based on null hypothesis that all parameter coefficients are zero, so Prob >|t| less than 0.05 indicates that the null hypothesis is not true and consequently

those coefficients are not zero. The lower Prob >|t| is, the more significant that coefficient is.

Response Condensate Recovery

Sorted Parameter Estimates

Term	Estimate	Std Error	t Ratio	Prob>|t|
Well Spacing[Half Diagonal]	-7.837012	0.808654	-9.69	<.0001*
Injection Time[Dew Point]	8.0175718	0.831914	9.64	<.0001*
Injection Time[Depleted]	-5.65935	0.836055	-6.77	<.0001*
Injection Well Type[Horizontal at bottom]*Production Well Type[Vertical]	-2.965476	0.834303	-3.55	0.0013*
Well Spacing[Half Diagonal]*Injection Time[Depleted]	4.0009112	1.166603	3.43	0.0018*
Permeability*Well Spacing[Half Diagonal]	2.9443131	0.950755	3.10	0.0043*
Injection Well Type[Vertical]*Production Well Type[Vertical]	2.5304339	0.829754	3.05	0.0049*
Injection Scheme[WAG]	1.6057839	0.571273	2.81	0.0088*
Permeability*Injection Time[Dew Point]	2.1327468	0.965351	2.21	0.0352*
Well Spacing[Two-Third Diagonal]	1.7728385	0.821708	2.16	0.0394*
Well Spacing[Half Diagonal]*Injection Scheme[WAG]	1.7272364	0.812631	2.13	0.0422*
Injection Time[Depleted]*Injection Scheme[WAG]	-1.704587	0.83691	-2.04	0.0509
Injection Scheme[WAG]*Kv/Kh	-1.396877	0.720288	-1.94	0.0622
Production Well Type[Vertical]*Injection Scheme[WAG]	1.1097583	0.594749	1.87	0.0722
Injection Well Type[Horizontal at bottom]	1.5006108	0.814273	1.84	0.0756
Production Well Type[Vertical]	-0.995948	0.584317	-1.70	0.0990
Injection Time[Dew Point]*Injection Scheme[WAG]	-1.410336	0.851026	-1.66	0.1083
Permeability*Injection Time[Depleted]	-1.556757	0.943412	-1.65	0.1097
Well Spacing[Two-Third Diagonal]*Production Well Type[Vertical]	1.3522158	0.82597	1.64	0.1124
Injection Well Type[Horizontal at bottom]*Well Spacing[Half Diagonal]	1.7536398	1.147334	1.53	0.1372
Kv/Kh(0.01,1)	-0.967847	0.674003	-1.44	0.1617
Permeability(10,1000)	0.9379115	0.67825	1.38	0.1773
Permeability*Injection Rate	1.0791899	0.794894	1.36	0.1850
Injection Well Type[Vertical]*Injection Time[Dew Point]	-1.591681	1.201744	-1.32	0.1957
Well Spacing[Two-Third Diagonal]*Injection Scheme[WAG]	-1.050767	0.810587	-1.30	0.2051
Injection Rate*Kv/Kh	1.087649	0.839924	1.29	0.2056
Well Spacing[Half Diagonal]*Injection Time[Dew Point]	-1.456298	1.168851	-1.25	0.2228
Injection Time[Depleted]*Production Well Type[Vertical]	1.0343133	0.833571	1.24	0.2246
Permeability*Permeability	-1.722711	1.443571	-1.19	0.2424
Permeability*Well Spacing[Two-Third Diagonal]	-1.073093	0.952462	-1.13	0.2691
Well Spacing[Two-Third Diagonal]*Injection Time[Depleted]	-1.329113	1.215896	-1.09	0.2833
Well Spacing[Half Diagonal]*Kv/Kh	-1.010324	0.959364	-1.05	0.3010
Injection Well Type[Vertical]*Injection Scheme[WAG]	-0.855643	0.835841	-1.02	0.3144
Injection Well Type[Horizontal at bottom]*Injection Time[Dew Point]	1.1894361	1.168913	1.02	0.3173
Injection Time[Depleted]*Kv/Kh	0.9344028	0.989641	0.94	0.3529

Figure 5.7: Sorted parameter coefficients for condensate recovery factor

Response Amount of CO2 stored

Sorted Parameter Estimates

Term	Estimate	Std Error	t Ratio	Prob>|t|
Injection Scheme[WAG]	-9.29615	0.357461	-26.01	<.0001*
Permeability(10,1000)	3.7640579	0.4244	8.87	<.0001*
Permeability*Injection Scheme[WAG]	-2.378056	0.453413	-5.24	<.0001*
Permeability*Permeability	-3.951086	0.903283	-4.37	0.0001*
Injection Time[Depleted]	2.1401354	0.523143	4.09	0.0003*
Injection Time[Depleted]*Injection Scheme[WAG]	-1.608324	0.523678	-3.07	0.0046*
Permeability*Production Well Type[Vertical]	-1.135549	0.439052	-2.59	0.0150*
Injection Well Type[Horizontal at bottom]*Injection Time[Depleted]	-1.571904	0.731356	-2.15	0.0401*
Well Spacing[Half Diagonal]	-1.086307	0.505997	-2.15	0.0403*
Permeability*Kv/Kh	1.0469492	0.525302	1.99	0.0557
Injection Rate*Well Spacing[Half Diagonal]	-1.183992	0.594498	-1.99	0.0559
Permeability*Well Spacing[Half Diagonal]	1.1829479	0.594914	1.99	0.0563
Injection Well Type[Vertical]*Injection Time[Dew Point]	-1.444868	0.751965	-1.92	0.0646
Production Well Type[Vertical]	-0.670432	0.365623	-1.83	0.0770
Injection Rate(4000,12000)	0.7913543	0.431697	1.83	0.0771
Production Well Type[Vertical]*Injection Scheme[WAG]	0.6819105	0.372151	1.83	0.0772
Permeability*Injection Well Type[Vertical]	-1.042842	0.601603	-1.73	0.0936
Injection Well Type[Horizontal at bottom]*Injection Time[Dew Point]	1.262966	0.731421	1.73	0.0949
Injection Rate*Production Well Type[Vertical]	0.7659388	0.444523	1.72	0.0955
Permeability*Injection Rate	0.8433736	0.497388	1.70	0.1007
Injection Scheme[WAG]*Kv/Kh	-0.725641	0.450704	-1.61	0.1182
Injection Rate*Injection Well Type[Vertical]	1.0047698	0.627458	1.60	0.1201
Injection Rate*Injection Time[Dew Point]	0.9492723	0.625084	1.52	0.1397
Injection Time[Dew Point]*Injection Scheme[WAG]	0.8050218	0.532511	1.51	0.1414
Well Spacing[Half Diagonal]*Injection Time[Depleted]	1.0965967	0.729976	1.50	0.1438
Injection Well Type[Horizontal at bottom]*Well Spacing[Half Diagonal]	0.9539005	0.717919	1.33	0.1943
Injection Rate*Injection Scheme[WAG]	-0.589914	0.444808	-1.33	0.1951
Injection Well Type[Vertical]*Injection Scheme[WAG]	0.6778472	0.523009	1.30	0.2052
Well Spacing[Two-Third Diagonal]*Injection Scheme[WAG]	0.5893624	0.507207	1.16	0.2547
Well Spacing[Two-Third Diagonal]*Injection Time[Depleted]	-0.844824	0.76082	-1.11	0.2759
Well Spacing[Half Diagonal]*Kv/Kh	-0.653853	0.600301	-1.09	0.2850
Permeability*Well Spacing[Two-Third Diagonal]	-0.644554	0.595982	-1.08	0.2884
Injection Well Type[Horizontal at bottom]*Well Spacing[Two-Third Diagonal]	-0.763902	0.741951	-1.03	0.3117
Well Spacing[Half Diagonal]*Production Well Type[Vertical]	0.4999341	0.512683	0.98	0.3376
Injection Well Type[Horizontal at bottom]*Production Well Type[Vertical]	-0.507093	0.522047	-0.97	0.3394

Figure 5.8: Sorted parameter coefficients for amount of CO_2 stored

For condensate recovery objective as shown in Figure 5.7, two most influential factors are well spacing, injection time and interaction effect of these two factors. Larger well spacing results in higher condensate recovery factor because CO_2 has to take more time to reach the production well which can prevent CO_2 breakthrough. Injection at dew point pressure provides higher condensate recovery

than injection after depletion. After gas is precedingly produced by natural depletion, injection at dew point pressure can maintain gas production rate longer or, in turn, more condensate is recovered by pressure maintenance, all contributing to enhanced condensate recovery. On the other hand, CO_2 injection after depletion can recover less condensate compared to injection at dew point pressure because constant condensate production period is shorter, resulting in low condensate recovery. While initial injection shows least condensate recovery because injection of CO_2 at the beginning will cause early CO_2 breakthrough although no condensate dropout occurs. Lastly, interaction effect of well spacing and injection time appears to be significant. Combination of half-diagonal spacing and injection after depletion has the most significant effect on condensate recovery among other combinations. At small well spacing, injection after depletion can prevent early CO_2 breakthrough together with the aid of small spacing to accelerate recovery process, and subsequently more condensate can be recovered unlike other injection time scenarios which will cause early CO_2 breakthrough.

For CO_2 sequestration objective, two most influential factors are injection scheme, permeability and interaction effect of injection scheme and permeability as depicted in Figure 5.8. Injection scheme shows the most influential effect on CO_2 sequestration objective. WAG injection has beneficial effect on mobility control which results in better condensate recovery but jeopardizes amount of CO_2 injected into the reservoir. Continuous CO_2 injection is more likely to cause early CO_2 breakthrough and less condensate recovery is consequently inflicted. However, a large amount of CO_2 can be injected into the reservoir, contributing to CO_2 sequestration objective. Permeability is another influential factor on CO_2 sequestration. Higher permeability assists CO_2 to channel through pore spaces more easily, and subsequently fracture pressure is not prematurely reached. This contributes to a large amount of CO_2 injected and stored in the reservoir. Lastly, interaction effect between injection scheme and permeability shows that amount of CO_2 increases with increasing permeability together with the aid of continuous CO_2 injection because CO_2 can easily channel through the pore spaces in high permeability reservoir as described before. On the other hand, WAG injection in high permeability shows

adverse effect on amount of CO_2 stored because water will occupy a large amount of pore space, which results in lower amount of CO_2 stored in the reservoir.

In order to see main and interaction effects at the same time, JMP can generate 3-D response surface using 'Surface Profiler' platform. One of the 3-D response surfaces for condensate recovery factor at different permeabilities and different injection rates in which other parameters are kept constant is shown in Figure 5.9.

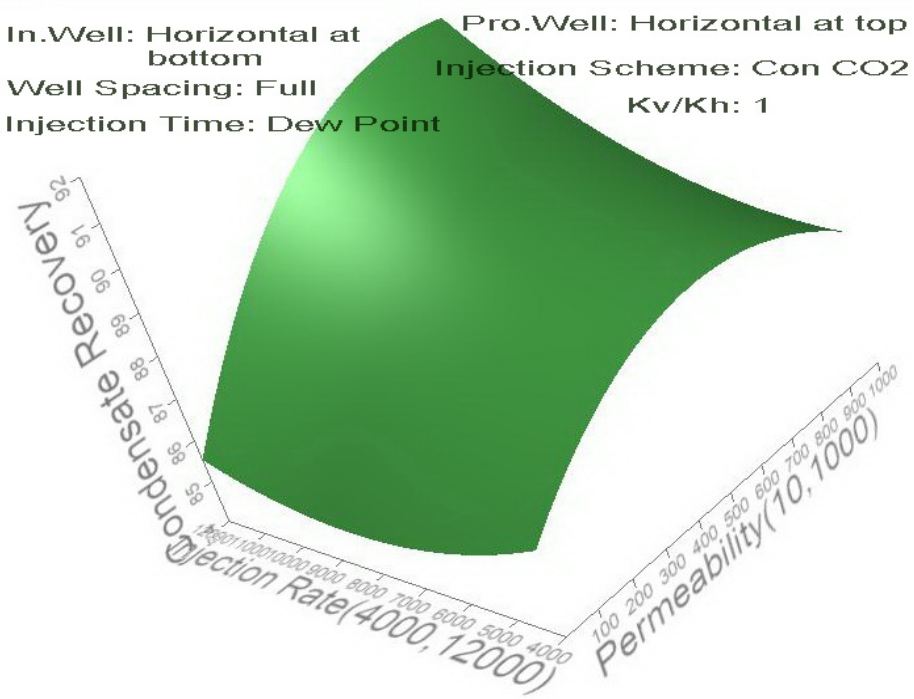

Figure 5.9: 3-D response surface for condensate recovery factor

From Figure 5.9, 3-D response surface presents two parameters on the x-axis; namely, permeability and injection rate, and condensate recovery factor on the y-axis. Interaction effects can be clearly seen in 3-D response. Focus on change of permeability shows that condensate recovery factor increases with increasing permeability. CO_2 in higher permeability reservoir will spread all over the reservoir more easily than low permeability case. Hence, CO_2 takes more time to reach the production well, which results in higher condensate recovery factor. Focus on change of injection rate shows that at low permeability condensate recovery factor decreases with increasing injection rate because high injection rate of CO_2 at low permeability will cause early breakthrough, which results in lower recovery. On the other hand, at high permeability, condensate recovery factor increases with increasing injection rate.

This is because high injection rate results in longer production lifetime and CO_2 can spread all over the reservoir with higher swept area and more time for CO_2 to break through, all contributing to the condensate recovery. Additionally, high k_v/k_h results in higher recovery factor only at high injection rate because the hydrocarbon production is enhanced by more amount of CO_2 injected. Full well spacing results in high condensate recovery because CO_2 injected into the reservoir has much enough time to flood hydrocarbon gas before reaching the production well. CO_2 injection at dew point pressure helps prolong condensate plateau production rate which results in high condensate recovery. Placing horizontal injection well at the bottom part of the reservoir lets CO_2 push much hydrocarbon gas upward due to large contact area of horizontal well and placing horizontal production well at the top part of the reservoir can obtain much of hydrocarbon gas due to large contact area. However, injection of continuous CO_2 does not show significant difference of condensate recovery factor compared to that of WAG injection.

Effects of parameters on amount of CO_2 stored are shown in Figure 5.10. Unlike 3-D response surface of condensate recovery factor, trend of this response behaves in the same way for change of both parameters. At low and high injection rate, the amount of CO_2 stored increases with increasing permeability because higher permeability causes CO_2 to easily channel through the pore space and more time for fracture pressure to be reached, benefiting amount of CO_2 stored. At low and high permeability, the amount of CO_2 stored increases with increasing injection rate due to higher amount of injected CO_2. Additionally, change of k_v/k_h shows effects on the response. High K_v/K_h has beneficial effect on amount of CO_2 stored because it is easy for CO_2 to travel down the reservoir and hence more CO_2 stored can be stored. CO_2 injection at dew point pressure shows good effect on amount of CO_2 stored because much hydrocarbon gas is produced without condensate dropout, so there are large available pore spaces for CO_2 to be stored. Placing horizontal injection well at the bottom part can displace much of hydrocarbon gas, and therefore large available pore spaces are available for CO_2 to be stored.

C

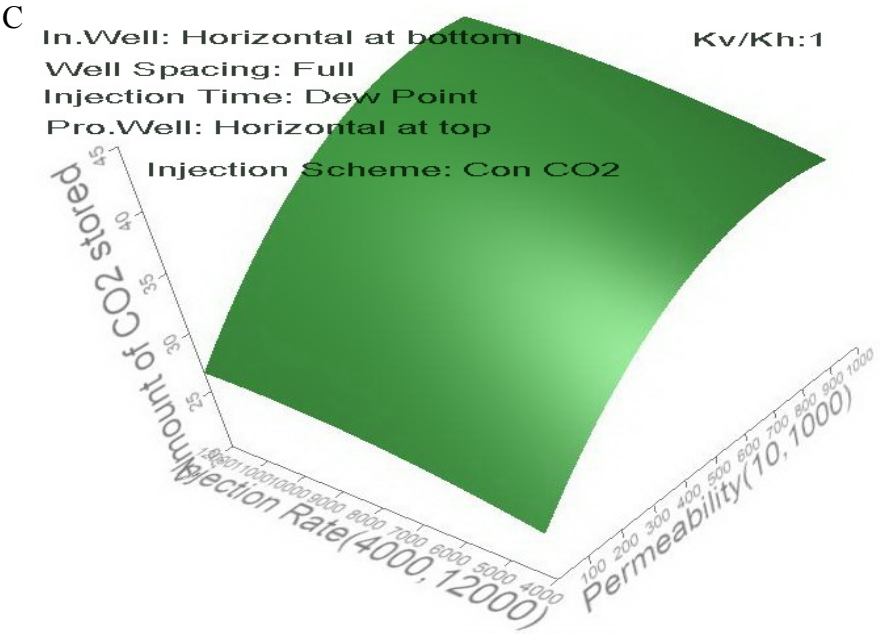

Figure 5.10: 3-D response surface for amount of CO_2 stored with continuous CO_2 injection

If the injection scheme which has the most influential effect on CO_2 storage is switched to WAG injection, the 3-D response surface for the amount of CO_2 stored is shown in Figure 5.11

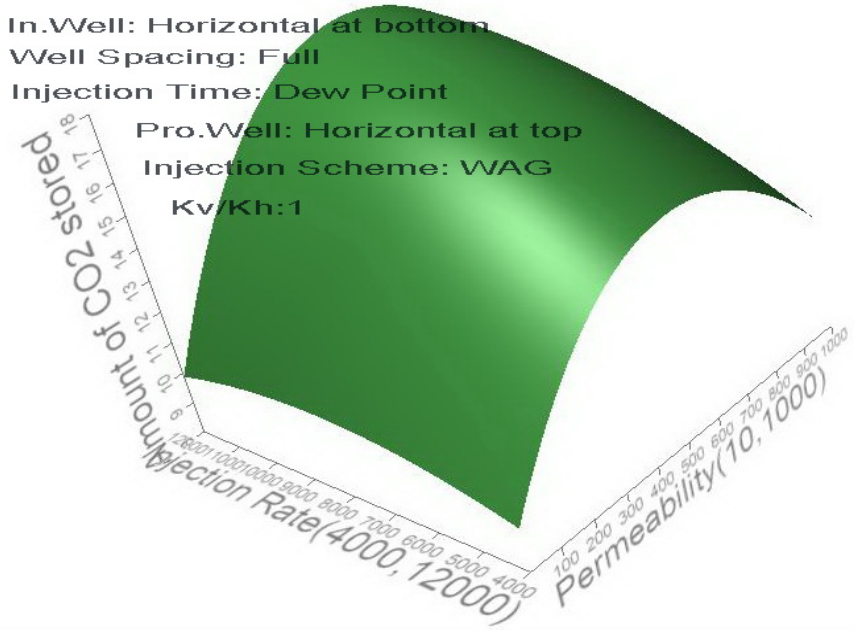

Figure 5.11: 3-D response surface for amount of CO_2 stored with WAG injection

Let's first focus on change of response at low permeability. The amount of CO_2 stored increases with increasing injection rate but tends to decrease after injection rate of 8000 Mscf/D is passed. At the beginning, higher injection rate results in increasing response due to additional amount of CO_2 injected. However, too high injection rate will cause early breakthrough, which results in lower response. On the other hand, at high permeability the response increases with increasing injection rate because high permeability causes CO_2 to channel through pore space more easily and more amount of CO_2 stored is gained. Focus on change of permeability shows that at every level of injection rate the response tends to increases first and then decreases after 700-mD permeability is passed. This is because at very high permeability, massive amount of water occupies pore space; so less amount of CO_2 can be stored due to less pore space. Large well spacing does not help increase the amount of CO_2 stored but in turn increases the amount of water in pore spaces. WAG injection at dew point pressure is not able to sustain the reservoir pressure as well as supercritical pure CO_2 is, resulting in low available pore spaces for CO_2 to be stored. Using horizontal wells allows a large amount of water to contact with reservoir, and consequently water occupies lot of pore spaces with decrease of amount of CO_2 stored.

5.2 Proxy Cross Validation Experiments

As stated in Section 4.5, cross-validation experiments are randomly generated by JMP to validate the proxy model. Relevant simulation results according to 30-case experiments are obtained as shown by Table 5.2.

Table 5.2: Simulation results of 30-case cross-validation experiments

Run ID	Validation Table								Condensate recovery factor (%)	Amount of CO_2 stored (Bscf)
	Permeability (md)	Injection rate (Mscf/D)	Injection well type	Well spacing	Injection time	Production well type	Injection scheme	kv/kh		
1	604	8800	Horizontal at bottom	Full diagonal	Depleted	Vertical	WAG	1	62.10	11.39
2	406	7200	Horizontal at bottom	Two-third diagonal	Dew point	Vertical	Continuous CO_2	0.01	71.55	31.80
3	208	4000	Horizontal at top	Full diagonal	Initial	Horizontal at top	Continuous CO_2	0.802	69.73	30.62
4	10	10400	Horizontal at top	Half diagonal	Dew point	Vertical	WAG	0.604	57.02	6.21
5	802	12000	Vertical	Full diagonal	Depleted	Horizontal at top	Continuous CO_2	0.208	59.89	40.42
6	1000	5600	Vertical	Two-third diagonal	Depleted	Vertical	WAG	0.406	61.06	12.82
7	802	10400	Horizontal at bottom	Half diagonal	Dew point	Horizontal at top	WAG	0.01	62.08	12.05
8	604	4000	Horizontal at bottom	Two-third diagonal	Depleted	Vertical	WAG	0.406	60.38	12.36
9	208	5600	Horizontal at top	Half diagonal	Initial	Horizontal at top	Continuous CO_2	1	56.06	26.50
10	1000	8800	Vertical	Full diagonal	Depleted	Horizontal at top	WAG	0.802	59.29	13.35
11	10	7200	Vertical	Half diagonal	Initial	Vertical	Continuous CO_2	0.208	44.14	15.62
12	406	12000	Horizontal at bottom	Full diagonal	Depleted	Vertical	Continuous CO_2	0.604	61.50	38.15
13	802	4000	Horizontal at bottom	Half diagonal	Depleted	Horizontal at top	WAG	0.208	58.67	12.90
14	10	7200	Horizontal at top	Full diagonal	Dew point	Horizontal at top	Continuous CO_2	0.406	86.95	24.42
15	604	10400	Horizontal at top	Two-third diagonal	Depleted	Horizontal at top	WAG	0.01	59.82	12.36
16	1000	8800	Vertical	Half diagonal	Initial	Horizontal at top	Continuous CO_2	0.604	58.02	32.08
17	406	5600	Horizontal at bottom	Full diagonal	Initial	Horizontal at top	Continuous CO_2	1	64.73	31.17
18	208	12000	Horizontal at bottom	Half diagonal	Dew point	Vertical	WAG	0.802	63.44	8.78
19	208	4000	Horizontal at top	Full diagonal	Dew point	Vertical	Continuous CO_2	0.802	76.59	31.29
20	1000	5600	Horizontal at top	Two-third diagonal	Initial	Vertical	WAG	0.406	63.55	9.28
21	604	8800	Vertical	Half diagonal	Depleted	Horizontal at top	Continuous CO_2	1	54.55	36.87
22	10	10400	Horizontal at bottom	Full diagonal	Initial	Horizontal at top	WAG	0.604	85.24	10.26
23	802	12000	Horizontal at bottom	Two-third diagonal	Dew point	Horizontal at Top	WAG	0.208	77.32	12.78

Table 5.2: Simulation results of 30-case cross-validation experiments (continued)

24	406	7200	Horizontal at top	Full diagonal	Initial	Vertical	WAG	0.01	74.27	10.15
25	604	7200	Horizontal at top	Two-third diagonal	Initial	Horizontal at top	Continuous CO_2	0.01	67.49	31.93
26	208	12000	Horizontal at bottom	Full diagonal	Dew point	Vertical	WAG	0.208	72.33	11.05
27	406	8800	Horizontal at bottom	Half diagonal	Dew point	Horizontal at top	Continuous CO_2	1	65.70	29.71
28	1000	10400	Horizontal at bottom	Two-third diagonal	Depleted	Vertical	Continuous CO_2	0.604	59.76	40.41
29	10	5600	Horizontal at top	Half diagonal	Initial	Horizontal at top	WAG	0.406	40.58	4.27
30	802	4000	Vertical	Full diagonal	Dew point	Horizontal at top	WAG	0.802	77.57	12.14

To validate the proxy model, two responses which are predicted by the proxy model have to be obtained. Hence, the following steps are conducted to construct the proxy model function which will be used to predict the responses.

1.) All parameter coefficients are obtained from JMP as shown in Figure 5.12

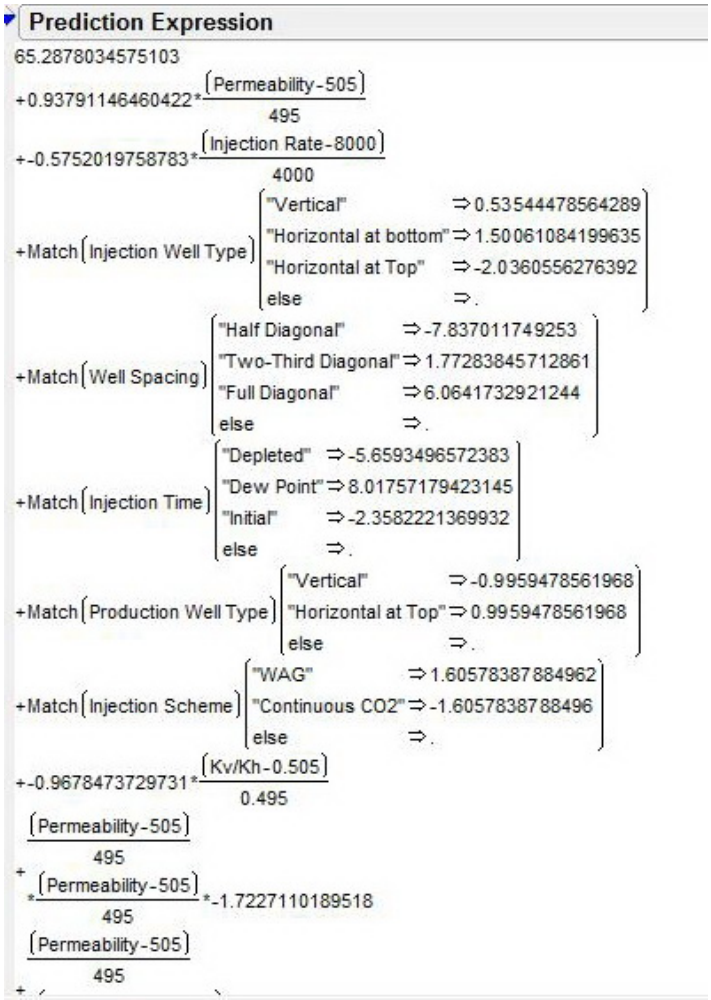

Figure 5.12: Parameter coefficients obtained from JMP

2.) Generate proxy model function using Visual Basic Application in Excel.

3.) The proxy model function with parameter input is prompted to be used as shown by Figure 5.13

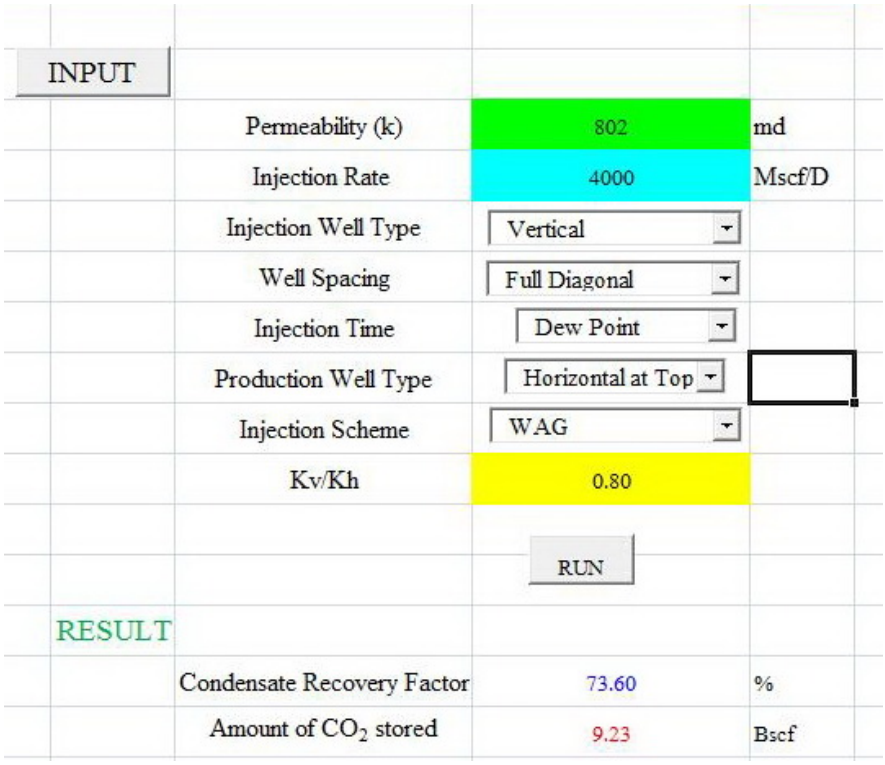

Figure 5.13: Proxy model function

Subsequently, the generated proxy model function can be used to predict the responses according to 30-case cross-validation experiments as shown by Table 5.3.

Table 5.3: ECLIPSE and predict responses of 30-case cross-validation experiments

Run ID	ECLIPSE condensate recovery factor (%)	Predicted condensate recovery Factor (%)	ECLIPSE amount of CO_2 stored (Bscf)	Predicted amount of CO_2 stored (Bscf)
1	62.10	57.06	11.39	11.63
2	71.55	73.72	31.80	27.48
3	69.73	71.57	30.62	26.97
4	57.02	56.89	6.21	4.66
5	59.89	57.95	40.42	40.24
6	61.06	60.98	12.82	7.72
7	62.08	60.32	12.05	17.13
8	60.38	58.71	12.36	8.36
9	56.06	39.42	26.50	19.18
10	59.29	53.53	13.35	13.13
11	44.14	45.16	15.62	18.89
12	61.50	60.51	38.15	35.20
13	58.67	65.51	12.90	15.87
14	86.95	79.76	24.42	23.59
15	59.82	54.05	12.36	14.58
16	58.02	52.66	32.08	31.27
17	64.73	72.65	31.17	31.72
18	63.44	63.69	8.78	11.00
19	76.59	79.09	31.29	26.44
20	63.55	63.28	9.28	8.42
21	54.55	53.77	36.87	38.53
22	85.24	79.86	10.26	6.00
23	77.32	81.27	12.78	17.66
24	74.27	74.66	10.15	13.51
25	67.49	58.16	31.93	31.51
26	72.33	77.84	11.05	15.84
27	65.70	68.49	29.71	30.87
28	59.76	55.73	40.41	35.00
29	40.58	53.97	4.27	3.35
30	77.57	73.32	12.14	10.40

After that, comparison between predicted and ECLIPSE responses has to be performed in order to investigate the difference between them by using statistical test called ‘Matched Pairs t-test’ platform as shown in Figure 5.14 and Figure 5.15.

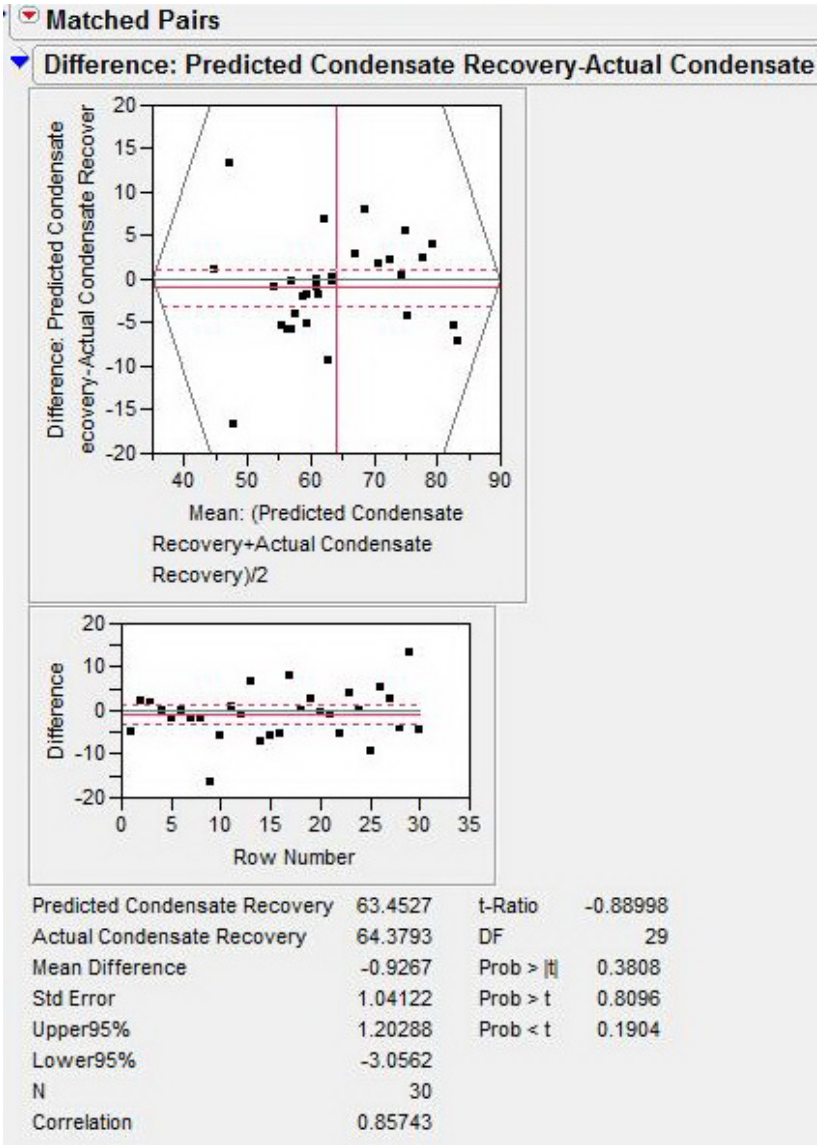

Figure 5.14: Matched pairs t-test between ECLIPSE and predicted responses for condensate recovery factor

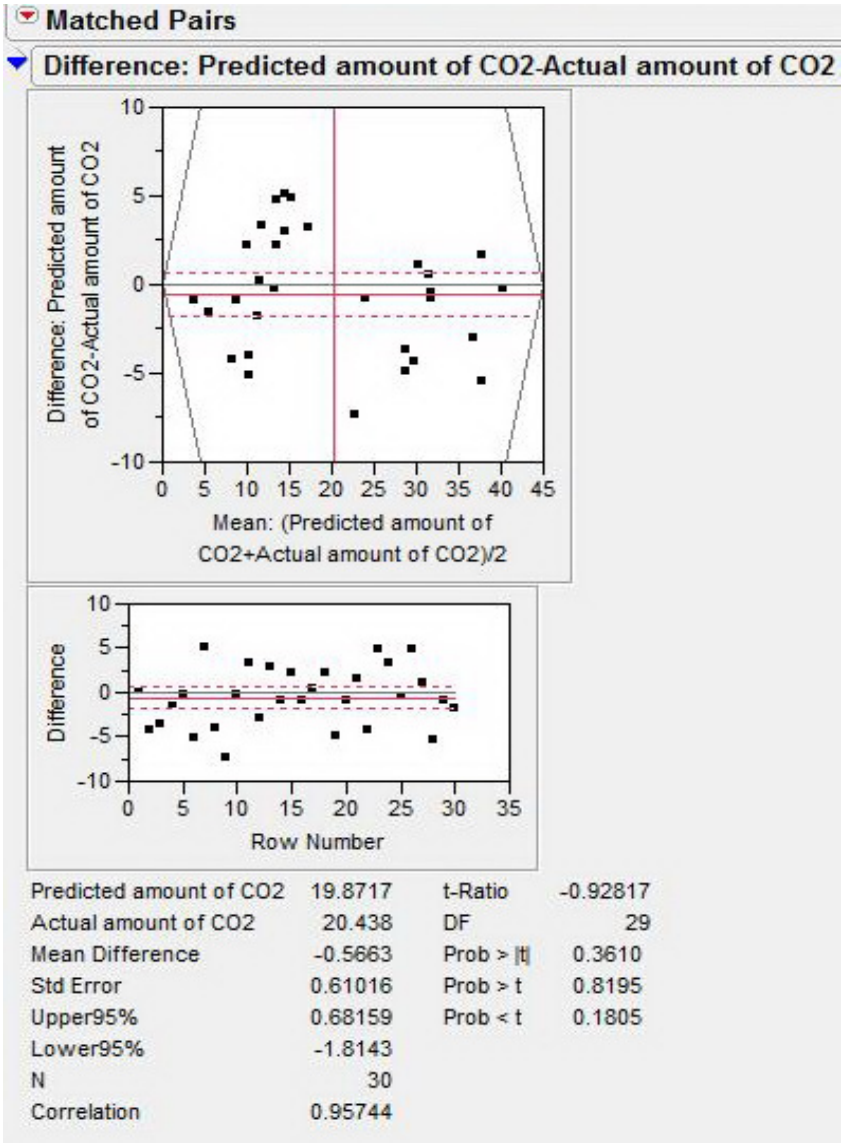

Figure 5.15: Matched pairs t-test between ECLIPSE and predicted responses for amount of CO_2 stored

Both figures plot the difference between predicted and ECLIPSE responses on the vertical axis and the mean of predicted and ECLIPSE responses on the horizontal axis. The horizontal solid line represents average difference of predicted and ECLIPSE responses whereas the vertical solid line represents average mean of both values. The horizontal dashed line shows 95% confidence interval of the difference. Graphically, the solid horizontal lines at zero in Figure 5.14 and Figure 5.15 both fall inside the confidence interval. This means that predicted and ECLIPSE responses are

not statistically different with 95% confidence. The interpretation can be confirmed by t-test results ("Prob>|t|", "Prob>t", and "Prob<t") which all are greater than 0.05.

Moreover, proxy model of amount of CO_2 stored has better predictability than that of condensate recovery factor by observing the plot between number of experiment points and difference. Almost all the differences between ECLIPSE and predicted recovery factor are within a range of +7% to -7% condensate recovery factor whereas those of amount of CO_2 stored are + 5 Bscf to -5 Bscf. T-test results of Figure 5.15 are greater than those of Figure 5.14 which also strengthens the interpretation that the amount of CO_2 stored has a better fit.

As a result, the quadratic proxy model can adequately fit the predicted results for both responses and therefore can be employed as a tool to predict optimum strategies and parameters of the candidate reservoir considered for maximizing condensate recovery and amount of CO_2 stored simultaneously in accordance with the objective of this study.

5.3 Parameter & Strategy Optimization

After validating the proxy model with cross-validation experiments in Section 5.2, the 'Prediction Profiler' in JMP is subsequently used to predict optimum parameters and strategies for maximizing two objective functions. Figure 5.16 presents optimum parameters & strategies predicted by 'Prediction Profiler' platform.

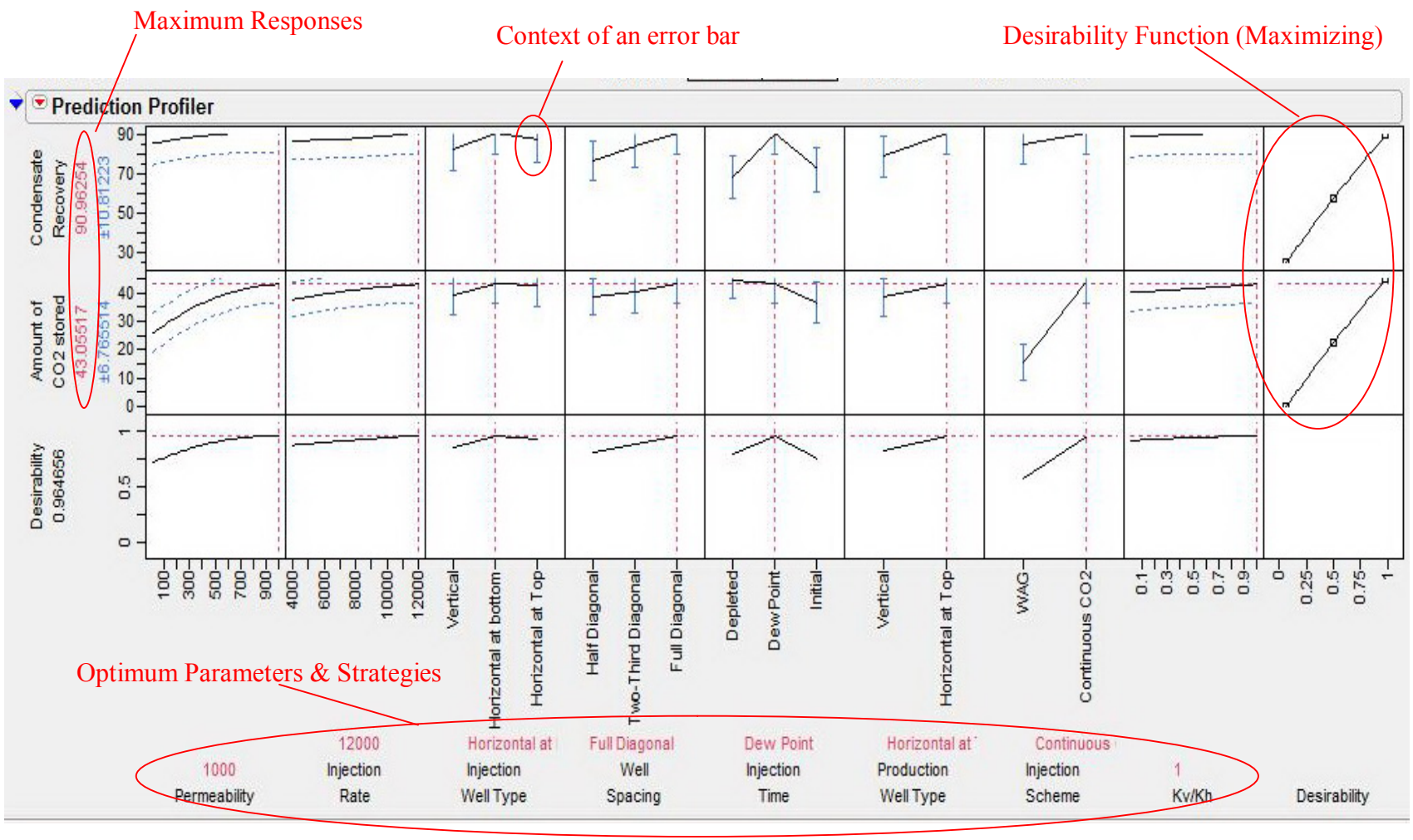

Figure 5.16: Optimum parameters & strategies predicted by 'Prediction Profiler' platform

Figure 5.16 shows optimum parameters & strategies on the horizontal line and both maximum predicted responses highlighted by red color on the vertical line. Blue values next to the response values represent 95% confidence interval of the responses. Desirability trace (solid curve) of each factor located at the bottom row shows how well the responses meet what the experimenter desires. Current desirability of each factor is shown by the intersection between the vertical and horizontal dashed lines. In this study, maximizing desirability function is set as the target which is represented by the right-hand desirability function traces. The more the response is, the more desirable the trace is. So, it can be seen that all intersection points represent as much as possible desirability, which in the figure is 0.964656, according to all optimum parameters and strategies. All these optimum parameters and strategies result in maximum condensate recovery factor and amount of CO_2 stored in accordance with the maximizing desirability function. The response or prediction line of each factor is all located in the top two rows in which one row is for condensate recovery factor and the other is for amount of CO_2 stored. Like desirability traces, current responses can be obtained from the intersection between the vertical and horizontal dashed lines, which leads to maximum predicted responses highlighted by red color for both objective functions. The 95% confidence interval of each response is represented by a dotted blue curve surrounding the predicted line for numerical parameters or by a context of an error bar for categorical parameters.

In summary, the optimum parameters and strategies as well as the predicted responses for both objectives are presented in Table 5.4

Table 5.4: Optimization scenario and predicted responses by proxy model

Parameters & Strategy	**Value**
Permeability (md)	1000
Injection rate (Mscf/D)	12000
Injection well type	Horizontal at Bottom
Well spacing	Full Spacing
Injection time	Dew Point
Production well type	Horizontal at Top
Injection scheme	Continuous CO_2
kv/kh	1
Condensate recovery factor (%)	**90.96**
CO_2 storage (Bscf)	**43.06**

The responses acquired from corresponding simulation run for the parameters and strategy shown in Table 5.4 which are 84.77% condensate recovery factor and 38.716 Bscf of CO_2 stored are compared to 90.96% and 43.06 Bscf obtained from the proxy model. The difference between predicted and ECLIPSE response of condensate recovery factor is 6.14% while that of amount of CO_2 stored is 4.34 Bscf. Considering the cross-validation process by t-test, the results from proxy model are acceptable although the predicted results are not exactly the same with ECLIPSE results but it can predict optimum parameters and strategy for maximizing both objective functions as a guideline for development planning in accordance with the objectives of this study.

The results shown in Table 5.4 suggest good candidate for implementing coupled CO_2 sequestration and enhanced condensate recovery project. High permeability gas condensate reservoirs with high kv/kh ratio are good candidates for coupled CO_2 sequestration and enhanced condensate recovery. CO_2 can more easily channels through the pore spaces in 1000-md permeability reservoir with high k_v/k_h compared to 10-md permeability reservoir and therefore CO_2 has longer time to be

sequestered till the fracture pressure constraint is reached as shown in Figure 5.17. This contributes to amount of CO_2 injected and stored into the reservoir as shown in Figure 5.18. At the same time, longer condensate plateau rate can be achieved due to lower pressure drop, resulting in more condensate production. Figure 5.19 shows bottomhole pressure of production well, and Figure 5.20 shows condensate production rate of 1000-md and 10-md permeability.

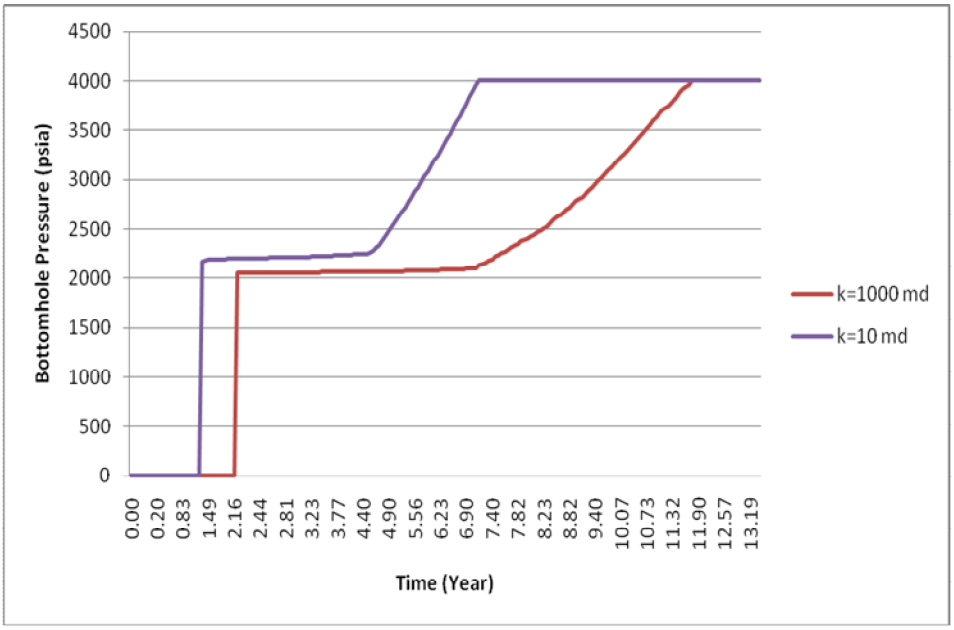

Figure 5.17: Bottomhole pressure of injector for 1000-md and 10-md permeability

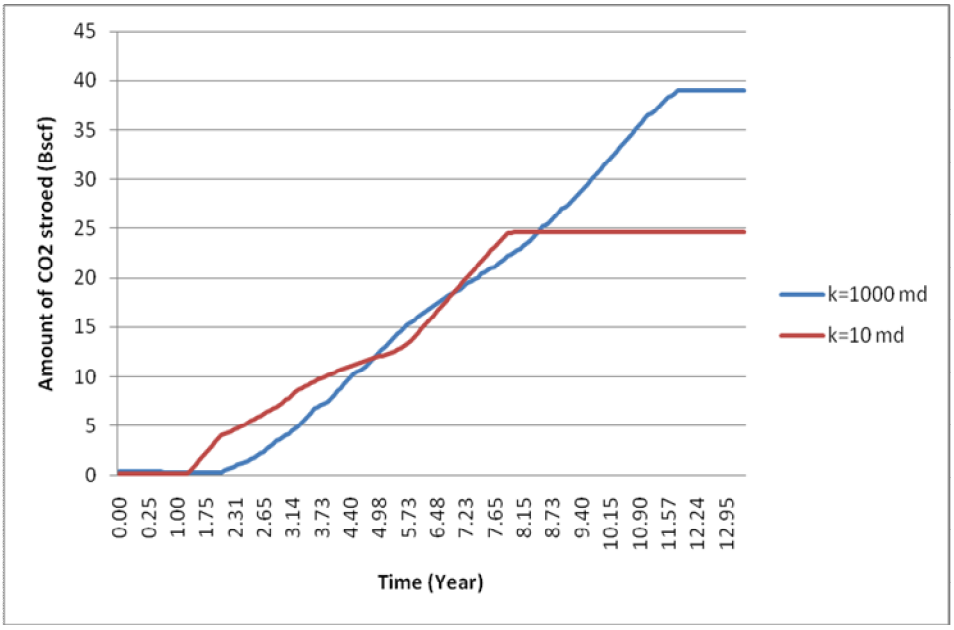

Figure 5.18: Amount of CO_2 stored for 1000-md and 10-md permeability

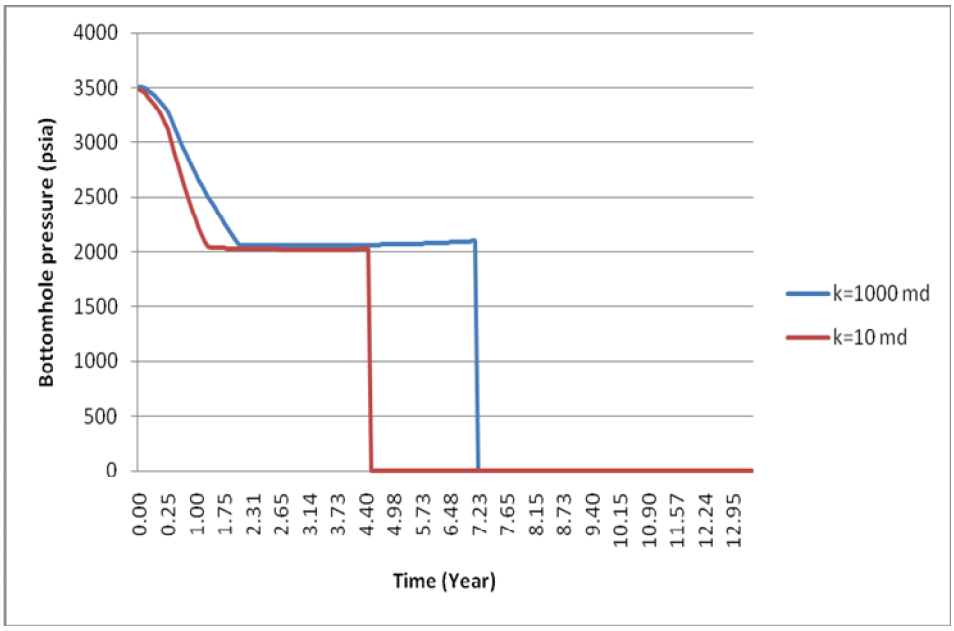

Figure 5.19: Bottomhole pressure of producer for 1000-md and 10-md permeability

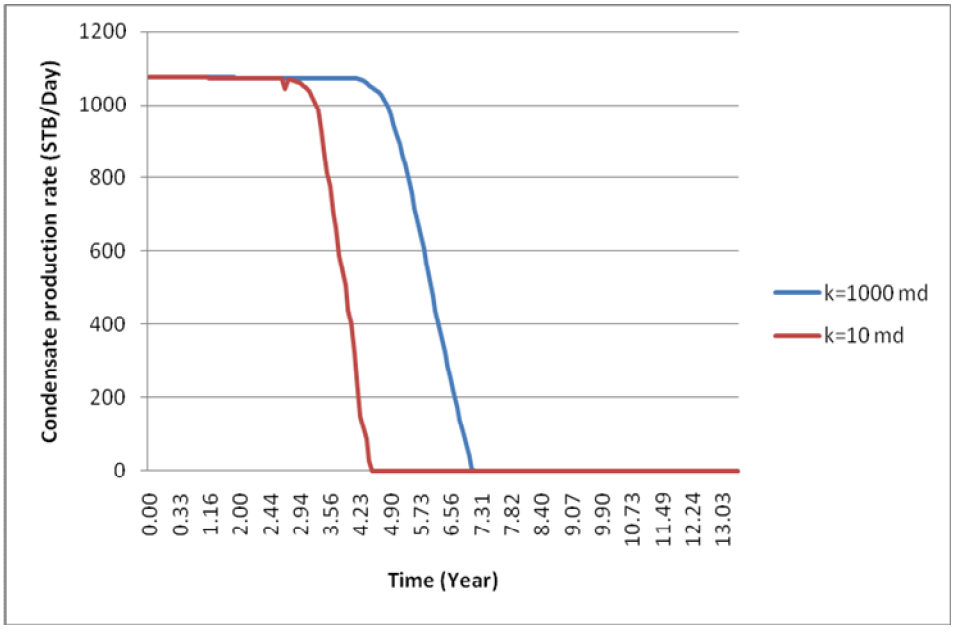

Figure 5.20: Condensate production rate for 1000-md and 10-md permeability

Injection with continuous CO_2 or pure CO_2 is more beneficial to the amount of CO_2 stored with the aid of full well spacing, allowing CO_2 to have more time to spread as much as possible in the pore spaces. Consequently, pure CO_2 injection shows higher amount of CO_2 stored when compared with WAG injection as shown in Figure 5.21. Less amount of injected CO_2 in WAG injection causes lower amount of CO_2 stored. Additionally, injected water occupies the pore spaces represented by water saturation as shown by Figure 5.22. The water impedes CO_2 to be injected due to high density of water, causing fracture pressure to be rapidly reached as shown in Figure 5.23, resulting in lower amount of CO_2 stored. For condensate recovery, there is no difference on total condensate production between these two injection schemes although pure CO_2 injection shows a little bit longer condensate plateau period. Figure 5.24 shows total condensate production, and Figure 5.25 shows condensate production rate of two injection schemes.

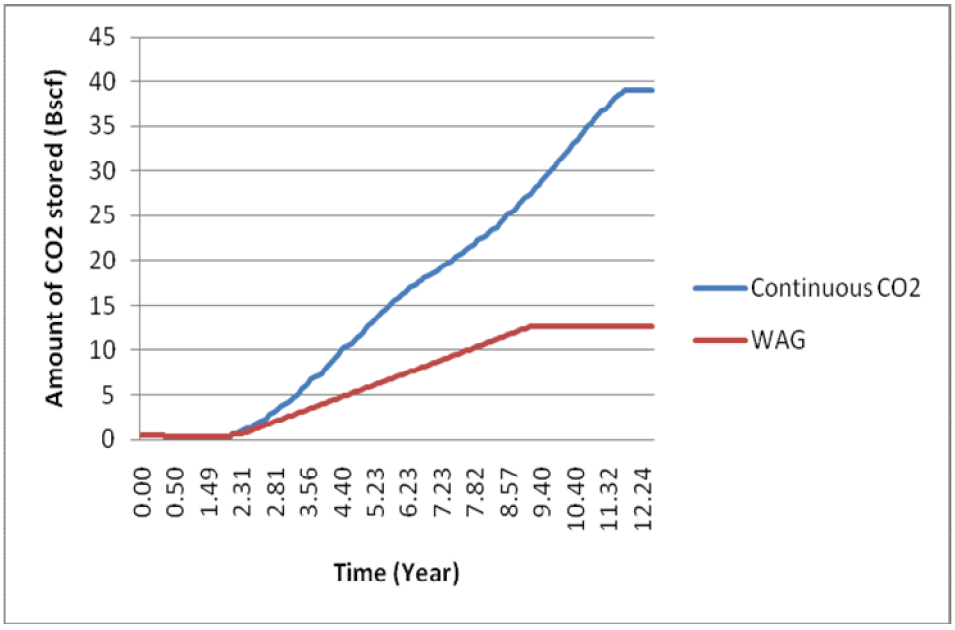

Figure 5.21: Amount of CO_2 stored for continuous CO_2 and WAG injection

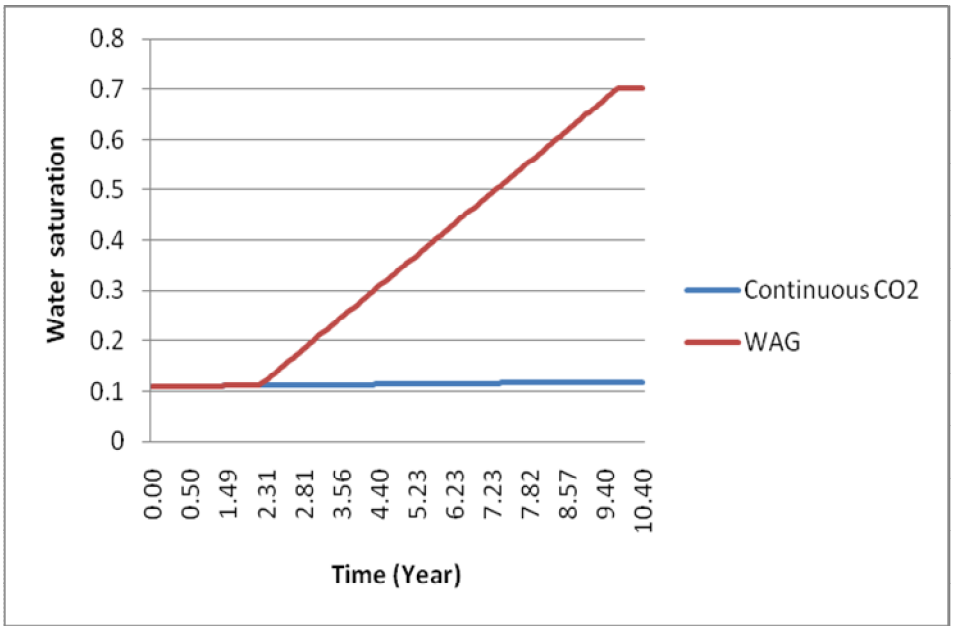

Figure 5.22: Water saturation for continuous CO_2 and WAG injection

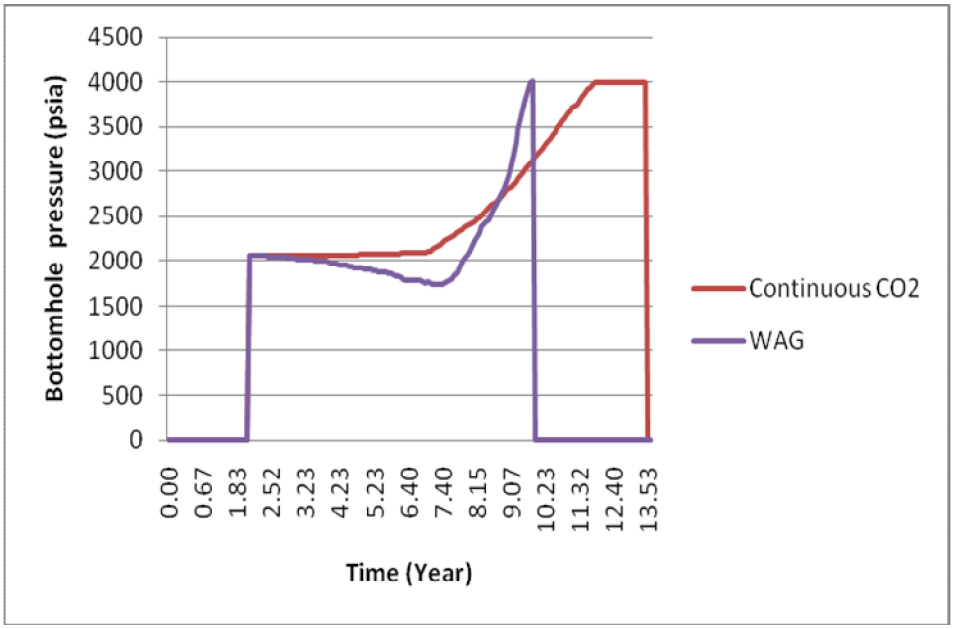

Figure 5.23: Bottomhole pressure of injector for continuous CO_2 and WAG injection

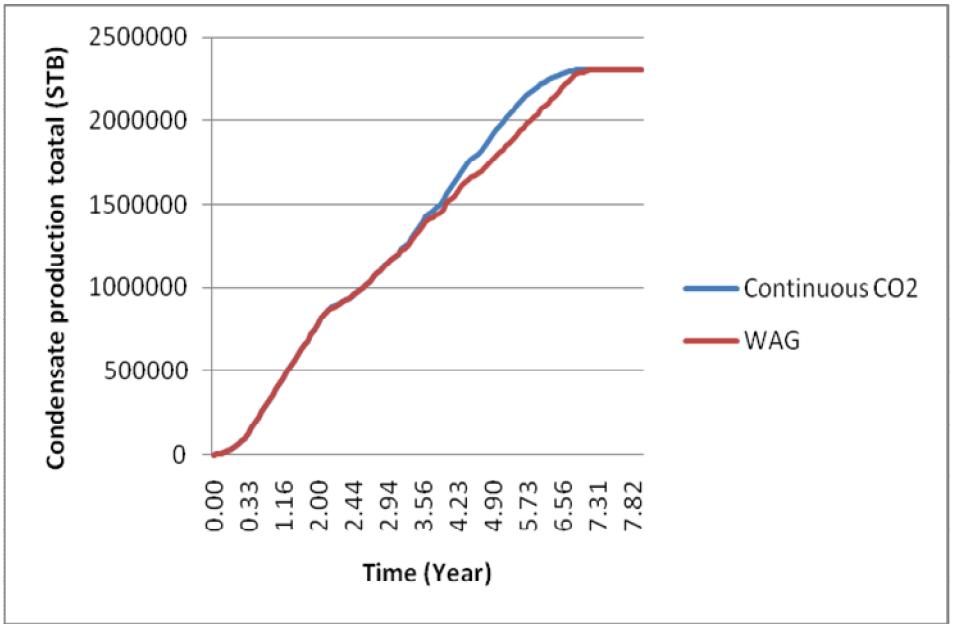

Figure 5.24: Condensate production total for continuous CO_2 and WAG injection

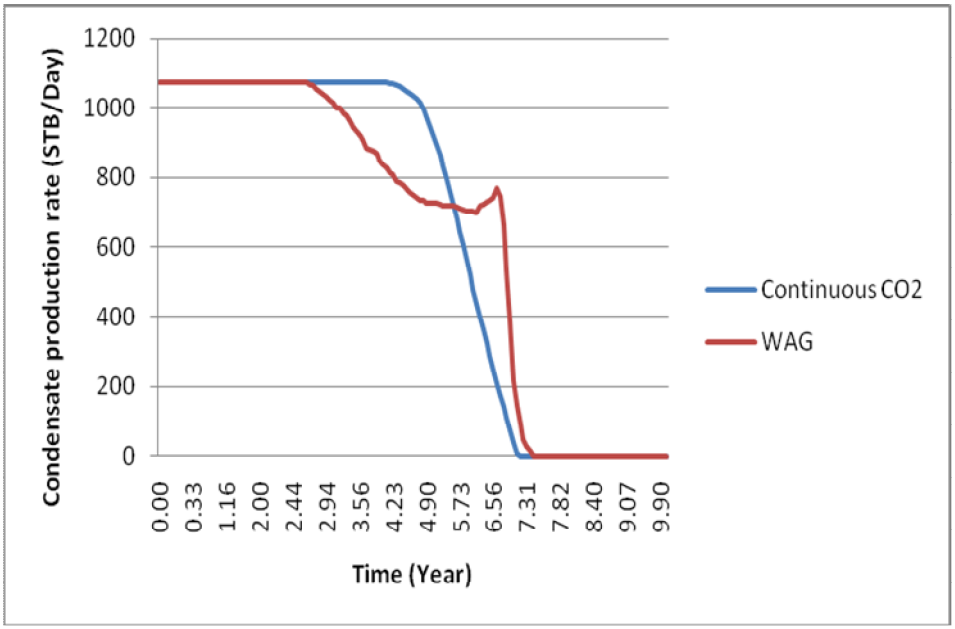

Figure 5.25: Condensate production rate for continuous CO_2 and WAG injection

Injection at the dew point shows much more condensate recovery when compared to the other cases because the condensate production plateau rate is sustained to be longer which contributes to enhanced condensate recovery. Although the amount of CO_2 stored for injection at dew point pressure is less than that of CO_2 injection after depletion, condensate production with injection at dew point pressure is quite higher than that of injection at depleted condition. So, injection at dew point is recommended in accordance with maximization on two responses. Injection at initial production shows both low condensate recovery and low amount of CO_2 stored because early CO_2 breakthrough causes impaired condensate recovery and fracture pressure is reached too rapidly, resulting in low amount of CO_2 stored. Figure 5.26 shows condensate production rate, and Figure 5.27 shows the amount of CO_2 stored for different injection times.

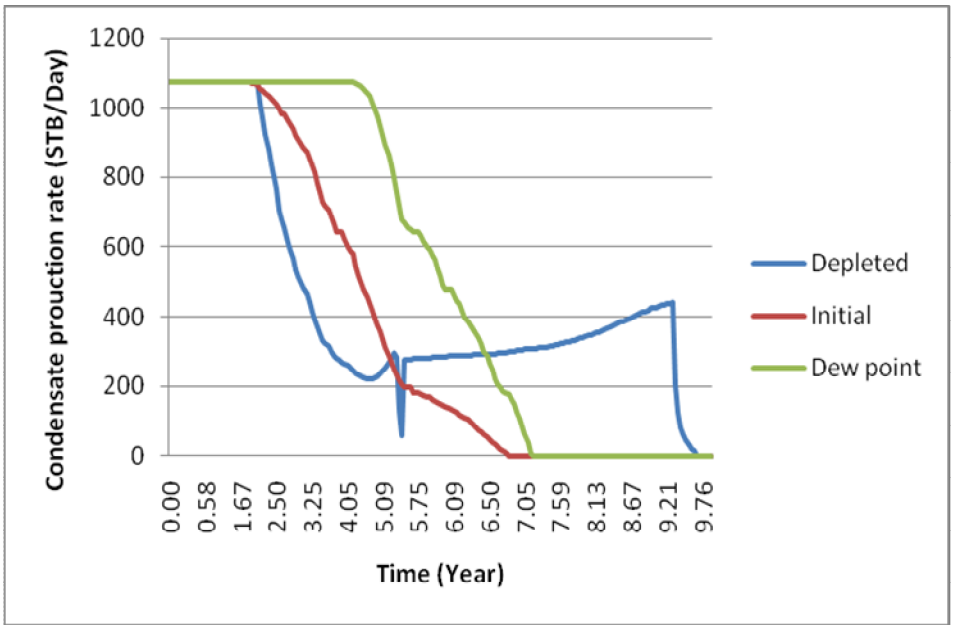

Figure 5.26: Condensate production rate for different injection times

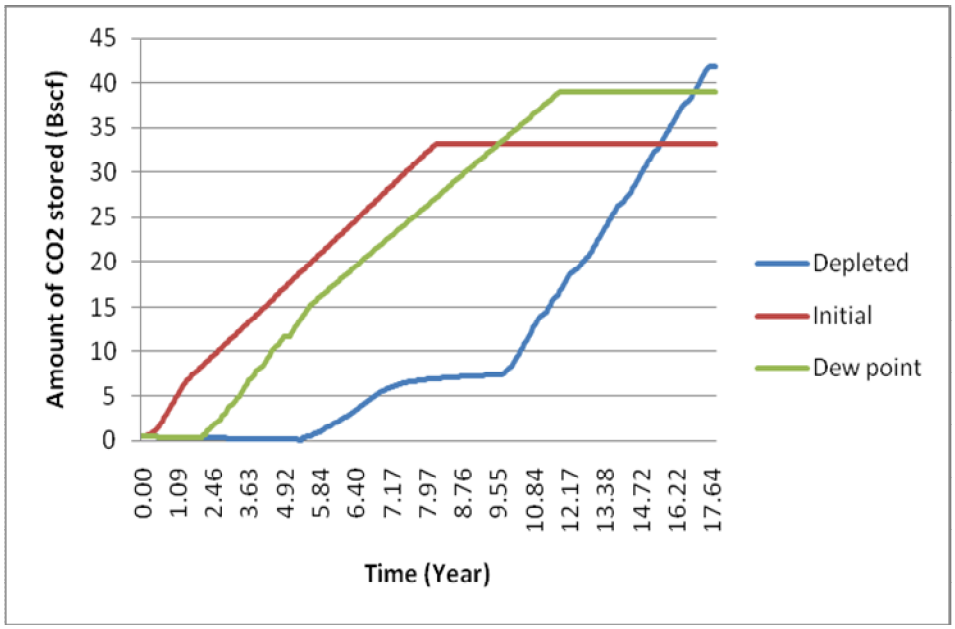

Figure 5.27: Amount of CO_2 stored for different injection times

High injection rate at 12000 Mscf/D assists in hydrocarbon displacement and increases more amount of CO_2 injected when compared to low injection rate at 4000 Mscf/D. Although low injection rate will hold CO_2 longer before reaching the production well which is represented by longer production period as shown in Figure 5.28, but finally total condensate recovery and amount of CO_2 injected by high injection rate is more than those obtained by low injection rate case. Consequently, higher amount of CO_2 stored is achieved. Figure 5.29 shows total condensate production for injection rate at 12000 Mscf/D and 4000 Mscf/D, and Figure 5.30 shows amount of CO_2 stored for both injection rates.

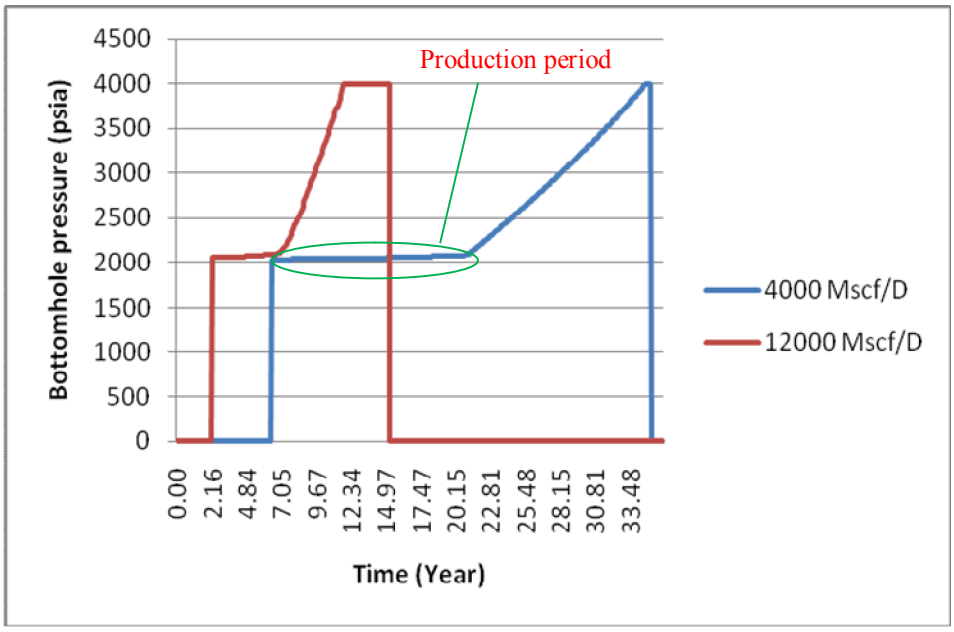

Figure 5.28: Bottomhole pressure of injector for 4000 Mscf/D and 12000 Mscf/D of injection rate

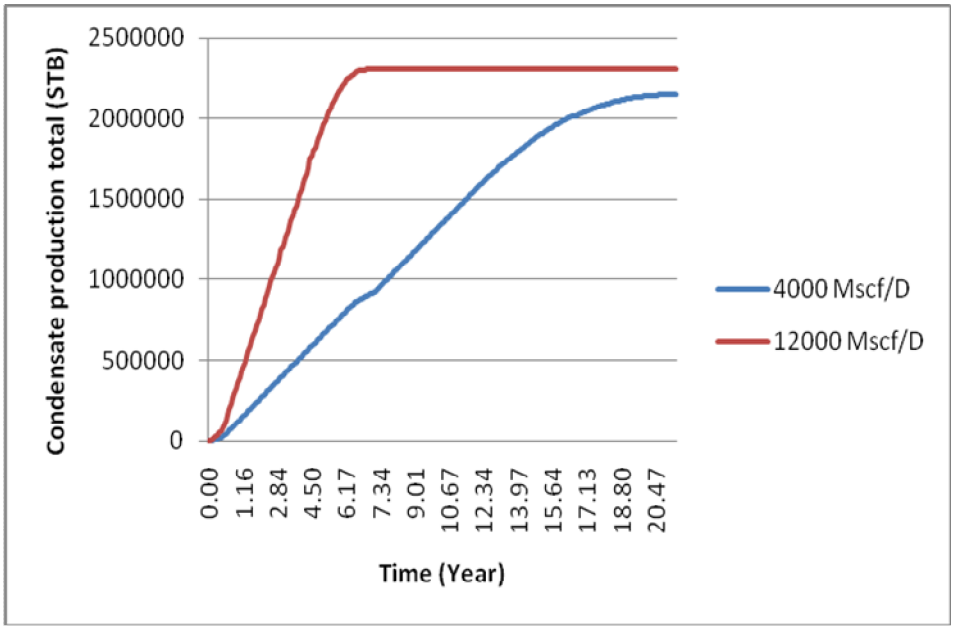

Figure 5.29: Condensate production total for 4000 Mscf/D and 12000 Mscf/D of injection rate

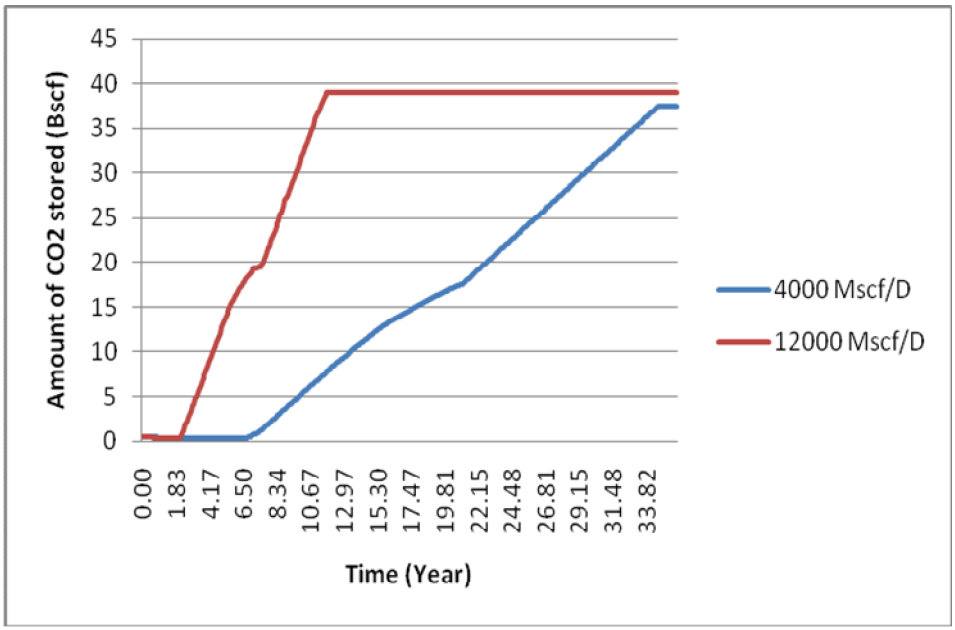

Figure 5.30: Amount of CO_2 stored for 4000 Mscf/D and 12000 Mscf/D of injection rate

Additionally, both horizontal wells have large contact area to the reservoir than that of vertical wells, providing more hydrocarbon recovery and also more amount of CO_2 to be injected. Placing the horizontal injector at the lower part of the reservoir helps displace hydrocarbon gas upward to the upper horizontal producer, contributing to more condensate recovery and more CO_2 stored due to available pore spaces. Supercritical CO_2 with high density will move down to the bottom part of the reservoir and move into the pore spaces, benefiting the amount of CO_2 stored. The schematic of both horizontal wells showing effect on gas recovery and amount of CO_2 stored is illustrated by Figure 5.31 and Figure 5.32, respectively.

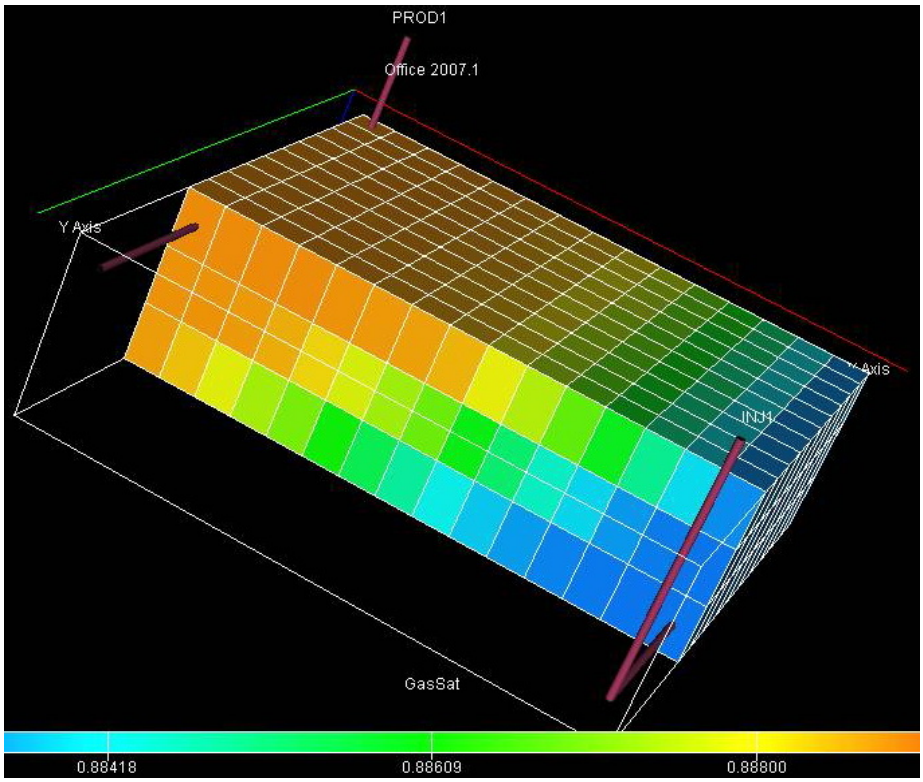

Figure 5.31: The schematic of both horizontal wells showing effect on gas recovery

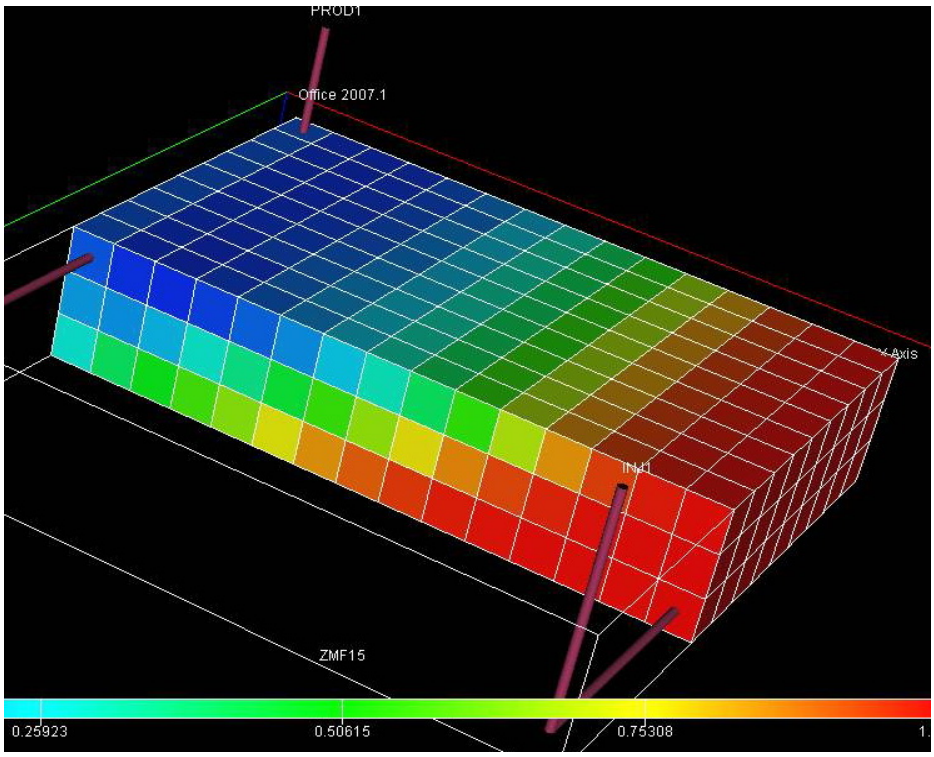

Figure 5.32: The schematic of both horizontal wells showing effect on amount of CO_2 stored

CHAPTER VI

CONCLUSIONS AND RECOMMENDATIONS

In this chapter, conclusions on the effects of CO_2 injection on coupled CO_2 sequestration and enhanced condensate recovery, usefulness of Experimental Design and Response Surface Methodology on coupled CO_2 sequestration and enhanced condensate recovery are presented. Recommendations for further study are also provided.

6.1 Conclusions

1. Experimental Design and Response Surface Methodology is proved to be an effective tool to predict maximum condensate recovery factor and amount of CO_2 stored in this study in place of exhaustive compositional simulations. D-optimal design which is selected as the design criteria is used to generate a quadratic proxy model with acceptable prediction efficiency. The prediction efficiency is guaranteed by cross-validation experiments and matched pairs t-test between ECLIPSE responses and predicted responses showing good model fitting. The differences between ECLIPSE and predicted recovery factor are within a range of +7% to -7% condensate recovery factor whereas those of amount of CO_2 stored are between + 5 Bscf to -5 Bscf.
2. Although the predicted results are not exactly the same as ECLIPSE results, the proxy model can be used as the guideline for implementing optimum strategies for maximizing the results with cost and time saving.
3. Lists of influential factors for both objective functions are obtained. Focus on those higher ranked benefits the economics of project in case of budget constraint. Well Spacing and injection time are two most influential factors on condensate recovery factor, and injection scheme and permeability are two most influential factors on amount of CO_2 stored.
4. The proxy model suggests that 1000 md-permeability gas condensate reservoirs with high k_v/k_h are good candidates for implementing coupled CO_2 sequestration and enhanced condensate recovery project. High permeability helps CO_2 travel

easily in the pore spaces, and consequently CO_2 has more time to be stored in the pore spaces till fracture pressure is reached, contributing to high amount of CO_2 stored. Additionally, better condensate recovery is achieved because of lower pressure drop, resulting in longer plateau production rate of condensate.

5. Using high injection rate at 12000 Mscf/D assists in hydrocarbon displacement and benefits the amount of CO_2 injected better although the fracture pressure is prematurely reached earlier than lower injection rate.
6. Pure CO_2 injection with full well spacing is recommended in this study. CO_2 has enough time to spread over the pore spaces by aid of full well spacing, resulting in a large amount of CO_2 stored in the pore spaces. On the other hand, WAG injection shows that total condensate recovery is equal to that of pure CO_2 injection but WAG injection impairs the amount of CO_2 stored. A large amount of water occupies the pore spaces and also causes fracture pressure to be prematurely reached due to high density of water.
7. CO_2 injection at dew point pressure sustains longer plateau condensate production than other starting times of injection time, resulting in higher condensate recovery. Injection after the reservoir is depleted shows the best amount of CO_2 stored but quite lower condensate recovery than that of injection at the dew point pressure. To meet the objectives of this study for equally maximizing two objective functions, CO_2 injection at dew point pressure is recommended.
8. Placing horizontal injection well at the bottom part and horizontal production well at the top part of the reservoir is recommended. Horizontal wells have more contact area to the reservoir than that of vertical wells which will assists in better hydrocarbon displacement and CO_2 can be injected more. Supercritical CO_2 can displace hydrocarbon gas upward toward the upper horizontal production well while supercritical CO_2 with high density move downward into the pore spaces, all contributing to enhanced condensate recovery and large amount of CO_2 stored.

6.2 Recommendations for Further Study

Although Experimental Design and Response Surface Methodology show good prediction efficiency on coupled CO_2 sequestration and enhanced condensate

recovery, it is valid only for reservoirs which have the same reservoir and fluid properties as those in this study. The prediction efficiency of the model can be used only within the levels of parameters used to construct the model. Hence, larger boundary of prediction can be achieved by investigation on larger levels of parameters which means surveillance and acquisition of more data are need, resulting in higher investment for the project. Besides, the prediction efficiency can also be improved by increasing design points within levels of parameters used.

REFERENCES

[1] Barrufet, M.A., Bacquet, A., and Falcone, G. Analysis of the Storage Capacity for CO_2 Sequestration of a Depleted Gas Condensate Reservoir and a Saline Aquifer. Journal of Canadian Petroleum Technology 49 (August 2010): 23-31.

[2] Thitaram, P. Effect of Fluid Composition on Carbon Dioxide Injection in Gas Condensate Reservoir. Master's Thesis, Department of Mining and Petroleum Engineering, Faculty of Enginnering, Chulalongkorn University, 2009.

[3] Chaback, J.J., and Willium, M.L. p-x Behavior of a Rich-Gas-Condensate Reservoir Fluid in Admixture of CO_2 and (N_2+O_2). Paper SPE 24132 presented at the 1992 SPE Sympsium on Enhanced Oil Recovery, Tulsa (April 1992)

[4] Lim, M.T., Khan, S.A., Sepehrnoori, K., and Pope, G.A. Simulation of Carbon Dioxide Flooding Using Horizontal Wells. Paper SPE 24929 presented at the SPE Annual Technical Conference and Exhibition, Washington, DC (October 1992)

[5] Jikich, S.A., Smith, D.H., Sams, W.N., and Bromhal, G.S. Enhanced Gas Recovery (EGR) with Carbon Dioxide Sequestration: A Simulation Study of Effects of Injection Strategy and Operational Parameters. Paper SPE 84813 presented at the SPE Eastern Regional/AAPG Eastern Section Joint Meeting, Pittsburgh, Pennsylvania (September 2003)

[6] Sobers, L.E., Frailey, A.M., and Lanal, A.S. Geological Sequestration of Carbon Dioxide in Depleted Gas Reservoirs. Paper SPE 89345 presented at the SPE/DOE Fourteenth Symposium on Improved Oil Recovery, Tulsa, Oklahoma (April 2004)

[7] Ramcharak, R., Aminian, K., and Ameri, S. Impact of Carbon Dioxide Sequestration in Gas/Condnesate Reservoirs. Paper SPE 139083 presented at the SPE Eastern Regional Meeting, Morgantown, West Virginias (October 2010)

[8] Cheong, Y.P. et al. Experimental Design Methodology for Quantifying UR Distribution Curve-Lessons Learnt and still to be learnt. Paper SPE 88585 presented at the 2004 SPE Asia Pacific Oil and Gas Conference and Exhibition, Perth, Australia (October 2004)

[9] Ghomian, Y., Sepehrnoori, K., and Pope, G.A. Efficient Investigation of Uncertainties in Flood Design Parameters for Coupled CO_2 Sequestration and Enhanced Oil Recovery. Paper SPE 139738 presented at the SPE International Conference on CO_2 Capture, Storage, and Utilization, New Orleans, Louisiana (November 2010)

[10] Forooghi, A., Hamouda, A.A., and Eilertsen, T. Co-optimization of CO_2 EOR and Sequestration Process in a North Sea Chalk Reservoir. Paper SPE 125550 presented at the SPE EUROPEC/EAGE Reservoir Characterization and Simulation Conference, Abu Dhabi, U.A.E. (October 2009)

[11] Arunmongkol, J. Design Optimization of a Horizontal Well in Thin Oil Column Reservoir in Gulf of Thailand Using Experimental Design Methodology. Master's Thesis, Department of Mining and Petroleum Engineering, Faculty of Engineering, Chulalongkorn University, 2010.

[12] Fan, L. et al. Understanding Gas-Condensate Reservoirs. Oilfield Review (2005): 14-27.

[13] Nemeth, L.K., and Kennedy, H.T. A Correlation of Dewpoint Pressure with Fluid Composition and Temperature. Paper SPE 1147 presented at the SPE 41th Annual Fall Meeting, Dallas, Texas (June 1967)

[14] Van Der Waals, J.D. Continuity of the Gaseous and Liquid States. Doctor's Thesis, Faculty of Mathematics and Natural Science, University at Leiden, 1873.

[15] Redlich, O., and Kwong, J.N.S. On the Thermodynamics of Solutions,V: An Equation of State. Fugacities of Gaseous Solutions. Chemical Reviews 44 (1949): 233.

[16] Soave, G. Equilibrium Constants from a Modified Redlich-Kwong EOS. Chemical Engineering Science 27 (1972): 1197.

[17] Peng, D.Y., and Robinson, D.B. A New-Constant EOS. Industrial & Engineering Chemistry Fundamentals 15 (1976): 59.

[18] Yisheng, F., Baozhu, L., Yongle, H. Condensate Gas Phase Behavior and Development. Paeper SPE 50925 presented at the 1998 SPE International Conference and Exhibition, Beijing, China (November 1998)

[19] Latil, M. Enhanced oil recovery. Houston, Texas: Gulf Publishing, 1980.

[20] Internal MMP IOR report. Correlations for Minimum Miscibility Pressures.

[21] Cronquist, C. Carbon Dioxide Miscibility with Light Reservoir Oils. Proceedings of the Fourth Annual U.S. DOE Symposium on Enhanced Oil and Gas Recovery and Improved Drilling Methods, Tulsa (August 1978)

[22] Glasø, O. Generalised Minimum Miscibility Pressure Correlation. SPE Journal 25 (December 1985): 927.

[23] Yuan, H., and Johns, R. T. Simplified methods for Calculation of Minimum Miscibility Pressure or Enrichment. Paper SPE 77381 presented at the Annual Technical Conference and Exhibition, San Antonio, Texas (29 September – 2 October, 2002)

[24] Essendelft, D., Taron, J., and Fitzgerald, M. CO_2 Sequestration through Deep Saline Injection and Photosynthetic Biological Fixation: System Design for Two Plausible CO_2 Sequestration Strategies. The Pensylvania State University, 2009.

[25] http://www.sciencedirect.com. Sequestration of CO_2 in geological media: criteria and approach for site selection in response to climate change [Online]. 2000. Available from: http://www.sciencedirect.com/science/article/pii/S0196890499001491 [2012, January 20]

[26] Kantham, M. Pre-Feasibility Study of Carbon Capture and Storage (CCS) Technologies: A Case Study of Offshore Natural Gas Field in Thailand. Master's Thesis, Department of Mining and Petroleum Engineering, Faculty of Engineering, Chulalongkorn University, 2010.

[27] Shtepani E. CO_2 Sequestration in Depleted Gas/Condensate Reservoirs. Paper SPE 102284 presented at the SPE Annual Technical Conference and Exhibition, San Antonio, Texas (September 2006)

[28] http://www.co2injection.com/. Sequestration of CO_2 in geological media: criteria and approach for site selection in response to climate change [Online]. 2007. Available from: http://www.co2injection.com/ [2012, January 20]

[29] Montgomery, D.C. Design and Analysis of Experiments. 5th Edition. International student version. Asia: John Wiley & Sons., 2005.

[30] United States Department of Commerce, NIST/SEMATECH. NIST/SEMATECH e-Handbook of Statistical Methods [Online]. 2003. Available from: http://www.itl.nist.gov/div898/handbook/index.htm [2012, January 01]

[31] Yeten, B. Castellini, A., Guyaguler,B., and Chen, W.H. A Comparison Study on Experimental Design and Response Surface Methodologies. Paper SPE 93347 presented at the 2005 SPE Reservoir Simulation Symposium, Houston, Texas (2005)

[32] Montgomery, D.C., and Runger, G.C. Applied Statistics and Probability for Engineers. 3rd Edition. Asia: John Wiley & Sons., 2003.

[33] Mogbo, O. CO_2 EOR and Sequestration in a Depleted Gas-condensate Reservoir: UKNS Case Study. Paper SPE 150752 presented at the Nigeria Annual International Conference and Exhibition, Abuja (2011)

[34] Klinnoi, P. Application of Experimental Design and Response Surface Methods for Field Production Forecast. Master's Thesis, Department of Mining and Petroleum Engineering, Faculty of Engineering, Chulalongkorn University, 2007.

[35] Gas Processors Suppliers Association. ENGINEERING DATA BOOK FPS VERSION. Volume I & II. Tulsa, Oklahoma, 1998.

APPENDIX

APPENDIX

1) Compressor Specification and Cost [34]

Compressor Spec

Type	:	Reciprocating
Design capacity	:	14.0 MMSCF/D
Operating capacity	:	12.5 MMSCF/D
Operating suction pressure	:	275 psig
Operating discharge pressure	:	1,350 psig (Δp = 1,075 psig)
Operating temperature	:	50 ^{o}C
Estimated required power	:	1,400 HP

Cost estimation of compressor

Items	Cost (1000 US$)
PDS Tariff	
- Detailed design	25.0
- Construction	30.0
- Project management	25.0
Materials	1,760
- Compressor package	
- Compressor frame and cylinders	
- F&G lube system	
- Pulsation dampener and separator	
- Air cooler	
- Gas engine driver	
- Skid	
- Water cooling system	
- PLC control unit	
- Drawings	
- Transportation and insurance for major equipment	137.5
- Foundation and grouting work	100.0
- Mechanical modification	50.0
- Instrumentation (replace the aging facility)	25.0

Items	Cost (1000 US$)
- Electrical modification (hook-up to power supply from the existing facility) - Soft starter panel, 110 kW, IP55 for fan motor - Cables - RCU - Small distribution board - Lightings - Splice box - Accessories	112.5
- Modification of fire and gas detection system - New sensor units (5 sets) - Modification of existing fire and gas alarm panel - Software	30.0
- Commissioning spare parts	0.0
- Other bulks	25.0
Construction and Commissioning Cost - Civil work - Mechanical work - Electrical work - Instrument work - Third party inspection of K-3850 at the factory - Installation, commissioning, and training (vendor) - Contingency (10%) Total	 20.0 37.5 20.0 5.0 15.0 60.0 247.75 2,725.25

The above costs form part of BI 5DXX

Notes: Cost for electrical facility has been based on the estimated electrical consumption (by the air cooler fan) of 90-110 kW.

2) Electrical/Power consumption calculations

Pumping power is defined as the time-rate of pumping work. It is related to pumping rate and pressure by

$$\text{power} = \frac{\text{work}}{\text{time}} = q\Delta p$$

The customary unit of power for combustion engines is horsepower (HP) and for electrical motors is the kilowatt (kw). The power units are related by

1 HP = 0.746 kw

The approximate compressor power

$$P = 0.23\, q_g \left[\left(\frac{p_2}{p_1}\right)^{0.2} - 1\right]$$

where

q_g is gas compression or injection rate (Mscf/D)

p_1 is compressor suction pressure (psia) = 289.7 psia

p_2 is compressor discharge pressure (psia) = 1,367.47 psia

P is compression power, HP

Note: Oil price = 97.9 $US/STB

Injection rate (Mscf/D)	**Power (HP)**	**Power (kw)**	**Consumption total power cost(USD/Year) EGAT power**	**Consumption total power cost(USD/D) EGAT power**	**Economic limit (STB/D)**
4000	344.7	257.15	101,151.5	277.13	3.57
5600	482.58	360	141,612.0	387.98	5.01
7200	620.46	462.87	182,072.6	498.83	6.44
8000	689.4	514.29	202,302.9	554.25	7.15
8800	758.34	565.72	222,533.2	609.68	7.87
10400	896.22	668.58	262,993.8	720.53	9.3
12000	1034.1	771.44	303,454.4	831.38	10.72

Vitae

Pitipong Santagarn was born on October 12th, 1984 in Phang-nga, Thailand. He received his Bachelor of Engineering in Civil Engineering from the Department of Civil Engineering, Faculty of Engineering, King Mongkut's University of Technology North Bangkok in 2008. He has then continued his further study in the Master's Degree program in Petroleum Engineering at the Department of Mining and Petroleum Engineering, Faculty of Engineering, Chulalongkorn University since 2008.